UNIVERSITÀ DEGLI STUDI DI CAMERINO

School of Advanced Studies

DOCTORAL COURSE IN

Physical and Chemical Processes in Earth Systems

XXXVI cycle

FAULT INTERACTION AND THE EVOLUTION OF SEISMICITY: THE CASE STUDY OF THE CENTRAL APENNINE FAULT SYSTEM (CAFS)

PhD Student
Giorgio Valentini

Supervisor
Prof. Emanuele Tondi

Co- supervisor
Dr. Tiziano Volatili

TABLE OF CONTENTS

LIST OF FIGURES

horizontal offset with slickenlines (rake=5°); (d) Broken and displaced root (No 149, 13/01/2021) showing 8 cm left-lateral offset; (e) coseismic rupture in paved road near the village of Brest Pokupski (No 121, 12/01/2021) showing 5 cm left-lateral offset and lower-hemisphere, equal-area projection of the overall coseismic ruptures with left-lateral offset. The inset shows a close-up of compressional jog. The numbers (No 1) refer to the observation points (indicated in Fig. 2.3) of the records in the database, while the dates refer to the photo acquisition.

Figure 2.5 (a) Virtual outcrop model of the Župić Fault exposed in a quarry in poorly-lithified Pliocene shallow marine calcareous deposits (see also Fig. 2.5c). (b) Geologic interpretation and structural data extracted from the VRGS software, depicts a positive flower structure composed of three main fault planes.

Figure 2.6 Examples of sliding, rockfall, fracture, sinkhole, and sand volcanism in the epicentral area of the Petrinja earthquake. (a) (15/01/2021) and (d) (5/01/2021) Examples of sand boil associated with liquefaction phenomena occurred in the valley of the Kupa river (No 165, 166, 205). (b) The earthquake triggered some rockfalls along the crown of the quarry close to the village of Hrastovica (No 64, 12/01/2021). (c) The largest sinkhole opened in the Mečenčani area with a diameter of about 20 meters (No 212, 14/01/2021). (e) Large fracture connected to the sinking of the river dam induced by liquefaction below (No 204, 5/01/2021). (f) Failure of river embankment induced by liquefaction (No 189, 14/01/2021). The numbers (No 1) refer to the observation points of the records in the dataset indicated in Fig. 2.3 and the dates refer to the photo acquisition.

Figure 2.7. Diagrams showing the main active faults activated during the 29 December 2020 Petrinja earthquake. (a) The Petrinja Fault Zone (PFZ) is a ca. 10 km wide right-lateral strike-slip shear zone composed by "conjugate" faults in which the Župić and the Kupa Faults represent (Y) and (X) shears, respectively. The inset shows the structural features of an idealized shear zone. (b) Tension cracks (T) and mole tracks (P) are developed coseismically within the NW-striking (Y) and NE-striking (X) shears (observation points No 173-176 in Fig. 2.3, photo acquisition date 13/01/2021). The NS oriented arrows indicate the horizontal maximum compression based on geological data, geophysical observations (Bada et al., 1999) and the field data obtained in this study. (c) Simplified sketch of Fig. 2.8b.

Figure 3.1 a) Map of the 15 seismic events with $5.8 \leq Mw \geq 7.0$ in the CAFS area since 1279CE. Main active fault traces on the topographic surface are also shown in red (CFFn – Colfiorito Fault nord; CFFs - Colfiorito Fault south; MVF – Monte Vettore Fault; NF – Norcia Fault; CF – Cascia Fault; CMF – Campotosto Fault; GSF – Gran Sasso Fault; PZF – Pizzoli Fault; PF – Paganica Fault; PTF – Pettino Fault) (Tondi, 2000; Galderisi and Galli, 2020; Tondi et al., 2020; Galli et al., 2022 and references therein). b) CAFS cumulative seismic moment (dyne/cm) as a function of time. Dashed lines show the hypothetical course of the seismic cycle if the system had been (i) ''energy-predictable'' and (ii) ''time-predictable'' (Shimazaki and Nakata, 1980; Tondi and Cello, 2003).

Figure 3.2 Simulations to test the influence of different fault models on CST. With a planar rectangular model (a), the receiver fault is negligibly influenced, whereas with elliptical faults

(b) the receiver fault tip shows higher stress values. By further adding the effect of the variable strike (c), a more heterogeneous stress pattern is noted on the receiver fault.

Figure 3.3 Comparison between the elliptical tip line loop of the fault (in red) and the commonly adopted rectangular shape (in green). The dashed part of the ellipse indicates the hypothetical continuation of the perimeter above the topographical surface. Center-to-perimeter faded colors show the ideal variation of displacement on the fault surface, maximum in the center and zero along the tip line loop.

Figure 3.4 CST on the Norcia fault (NF) caused by the slip of the a) Colfiorito north fault (CFFn), b) Colfiorito south fault (CFFs) and c) simultaneous activation of both faults. The pictures on the right side show the fault location in map view.

Figure 3.5 Map view of the spatial distribution of the CST caused by the simultaneous activation of Colfiorito north and South faults, the calculation was performed on a plane at 7.5km depth.Contour lines of equal stress variation on the receiver fault are drawn in black (numbers are stress in bars). The red traces are the surface traces of the faults (CFFn-Colfiorito north fault, CFFs- Colfiorito south fault, NF-Norcia fault).

Figure 3.6 CST on the Cascia fault (CF) following the 1328 Mw6.49 seismic event caused by the slip on the Norcia fault (NF). a) Plan view of the spatial distribution of the CST on a plane at 7.5km depth. Contour lines of equal stress variation on the receiver fault are drawn in black (numbers are stress in bars). The red traces are the surface traces of the faults. b) 3D view of the CST on fault surfaces.

Figure 3.7 CST on the Cascia fault (CF) following the 1328 Mw6.49 seismic event caused by the slip on the Norcia fault (NF). a) Plan view of the spatial distribution of the CST on a plane at 7.5km depth.Contour lines of equal stress variation on the receiver fault are drawn in black (numbers are stress in bars). The red traces are the surface traces of the faults. b) 3D view of the CST on fault surfaces.

Figure 4.1 Map of the 15 seismic events with $5.8 \leq Mw \geq 7.0$ in the CAFS area since 1279CE. Main active fault traces on the topographic surface are also shown in red (CFFn – Colfiorito Fault nord; CFFs - Colfiorito Fault south; MVF – Monte Vettore Fault; NF – Norcia Fault; CF – Cascia Fault; CMF – Campotosto Fault; GSF – Gran Sasso Fault; MF – Marine Fault; PF – Paganica-San Demetrio Fault; PTF – Pettino Fault) (Tondi, 2000; Galderisi and Galli, 2020; Tondi et al., 2020; Galli et al., 2022 and references therein). Modified after Valentini et al. (2023).

Figure 4.2 a) oblique view of the CST distribution on a plane located at a depth of 5 km. The causative faults are Colfiorito North and South, and the receiver fault is the Norcia Fault. b) Cross-sections perpendicular to the receiver fault (NF) one at the northernmost part of the fault, near the causative fault and the other at the southern portion of the Norcia fault. Note the difference in the CST pattern when moving just a few kilometers away from the causative fault. c) 3D view of the causative and receiver faults. Note that the CST is calculated on each of the rectangles that make up the entirety of the faults.

Figure 4.3 a) Plan view of the CST distribution on a plane located at a depth of 5 km. The causative fault is the Gran Sasso Fault, and the receiver fault is the Paganica Fault. b) 3D view of the causative and receiver faults. Note that the CST is calculated on each of the rectangles that make up the entirety of the faults. c) Cross-sections perpendicular to the receiver fault (PF), one at the northernmost part of the fault and the other Cross-section at the southern portion of the Paganica fault.

Figure 4.4 a) Plan view of the CST distribution on a plane located at a depth of 5 km. The causative faults belong to the Norcia Fault System and the receiver fault is the Paganica Fault. b) 3D view of the causative and receiver faults. Note that the CST is calculated on each of the rectangles that make up the entirety of the faults. c) Cross-sections perpendicular to the receiver faults (MF and PF), one at the northernmost part of the MF, near the causative faults and the other Cross-section on the PF. Note the difference in the CST pattern when moving just a few kilometers away from the causative fault.

Figure 4.5 a) Plan view of the CST distribution on a plane located at a depth of 5 km. The causative faults are the Marine, Pettino and Paganica-San Demetrio faults (Upper Aterno Fault System) and the receiver fault is the Norcia Fault. b) 3D view of the causative and receiver faults. Note that the CST is calculated on each of the rectangles that make up the entirety of the faults.

Figure 4.6 a) Plan view of the CST distribution on a plane located at a depth of 5 km. The causative faults are Colfiorito North and South, and the receiver fault is the Mt. Vettore Fault. b) 3D view of the causative and receiver faults. Note that the CST is calculated on each of the rectangles that make up the entirety of the faults. c) Cross-section perpendicular to the receiver fault (MVF).

Figure 4.7 Plan view of the CST distribution on a plane located at a depth of 5 km. The causative fault is the Paganica-San Demetrio fault, and the receiver fault is the Mt. Vettore Fault.

Figure 4.8 CST related to the 24/08/2016 earthquake. a) Oblique view of the CST distribution on a plane located at a depth of 5 km. The causative fault is the southernmost portion of the Mt. Vettore Fault and the receiver is its central and northern portion. b) 3D view of the CST on the Mt. Vettore Fault. Note that the CST is calculated on each of the rectangles that make up the entirety of the fault. c) Cross-sections perpendicular to the MVF, one near the southern partial rupture and the other cross-section at the central portion of the MVF. Note the difference in the CST pattern when moving just a few kilometers away from the rupture.

Figure 4.9 CST related to the 26/10/2016 earthquake. a) Oblique view of the CST distribution on a plane located at a depth of 5 km. The causative fault is the northernmost portion of the Mt. Vettore Fault and the receiver is its central and southern portion. b) 3D view of the CST on the Mt. Vettore Fault. Note that the CST is calculated on each of the rectangles that make up the entirety of the fault. c) Cross-sections perpendicular to the MVF, one near the northern partial rupture and the other cross-section at the central portion of the MVF. Note the difference in the CST pattern when moving just a few kilometers away from the rupture.

Figure 4.10 CST related to the 30/10/2016 earthquake. a) Oblique view of the CST distribution on a plane located at a depth of 5 km. The causative fault is the Mt. Vettore Fault and the receiver is the Norcia fault. b) 3D view of the CST on the causative and receiver faults. Note that the CST is calculated on each of the rectangles that make up the entirety of the fault. c) three cross-sections perpendicular to the Norcia fault placed in different portions along the receiver fault.

Figure 4.11 a) 3D view of the cumulative CST in the CAFS following the 1997, 2009 and 2016 seismic sequences. Note that the CST is calculated on each of the small rectangles that make up the entirety of the faults. b) Cumulative CST distribution at a depth of 5 km (plan view) following the 1997, 2009 and 2016 seismic sequences.

Figure 4.12 Summary visualization of the Calculated CST at a Depth of 5 km among the faults of the CAFS for each of the analyzed historical earthquakes. a) CST generated by the Colfiorito Fault System in April 1279. b) CST generated by the Gran Sasso Fault in September 1349. c) CST generated by the Norcia and Cascia Faults in January 1703. d) CST generated by the Paganica-San Demetrio fault, Marine, and Pettino Faults in February 1703. The fault traces drawn in black represent the causative faults. The insets of each figure illustrate the spatial distribution of the CST within the crust on a plane located at a depth of 5 km.

Figure 4.13 Summary visualization of the Calculated CST at a Depth of 5 km among the faults of the CAFS for each of the analyzed instrumental earthquakes. a) CST generated by the Colfiorito Fault System in September 1997. b) CST generated by the Paganica-San Demetrio Fault in April 2009. c) CST generated by the southern portion of the Mt. Vettore fault in August 2016. d) CST generated by the northern portion of the Mt. Vettore fault in October 26th 2016. e) CST generated by the complete rupture of the Mt. Vettore fault in October 30th 2016. f) Cumulative CST from the last five instrumental earthquakes. The fault traces drawn in black represent the causative faults. The insets of each figure illustrate the spatial distribution of the CST within the crust on a plane located at a depth of 5 km.

Figure 5.1 Comparison between a) the seismic cycle of the CAFS before the revision of historical events and the addition of the latest seismic events of 2009 and 2016 (modified after Tondi and Cello, 2003) and b) the updated seismic cycle by Valentini et al. (2023).

Figure 5.2 Distribution of seismic moment from the year 1100 to the present.

LIST OF TABLES

LIST OF ABBREVIATIONS

ASTER: Advanced Spaceborne Thermal Emission and Reflection Radiometer

CAFS: Central Apennine Fault System

CF: Cascia Fault

CFFn: Colfiorito Fault nord

CFFs: Colfiorito Fault south

CFTI : Catalogue of Strong Earthquakes in Italy

CMF: Campotosto Fault

CPTI : Parametric Catalogue of Italian Earthquakes

CST: Coulomb Stress Transfer

DBMI : Macroseismic Database of Italian Earthquakes

DISS : Database of Individual Seismogenic Sources

EMSC: European-Mediterranean Seismological Centre

GDEM: Global Digital Elevation Model

GPS: Global Positioning System

GSF: Gran Sasso Fault

INGV : National Institute of Geophysics and Volcanology

InSAR: Interferometric Synthetic-Aperture Radar

ITHACA: ITaly HAzard from CApable faults

KF: Kasina Fault

LOS: satellite's line of sight

M0: Seismic Moment

MAF: Mount Alvagnano Fault

MF: Marine Fault

MVF: Monte Vettore Fault

Mw: Moment Magnitude

NF: Norcia Fault

NFS: Norcia Fault System

NMF: north Medvednica Fault

NoHard: Novel Approach for Seismic Hazard Analysis

PDZ: Principal Displacement Zone

PF: Paganica Fault

PF: Pokuplje fault

PFZ: Petrinja Fault Zone

PSDFS: Paganica-San Demetrio Fault System

PTF: Pettino Fault

PZF: Pizzoli Fault

SF: Sava Fault

SfM: Structure from Motion

UAFS: Upper Aterno Fault System

UAV: Unmanned Aerial Vehicle

VOMs: Virtual Outcrop Models

VRGS: Virtual Reality Geologic Studio

ΔCST: Change in Coulomb Stress Transfer

$\Delta\sigma n$: alterations in normal stress

$\Delta\tau s$: shifts in shear stress

ABSTRACT

This thesis presents an integrated study of the Central Apennine Fault System (CAFS), focusing on the dynamics of fault interactions and the role of Coulomb Stress Transfer (CST) in shaping seismicity. The CAFS, a seismically active region in central Italy, has witnessed numerous destructive earthquakes recorded in extensive national seismic catalogs, making it an ideal subject for investigating the mechanisms underlying seismic events and their respective seismic cycles. In addition to the CAFS, the thesis incorporates findings from a field-based analysis of the Mw 6.4 Petrinja earthquake in Croatia. Although geographically distinct from the CAFS, this study contributes valuable insights into the processes of coseismic faulting and fault interaction in a strike-slip environment, enhancing our understanding of fault dynamics across different tectonic settings.

The proposed study spans a variety of tectonic regimes but aims to converge on a detailed examination of fault interaction and the related seismic activity. The primary focus is, therefore, on understanding how the CST influences the activation and interaction of faults within this intricate system in central Italy. A significant aspect of this research involves the analysis of both historical and instrumental seismic events within the CAFS, spanning from the year 1200 AD to the present day. Employing advanced modeling techniques, including innovative three-dimensional elliptical models, the study provides new insights into the role of CST in fault activity. The research demonstrates that CST plays a pivotal role in either promoting or inhibiting seismic events, highlighting the importance of this mechanism in understanding the seismic cycle of the region.

This thesis aims to advance the knowledge of Earthquake Geology by providing a comprehensive understanding of the seismic mechanisms within the CAFS and in regions that are geographically and geologically distinct (e.g., Petrinja, Croatia). The findings of this research might have significant implicationsfor seismic hazard assessment and risk management, contributing to the development of targeted seismic risk mitigation strategies and enhancing efforts in earthquake preparedness and response in seismically active regions.

CHAPTER 1: Introduction

In the fields of structural geology and seismology, the complex dynamics of fault interactions and their influence on the evolution of seismicity represent a fundamental research aspect. This field focuses on understanding how faults interact to shape the seismic cycle, subsequently influencing both the spatial and temporal distribution of earthquakes. A crucial aspect of this research is the analysis of the evolution of seismicity, including the stress transfer along fault systems and how these interactions contribute to the occurrence of strong seismic events.

The Central Apennine Fault System (CAFS, Cello et al., 1997), located in central Italy, serves as an exemplary case study to investigate these dynamics. Characterized by a robust seismic history, the CAFS has been the site of numerous destructive earthquakes over the millennia (CPTI15; Rovida et al., 2022). This region's seismic activity, capable of magnitudes up to Mw=7.0 (Roberts & Michetti, 2004; Galli et al., 2008, 2022), results from the ongoing tectonic interaction between the African and Eurasian plates, leading to the development of a complex array of active faults spanning over 130 km from the Colfiorito basin to the L'Aquila basin.

The seismicity of the CAFS is primarily driven by an extensional tectonic regime active since the early Pleistocene. This regime has led to the formation of predominantly normal-oblique faults, which, in some cases, have significantly modified and overwritten pre-existing compressive structures (Cello et al., 1995, 1997; Boncio and Lavecchia, 2000; Tondi, 2000; Boncio et al., 2004; Iezzi et al., 2019; Tondi et al., 2021). The region's structural complexity is evident in its network of normal-oblique kinematic faults, which have been the source of numerous devastating earthquakes over the past millennium. The seismic history of the CAFS is well-documented in national seismic catalogs, which, thanks to the long and significant Italian history, are among the most complete in the world. These catalogs have recorded hundreds of earthquakes, which, through detailed macroseismic and paleoseismological analyses, have been precisely located, and their magnitudes have been adequately estimated (although these estimates can sometimes be subject to considerable error; Vannucci et al., 2021). This robust starting point has allowed us to analyze the seismic cycle of the CAFS with a precision rarely found in other

geotectonic situations globally and a time span of about 800 years, long enough to allow the repetition of multiple seismic events caused by the same faults. This aspect is crucial in determining how fault interaction can influence the characteristic return time of a historical earthquake.

The role of Coulomb Stress Transfer (CST) (Harris and Simpson, 1992; Reasenberg and Simpson, 1992; King et al., 1994), which involves the transfer of static stress from one fault to another, is crucial in understanding seismicity within the CAFS is. The impact of CST on fault interactions has been the subject of extensive study, underscoring its importance in seismic events. However, specific investigations of CST in the context of the CAFS are less frequent (Nostro et al., 2005; Wedmore et al., 2017; Wang et al., 2018; Improta et al., 2019; Mildon et al., 2019, 2022; Pino et al., 2019; Galderisi and Galli, 2020; Roberts et al., 2024), justifying a more in-depth exploration of its effects on both historical and instrumental seismic events of significant magnitude associated with the CAFS.

This thesis aims to integrate the results of multiple studies to offer a cohesive narrative that clarifies the complex relationship between fault interactions, CST, and the evolution of seismicity within the CAFS. It presents a comprehensive exploration of the dynamics governing the CAFS, highlighting the critical role of CST in shaping the seismic landscape of this tectonically active region.

A notable study included in this thesis investigates the coseismic surface effects of the Petrinja earthquake on December 29, 2020, in Croatia (Tondi et al., 2021), highlighting the significance of conjugate faults within a shear zone context. The findings reveal that the earthquake activated a conjugate fault system, with right-lateral displacements up to 36 cm, unveiling a complex interaction among fault structures. This research enhances understanding of fault dynamics in environments distinct from the CAFS, emphasizing the necessity of accurately mapping coseismic deformations to assess seismic risk and better comprehend faulting processes and fault interactions in regions characterized by complex fault arrays.

Through the integration of diverse research results, this thesis advances the field of Earthquake Geology, providing valuable insights for seismic risk assessment and

management in one of Europe's most seismically active regions. The synthesis of these studies not only deepens our understanding of the seismic mechanisms at play within the CAFS but also contributes to the global discourse on earthquake preparedness and response.

The main goals of this research are listed below:

1) Coulomb Stress Transfer (CST) and fault interactions.

A key aspect of this research is the examination of CST and its influence on fault interactions within the CAFS. The study assesses how stress transfer among faults contributes to the activation or inhibition of faults.

2) Modeling techniques and analysis.

The thesis employs advanced modeling techniques, including strike-variable three-dimensional elliptical models, to analyze CST within the CAFS. This approach allows for a more accurate representation of fault geometry and a better understanding of stress distribution along and between faults.

3) Analysis and modeling of the CAFS seismic cycle.

Utilizing reliable and comprehensive seismic catalogs, the CAFS seismic cycle is aimed to be reconstructed as previously done by Tondi and Cello (2003), including the most recent seismic events. The resulting seismic cycle also emerges from revisions of the seismic moment generated by historical earthquakes in light of new paleoseismological investigations (Falcucci et al., 2015; Blumetti, 1995; Galadini and Galli, 2003; Galli et al., 2005; 2008; 2011; 2018; 2020; 2022; 2023; Iezzi et al., 2023). The goal is to seek a cyclicity or a systematic repetition in time and space of seismic events, in order to identify possible seismic gaps and hypothesize how much fault interaction may have influenced their trend.

4) Analysis of external seismic events.

In addition to focusing on the CAFS, the thesis includes an analysis of the Mw 6.4 Petrinja earthquake in Croatia. This study provides insights into similar processes of

coseismic faulting in strike-slip environments, offering broader applicability to the findings and enhancing our understanding of seismic dynamics in tectonically comparable regions.

The present PhD research project aims to contribute significantly to the field of Earthquake Geology. By enhancing our understanding of the dynamics of fault interactions and the role of CST in seismicity, this study provides valuable insights for developing effective seismic risk mitigation strategies and for improving efforts in earthquake preparedness and response, particularly in regions similar to the CAFS.

This doctoral thesis is organized as a collection of scientific papers. Chapter 1 provides an introductive overview and a specific explanation of the significance of Coulomb Stress Transfer (CST). Chapters 2, 3, and 4 constitute the core of the thesis, presenting the scientific articles authored during the research journey. Chapter 5 draws conclusions, summarizes, and critically discusses the main findings of the research, and reflects on future work. Below is a summary that outlines the content of the chapters concerning scientific outputs:

- ***Chapter 2 – 'CONJUGATE' COSEISMIC SURFACE FAULTING RELATED WITH THE 29 DECEMBER 2020, MW 6.4, PETRINJA EARTHQUAKE (SISAK-MOSLAVINA, CROATIA).***

  "Published on Scientific Reports"

The paper provides an essential analysis of the coseismic surface effects of the Mw 6.4 Petrinja earthquake that hit central Croatia on December 29, 2020. This earthquake, one of the strongest in Croatia in two centuries (Stucchi et al., 2013; Grünthal et al., 2012, ISIDe Working Group, 2007) struck near Petrinja and was significant due to its location at the boundary between the Dinarides mountain belt and the Pannonian Basin, a key area in the Alpine collision between the Eurasian and Adriatic tectonic plates (Tomljenović, et al., 2008).

The study highlights the importance of observing surface coseismic effects, as they provide insights into short-term time scale deformation, aiding in the robust

interpretation of long-term geological features for seismic and surface faulting hazard evaluation (Villani et al., 2018).

A novel approach involving Unmanned Aerial Vehicle (UAV) surveys and Structure from Motion (SfM) photogrammetry was employed. This methodology allowed for constructing 3D digital virtual outcrop models (VOMs) (Tavani et al., 2014; Pitts et al., 2017; Jablonska et al., 2021; Pitts et al., 2020) and enabled detailed digital geologic interpretations and structural data extraction, marking a significant advancement in earthquake geology research methods.

The primary surface ruptures observed and mapped in the epicentral area consisted of two sets of coseismic shear fractures with different orientations and slip characteristics. The NW–SE-trending shear fractures exhibited right-lateral strike-slip offset up to 36 cm, while the NE-SW-trending shear fractures showed left-lateral strike-slip offsets of up to 10 cm. These ruptures were observed along pre-existing fault zones, including the Župić Fault and the Kupa Fault, with significant horizontal offsets.

Secondary effects related to ground shaking, such as landslides, sinkholes, and sand boils, were identified, especially along the NE-SW oriented fault zone in the Kupa River's alluvial plain. These phenomena, often associated with surface ruptures, highlighted the broader impact of the earthquake in the landscape.

This research is fundamental in understanding the relationship between seismic sources at depth and their primary evidence at the surface. The study also provides new data on surface coseismic faulting in strike-slip settings, specifically relevant to the central Mediterranean region. The mapped pattern of coseismic fault ruptures is crucial for improving seismic and surface faulting hazard assessments, contributing significantly to our understanding of earthquake faulting processes and aiding in better forecasting the impact of more energetic earthquakes expected in such tectonic settings.

- ***Chapter 3 – NEW METHODOLOGICAL APPROACH IN THE EVALUATION OF FAULT INTERACTION: INSIGHTS FROM THE CENTRAL APENNINES FAULT SYSTEM***

The study focuses on the Central Apennine Fault System (CAFS) in Italy, known for its seismic activity including significant earthquakes in Colfiorito (1997) (Amato et al.,1998; Cello et al.,1998; Tondi, 2000; Vittori et al., 2000), L'Aquila (2009) (Chiarabba et al., 2009; Chiaraluce et al., 2011; Vannoli et al., 2012), and the Marche, Umbria, and Lazio regions (2016) (Chiaraluce et al., 2017). This work introduces a novel methodological approach to studying fault interaction within the CAFS, employing a more complex elliptical fault geometry model for Coulomb Stress Transfer (CST) analysis, aiming to reduce uncertainties in fault interaction.

The CAFS is characterized by several active normal to oblique faults responsible for numerous destructive earthquakes over the last millennium. Seismic events associated with these faults range from Mw 5.8 to 7.0 (relying on the empirical relationship by Galli et al. (2008)). The study identifies three main time windows of seismic activity in the CAFS: the 13th-14th centuries, the 17th-18th centuries, and from the late 20th century to the present day. This periodization of seismic activity underscores the importance of understanding the mechanisms influencing fault recurrence intervals and the role of CST in triggering fault ruptures.

The paper's innovative approach to CST and fault modeling involves using an elliptical shape to represent fault geometry more accurately, recognizing that this shape better reflects actual fault shapes at depth (Barnett et al., 1987; Walsh and Watterson, 1987; Gupta and Scholz, 2000). This model contrasts with the traditional planar and rectangular geometries used in previous CST calculations. By utilizing the "3D Faults" MATLAB code (Mildon et al., 2016), the study performed CST simulations respecting actual rupture conditions of earthquakes and calculated stress transfer between causative and adjacent faults.

Results indicate that the cumulative seismic moment released in the CAFS over the past millennium aligns with three distinct intervals, approximately 300-350 years apart (Tondi and Cello, 2003). However, the energy released varied across these time windows, with the first window exhibiting the highest seismic moment. The use of elliptical fault models in static CST modeling revealed significant differences in stress

transfer and patterns on receiver faults compared to traditional planar models, indicating a more robust interaction between faults and a higher degree of stress transfer.

The CST results are encouraging, demonstrating significant differences from classical methodologies. The method was tested on faults associated with historical earthquakes, revealing a strong correlation between the spatiotemporal evolution of the CAFS earthquake sequence and the static stress transferred to nearby faults. Faults in stress shadows were inhibited in reactivation after a major earthquake, while those under increased stress showed ruptures in shorter times than their usual return periods.

- ***Chapter 4 - INVESTIGATING THE LAST MILLENNIUM COULOMB STRESS TRANSFER IN THE CENTRAL APENNINE FAULT SYSTEM (CAFS)***

  "Submitted to Tectonics"

The paper examines the role of Coulomb Stress Transfer (CST) within the CAFS over the last millennium. The research analyzes significant seismic events of magnitudes over Mw 6.0 to understand CST's influence on fault activation and interaction.

Utilizing a three-dimensional elliptical model for fault representation, the study offers a more accurate depiction of fault geometry and stress distribution, essential for understanding seismic activity in the CAFS.

The key findings of the research demonstrate that CST significantly impacts the activation or inhibition of faults within the CAFS. The study provides insights into how the transfer of stress among faults can lead to reactivation or inhibition of seismic events. The research also explores the cumulative effect of CST arising from seismic events between 1997 and 2016, revealing complex interactions between positive and negative stress lobes generated by different earthquakes.

The paper contributes significantly to the field of Earthquake Geology by providing a comprehensive understanding of the seismic mechanisms within the CAFS. The findings have important implications for seismic risk assessment and management,

contributing to the development of targeted seismic risk mitigation strategies and enhancing earthquake preparedness and response efforts in seismically active regions.

Discussion, conclusions and final considerations are presented in Chapter 5.

1.1 COULOMB STRESS TRANSFER (CST)

Coulomb Stress Transfer (CST) (Harris and Simpson, 1992; Reasenberg and Simpson, 1992; King et al., 1994) is a fundamental concept in understanding earthquake mechanics. CST refers to the stress change caused by an earthquake on surrounding crust, influencing subsequent seismic activity. It is based on Coulomb's failure criterion (Handin, 1969), which posits that a fault will fail when the shear stress acting on it exceeds the frictional resistance enhanced by the normal stress. The concept of CST has revolutionized our understanding of earthquake interactions, sequences, and aftershocks.

CST involves the transfer of shear and normal stresses due to the permanent deformation caused by an earthquake. When an earthquake occurs, it modifies the stress state in the surrounding crust, which can either promote or inhibit subsequent seismic events on nearby faults (King et al.,1994). This stress change is quantified as the Coulomb stress change, which is a combination of shear stress change and the change in normal stress, weighted by the coefficient of friction on the fault surface. Positive Coulomb stress changes tend to encourage fault slip, whereas negative changes inhibit it (Stein, 1999).

Calculating CST requires understanding the fault's geometry, slip distribution of the earthquake, and the region's frictional properties. This calculation helps estimate the likelihood of subsequent seismic events.
The role of CST in earthquake sequences, including aftershocks, is significant. Aftershocks typically occur in regions where the mainshock has increased the Coulomb stress. Stein (2003) highlights how changes in seismicity rates are associated with the redistribution of stress by earthquakes. This relationship is crucial in understanding earthquake clustering and the spatial-temporal patterns of aftershocks.

The CAFS is an exemplary case for studying CST. It comprises several active normal-oblique faults, responsible for numerous destructive earthquakes. Valentini et al. (2023, 2024) investigated CST in the CAFS over the last millennium, focusing on significant seismic events (Mw > 6.0). The study utilized a three-dimensional elliptical

model for fault representation, enhancing the accuracy of fault geometry and stress distribution analysis. This approach provided insights into how CST influenced the reactivation or inhibition of faults within the CAFS, contributing significantly to the understanding of seismic mechanisms in this tectonically active region.

The alteration in Coulomb stress depends on several factors, such as the neighboring faults' proximity, geometry, kinematics, and the causative fault's slip pattern. Utilizing "Coulomb 3.4," (Lin and Stein, 2004; Toda et al., 2005) the Coulomb Stress Transfer (CST) has been calculated employing the formula:

$$\Delta CST = \Delta\tau s + \mu\Delta\sigma n$$

with ΔCST being the stress change, Δτs the shear stress change, μ the friction coefficient (set at 0.6 for the central Apennine, following Galderisi and Galli, 2020), and Δσn the normal stress change. Our analysis assumed established parameters, including a Poisson's ratio of 0.25 and Young's modulus of 800,000 bar.

Our CST calculations employed a three-dimensional model to precisely mimic the CAFS, minimizing errors through an elliptical and strike-variable fault shape (Valentini et al., 2023). The simulations, aimed at replicating actual seismic ruptures, considered factors like slip distribution (where available) and rupture extent.

To achieve detailed and accurate fault shape, a 1 km grid system has been introduced, a deviation from the usual 2 km segmentation, for a balance between detail and computation time. "Faults 3D" (Mildon et al., 2016) software was used for creating 3D fault models and slip distribution was assigned based on actual data or assumed patterns for less documented earthquakes, with adjustments made based on seismic moment.

For the visualization of CST data, a conventional CST map at a depth of 5 km was created. The data was then converted into KML format for visualization in Google Earth Pro. Additionally, cross-sectional views and a 3D model of the fault planes were developed, allowing for a segment-by-segment analysis of the CST.

The integration of CST into probabilistic seismic hazard assessment is a significant advancement. This approach allows for a more dynamic and accurate representation of seismic hazard, considering the transient changes in stress state following an earthquake.

References

Amato A., Azzara R., Chiarabba C., Cimini G. B., Cocco M., Di Bona M., Margheriti L., Mele F., Selvaggi G., Basili A., Boschi E., Courbolex F., Deschamps A., Gaffet S., Bittarelli G., Chiaraluce L., Piccinini D. and Ripepe M.; 1998: The 1997 Umbria-Marche, Italy, earthquake sequence: A first look at the main shocks and aftershocks. Geophysical Research Letters, 25(15), 2861-2864.

Barnett J. A., Mortimer J., Rippon J. H., Walsh J. J. and Watterson J.; 1987: Displacement geometry in the volume containing a single normal fault. AAPG Bulletin, 71(8), 925-937.

Blumetti A.M., 1995. Neotectonic investigation of evidence of paleoseismicity in the epicentral area of the January–February 1703, central Italy, earthquakes, Perspectives in Paleoseismology, Assoc. Eng. Geol. Bull., Special Publ.6, 83–100

Boncio, P., & Lavecchia, G. (2000). A structural model for active extension in Central Italy. Journal of Geodynamics, 29(3-5), 233-244.

Boncio, P., Lavecchia, G., & Pace, B. (2004). Defining a model of 3D seismogenic sources for Seismic Hazard Assessment applications: the case of central Apennines (Italy). Journal of Seismology, 8, 407-425.

Cello G, Mazzoli S, Tondi E, Turco E (1997) Active tectonics in the central Apennines and possible implications for seismic hazard analysis in peninsular Italy. Tectonophysics 272(1):43–68. https:// doi.org/ 10. 1016/ S0040- 1951(96) 00275-2

Cello G., Deiana G., Mangano P., Mazzoli S., Tondi E., Ferreli L., Maschio L., Michetti A.M., Serva L. and Vittori E.; 1998: Evidence for surface faulting during the September 26, 1997, Colfiorito (Central Italy) earthquakes. Journal of Earthquake Engineering, 2(2), 303-324.

Cello, G., Mazzoli, S., Tondi, E., & Turco, E. (1995). Tettonica attiva in Appennino centrale ed implicazioni per l'analisi della pericolosità sismica del settore assiale della catena umbro-marchigiana-abruzzese. STUDI GEOLOGICI CAMERTI. NUOVA SERIE, 13(1), 115-138.

Chiarabba C., Amato A., Anselmi M., Baccheschi P., Bianchi I., Cattaneo M., Cecere G., Chiaraluce L., Ciaccio M. G., De Gori P., De Luca G., Di Bona M., Di Stefano R., Faenza L., Govoni A., Improta L., Lucente F. P., Marchetti A., Margheriti L., Mele F., Michelini A., Monachesi G., Moretti M., Pastori M., Piana Agostinetti N., Piccinini D., Roselli P., Seccia D., Valoroso L.; 2009: The 2009 L'Aquila (central Italy) MW6.3 earthquake: Main shock and aftershocks. Geophysical Research Letters, 36(18).

Chiaraluce L., Di Stefano R., Tinti E., Scognamiglio L., Michele M., Casarotti E., Cattaneo M., De Gori P., Chiarabba C., Monachesi G., Lombardi A., Valoroso L., Latorre D. and Marzorati S.; 2017: The 2016 central Italy seismic sequence: A first look at the mainshocks, aftershocks, and source models. Seismological Research Letters, 88(3), 757-771.

Chiaraluce, L. (2012). Unravelling the complexity of Apenninic extensional fault systems: A review of the 2009 L'Aquila earthquake (Central Apennines, Italy). Journal of Structural Geology, 42, 2-18.

Falcucci, E., Gori, S., Moro, M., Fubelli, G., Saroli, M., Chiarabba, C., & Galadini, F. (2015). Deep reaching versus vertically restricted Quaternary normal faults: Implications on seismic potential assessment in tectonically active regions: Lessons from the middle Aterno valley fault system, central Italy. Tectonophysics, 651, 186-198.

Galadini F. , Galli P., 2003. Paleoseismology of silent faults in the Central Apennines (Italy): the Mt. Vettore and Laga Mts. faults, Ann. Geophys.465, 815–836.

Galderisi A. and Galli P.; 2020: Coulomb stress transfer between parallel faults. The case of Norcia and Mt Vettore normal faults (Italy, 2016 Mw 6.6 earthquake). Results in Geophysical Sciences, 1, 100003.

Galli P. A., Giaccio B., Messina P., Peronace E. and Zuppi G. M.; 2011: Palaeoseismology of the L'Aquila faults (central Italy, 2009, M w 6.3 earthquake): Implications for active fault linkage. Geophysical Journal International, 187(3), 1119-1134.

Galli P., Galadini F. and Calzoni F.; 2005: Surface faulting in Norcia (central Italy): a "paleoseismological perspective". Tectonophysics, 403(1-4), 117-130.

Galli P., Galadini F. and Pantosti D.; 2008: Twenty years of paleoseismology in Italy. Earth-Science Reviews, 88(1-2), 89-117.

Galli P., Galderisi A., Messina P. and Peronace E.; 2022: The Gran Sasso fault system: Paleoseismological constraints on the catastrophic 1349 earthquake in Central Italy. Tectonophysics, 822, 229156.

Galli P., Galderisi, A., Ilardo, I., Piscitelli, S., Scionti, V., Bellanova, J. and Calzoni, F.; 2018: Holocene paleoseismology of the Norcia fault system (Central Italy). Tectonophysics, 745, 154-169.

Galli P., Peronace E. and Messina P.; 2022: Archaeoseismic evidence of surface faulting in 1703 Norcia earthquake (Central Italian Apennines, Mw 6.9). Geosciences, 12(1), 14.

Galli P.; 2020: Recurrence times of central-southern Apennine faults (Italy): hints from palaeoseismology. Terra Nova, 32(6), 399-407.

Galli, P., Messina, P., Peronace, E., Galderisi, A., Ilardo, I., & Polpetta, F. (2023). Paleoseismic evidence of five magnitude 7 earthquakes on the Norcia fault system in the past 8,000 years (Central Italy). Frontiers in Earth Science, 11, 1188602.

Grünthal, G. and Wahlström, R. The European-Mediterranean Earthquake Catalogue (EMEC) for the last millennium. Journal of Seismology, 16, 535-570, DOI: https://doi.org/10.1007/s10950-012-9302-y (2012).

Gupta A. and Scholz C. H.; 2000: A model of normal fault interaction based on observations and theory. Journal of structural Geology, 22(7), 865-879.

Handin, J. (1969). On the Coulomb-Mohr failure criterion. Journal of Geophysical Research, 74(22), 5343-5348.

Harris, R. A., and R. W. Simpson (1992), Changes in static stress on southern California faults after the 1992 Landers earthquake, Nature, 360(6401), 251–254, doi:10.1038/360251a0.

Harris, R. A., and R. W. Simpson (1992), Changes in static stress on southern California faults after the 1992 Landers earthquake, Nature, 360(6401), 251–254, doi:10.1038/360251a0.

Iezzi, F., Francescone, M., Pizzi, A., Blumetti, A. M., Boncio, P., Di Manna, P., ... & Urbini, S. (2022, September). Paleoseismological surveys for the identification of capable faults in urban areas:

the case of the Mt. Marine Fault (Central Apennines, Italy). In 11th International INQUA Meeting on Paleoseismology, Active Tectonics and Archeoseismology (PATA), France.

Iezzi, F., Roberts, G., Walker, J. F., & Papanikolaou, I. (2019). Occurrence of partial and total coseismic ruptures of segmented normal fault systems: Insights from the Central Apennines, Italy. Journal of Structural Geology, 126, 83-99.

Improta, L., Latorre, D., Margheriti, L., Nardi, A., Marchetti, A., Lombardi, A. M., ... & Moretti, M. (2019). Multi-segment rupture of the 2016 Amatrice-Visso-Norcia seismic sequence (central Italy) constrained by the first high-quality catalog of Early Aftershocks. Scientific Reports, 9(1), 6921.

ISIDe Working Group. Italian Seismological Instrumental and Parametric Database (ISIDe). Istituto Nazionale di Geofisica e Vulcanologia (INGV). DOI: https://doi.org/10.13127/ISIDE (2007).

Jablonska, D., Pitts, A., Di Celma, C., Volatili, T., Alsop, G. I., & Tondi, E. (2021). 3D outcrop modelling of large discordant breccia bodies in basinal carbonates of the Apulian margin, Italy. Marine and Petroleum Geology, 123, 104732.

King G. C., Stein R. S. and Lin, J.; 1994: Static stress changes and the triggering of earthquakes. Bulletin of the Seismological Society of America, **84**(3), 935-953.

Lin J. and Stein R. S.; 2004: Stress triggering in thrust and subduction earthquakes and stress interaction between the southern San Andreas and nearby thrust and strike-slip faults. Journal of Geophysical Research: Solid Earth, **109**(B2).

Mildon, Z. K., Toda, S., Faure Walker, J. P., & Roberts, G. P. (2016). Evaluating models of Coulomb stress transfer: Is variable fault geometry important?. Geophysical Research Letters, 43(24), 12-407.

Mildon, Z. K., Roberts, G. P., Faure Walker, J. P., & Toda, S. (2019). Coulomb pre-stress and fault bends are ignored yet vital factors for earthquake triggering and hazard. Nature communications, 10(1), 2744.

Mildon, Z. K., Roberts, G. P., Faure Walker, J. P., Beck, J., Papanikolaou, I., Michetti, A. M., ... & Vittori, E. (2022). Surface faulting earthquake clustering controlled by fault and shear-zone interactions. *Nature Communications*, *13*(1), 7126.

Nostro, C., Chiaraluce, L., Cocco, M., Baumont, D., & Scotti, O. (2005). Coulomb stress changes caused by repeated normal faulting earthquakes during the 1997 Umbria-Marche (central Italy) seismic sequence. Journal of Geophysical Research: Solid Earth, 110(B5).

Pino, N. A., Convertito, V., & Madariaga, R. (2019). Clock advance and magnitude limitation through fault interaction: the case of the 2016 central Italy earthquake sequence. Scientific reports, 9(1), 5005.

Pitts, A.D. et al. Integrating traditional field methods with emerging digital techniques for enhanced outcrop analysis of deep water channel-fill deposits. Mar. Petrol. Geol., 87 https://doi.org/10.1016/j.marpetgeo.2017.05.001 (2017).

Pitts, A.D. et al. Sedimentological and stratigraphic signature of the Plio-Pleistocene tectonic events in the Southern Apennines, Italy: the Calvello-Anzi Basin case study. Mar. Petrol. Geol., 116, 104198. https://doi.org/10.1016/j.marpetgeo.2019.104198 (2020).

Reasenberg, P. A., and R. W. Simpson (1992), Response of regional seismicity to the static stress change produced by the loma prieta earthquake, Science, 255(5052), 1687–1690, doi:10.1126/science.255.5052.1687.

Roberts, G. P., & Michetti, A. M. (2004). Spatial and temporal variations in growth rates along active normal fault systems: an example from The Lazio–Abruzzo Apennines, central Italy. *Journal of Structural Geology*, *26*(2), 339-376.

Roberts, G. P., Sgambato, C., Mildon, Z. K., Iezzi, F., Beck, J., Robertson, J., ... & Mitchell, S. (2024). Spatial migration of temporal earthquake clusters driven by the transfer of differential stress between neighbouring fault/shear-zone structures. *Journal of Structural Geology*, *181*, 105096.

Rovida A., Locati M., Camassi R., Lolli B., Gasperini P. and Antonucci A.; 2022: Catalogo Parametrico dei Terremoti Italiani CPTI15, versione 4.0.

Stein, R. S. (1999). The role of stress transfer in earthquake occurrence. Nature, 402(6762), 605-609.

Stein, R. S. (2003). Earthquake conversations. Scientific American, 288(1), 72-79.

Stucchi, M. et al. The SHARE European Earthquake Catalogue (SHEEC) 1000–1899. Journal of Seismology, 17, 523–544, https://doi.org/10.1007/s10950-012-9335-2 (2013).

Tavani, S. et al. Building a virtual outcrop, extracting geological information from it, and sharing the results in Google Earth via OpenPlot and Photoscan: an example from the Khaviz Anticline (Iran). Comput. Geosci., 63, 44–53 (2014).

Toda S., Stein R. S., Richards-Dinger K. and Bozkurt S. B.; 2005: Forecasting the evolution of seismicity in southern California: Animations built on earthquake stress transfer. Journal of Geophysical Research: Solid Earth, **110**(B5).

Tomljenović, B., Csontos, L., Márton, E. & Márton, P. Tectonic evolution of the northwestern Internal Dinarides as constrained by structures and rotation of Medvednica Mountains, North Croatia. Geological Society, London, Special Publications, 298, 145-167. DOI: http://doi.org/10.1144/SP298.8 (2008).

Tondi E. and Cello G.; 2003: Spatiotemporal evolution of the Central Apennines fault system (Italy). Journal of Geodynamics, 36(1-2), 113-128.

Tondi E., Jablonská D., Volatili T., Michele M., Mazzoli S. and Pierantoni P. P.; 2020: The Campotosto linkage fault zone between the 2009 and 2016 seismic sequences of central Italy: Implications for seismic hazard analysis. GSA Bulletin, 133(7-8), 1679-1694.

Tondi E.; 2000: Geological analysis and seismic hazard in the central Apennines (Italy). Journal of Geodynamics, 29(3-5), 517-533.

Valentini, G., Volatili, T., Galli, P., & Tondi, E. (2023). New methodological approach in the evaluation of fault interaction: insights from the central Apennines fault system. BULLETIN OF GEOPHYSICS AND OCEANOGRAPHY, 64(4), 387-404.

Valentini, G., Volatili, T., Galli, P., & Tondi, E. (2024). Investigating the Last Millennium Coulomb Stress Transfer in the Central Apennine Fault System (CAFS) – Submitted to Tectonics

Vannoli P., Burrato P., Fracassi U. and Valensise G.; 2012: A fresh look at the seismotectonics of the Abruzzi (Central Apennines) following the 6 April 2009 L'Aquila earthquake (Mw 6.3). Italian Journal of Geosciences, 131(3), 309-329Vannucci et al., 2021

Villani, F. et al., A database of the coseismic effects following the 30 October 2016 Norcia earthquake in Central Italy. Sci Data, 5, 180049, https://doi.org/10.1038/sdata.2018.49 (2018)

Vittori E., Deiana G., Esposito E., Ferreli L., Marchegiani L., Mastrolorenzo G., Michetti A.M., Porfido S., Serva L., Simonelli A.L. and Tondi E.; 2000: Ground effects and surface faulting in the September–October 1997 Umbria–Marche (Central Italy) seismic sequence. Journal of Geodynamics, 29(3-5), 535-564.

Walsh J. J. and Watterson J.; 1987: Distributions of cumulative displacement and seismic slip on a single normal fault surface. Journal of Structural Geology, 9(8), 1039-1046.

Wang, L., Gao, H., Feng, G., & Xu, W. (2018). Source parameters and triggering links of the earthquake sequence in central Italy from 2009 to 2016 analyzed with GPS and InSAR data. Tectonophysics, 744, 285-295.

Wedmore L. N. J., Faure Walker J. P., Roberts G. P., Sammonds P. R., McCaffrey K. J. W. and Cowie P. A.; 2017: A 667 year record of coseismic and interseismic Coulomb stress changes in central Italy reveals the role of fault interaction in controlling irregular earthquake recurrence intervals. Journal of Geophysical Research: Solid Earth, 122(7), 5691-5711.

CHAPTER 2: 'Conjugate' Coseismic Surface Faulting Related With The 29 December 2020, Mw 6.4, Petrinja Earthquake (Sisak-Moslavina, Croatia).

Emanuele Tondi[1,6], Anna Maria Blumetti[2], Mišo Čičak[3], Pio Di Manna[2], Paolo Galli[4], Chiara Invernizzi[1], Stefano Mazzoli[1], Luigi Piccardi[5], Giorgio Valentini[1], Eutizio Vittori[5] & Tiziano Volatili[1]

[1]*School of Science and Technology, Geology Division, University of Camerino, Camerino, Italy.*

[2]*Italian Institute for Environmental Protection and Research - Geological Survey of Italy, Roma, Italy.*

[3]*Water Management Department for Middle and Lower Sava Flood Protection Service, Croatian Waters, Slavonski Brod, Croatia.*

[4]*Civil Protection Department, Presidency of the Council of Ministers, Roma, Italy.*

[5]*Institute of Geosciences and Earth Resources, National Research Council, Firenze, Italy.*

[6]*National Institute of Geophysics and Volcanology, Roma, Italy*

www.nature.com/scientificreports

scientific reports

Check for updates

OPEN

'Conjugate' coseismic surface faulting related with the 29 December 2020, Mw 6.4, Petrinja earthquake (Sisak-Moslavina, Croatia)

Emanuele Tondi[1,6], Anna Maria Blumetti[2], Mišo Čičak[3], Pio Di Manna[2], Paolo Galli[4], Chiara Invernizzi[1], Stefano Mazzoli[1], Luigi Piccardi[5], Giorgio Valentini[1], Eutizio Vittori[5] & Tiziano Volatili[1]✉

We provide here a first-hand description of the coseismic surface effects caused by the Mw 6.4 Petrinja earthquake that hit central Croatia on 29 December 2020. This was one of the strongest seismic events that occurred in Croatia in the last two centuries. Field surveys in the epicentral area allowed us to observe and map primary coseismic effects, including geometry and kinematics of surface faulting, as well as secondary effects, such as liquefaction, sinkholes and landslides. The resulting dataset consists of homogeneous georeferenced records identifying 222 observation points, each of which contains a minimum of 5 to a maximum of 14 numeric and string fields of relevant information. The earthquake caused surface faulting defining a typical 'conjugate' fault pattern characterized by Y and X shears, tension cracks (T fractures), and compression structures (P shears) within a ca. 10 km wide (across strike), NW–SE striking right-lateral strike-slip shear zone (i.e., the Petrinja Fault Zone, PFZ). We believe that the results of the field survey provide fundamental information to improve the interpretation of seismological, GPS and InSAR data of this earthquake. Moreover, the data related to the surface faulting may impact future studies focused on earthquake processes in active strike-slip settings, integrating the estimates of slip amount and distribution in assessing the hazard associated with capable transcurrent faults.

On 29 December 2020 at 11:19 (UTC), a moment magnitude (Mw) 6.4 earthquake struck central Croatia near the city of Petrinja, a settlement of about 25,000 inhabitants in the region of Sisak-Moslavina, causing 7 casualties and thousands homeless. The epicentre was 15 km SW of Sisak, the main town of the region, and 45 km SSE of Zagreb (Figs. 1, 2;[1–5]). The mainshock was preceded the day before by two foreshocks at 05:28 and 06:49 (UTC time), with Mw 5.2 and 4.8, respectively.

The seismic sequence came nine months after the Zagreb earthquake, a mainshock of Mw 5.5 that was followed by a largest aftershock of Mw 4.9, both occurred on March 22, between 4 and 7 km north-northwest of Zagreb[6] (Figs. 1, 2). In the last two centuries the same area was affected by three moderate earthquakes: on December 18, 1861 (Mw 5.4), on February 11, 1883 (Mw 5.1), and on October 8, 1909 (Mw 5.7)[2] (Fig. 2). The Mw 6.4 Petrinja earthquake occurred at the boundary of the two main geological provinces of Croatia: the Dinarides mountain belt and the Pannonian Basin (Fig. 1;[7,8]). The Dinarides, a wide NW–SE striking fold-and-thrust belt stretching from southwestern Slovenia to Montenegro along the Adriatic coast of Croatia and inland, are the result of the Alpine collision between the Eurasian and Adriatic tectonic plates (e.g.,[9–12]). The most prominent structures of the Dinarides are NW–SE trending folds and thrusts exposed along the SW margin of the Pannonian

[1]School of Science and Technology, Geology Division, University of Camerino, Camerino, Italy. [2]Italian Institute for Environmental Protection and Research - Geological Survey of Italy, Roma, Italy. [3]Water Management Department for Middle and Lower Sava Flood Protection Service, Croatian Waters, Slavonski Brod, Croatia. [4]Civil Protection Department, Presidency of the Council of Ministers, Roma, Italy. [5]Institute of Geosciences and Earth Resources, National Research Council, Firenze, Italy. [6]National Institute of Geophysics and Volcanology, Roma, Italy. ✉email: tiziano.volatili@unicam.it

Abstract

We provide here a first-hand description of the coseismic surface effects caused by the Mw 6.4 Petrinja earthquake that hit central Croatia on 29 December 2020. This was one of the strongest seismic events that occurred in Croatia in the last two centuries. Field surveys in the epicentral area allowed us to observe and map primary coseismic effects, including geometry and kinematics of surface faulting, as well as secondary effects, such as liquefaction, sinkholes and landslides. The resulting dataset consists of homogeneous georeferenced records identifying 222 observation points, each of which contains a minimum of 5 to a maximum of 14 numeric and string fields of relevant information. The earthquake caused surface faulting defining a typical 'conjugate' fault pattern characterized by Y and X shears, tension cracks (T fractures), and compression structures (P shears) within a ca. 10 km wide (across strike), NW-SE striking right-lateral strike-slip shear zone (i.e., the Petrinja Fault Zone, PFZ). We believe that the results of the field survey provide fundamental information to improve the interpretation of seismological, GPS and InSAR data of this earthquake. Moreover, the data related to the surface faulting may impact future studies focused on earthquake processes in active strike-slip settings, integrating the estimates of slip amount and distribution in assessing the hazard associated with capable transcurrent faults.

2.1 INTRODUCTION

On 29 December 2020 at 11:19 (UTC), a moment magnitude (Mw) 6.4 earthquake struck central Croatia near the city of Petrinja, a settlement of about 25,000 inhabitants in the region of Sisak-Moslavina, causing 7 casualties and thousands homeless. The epicentre was 15 km SW of Sisak, the main town of the region, and 45 km SSE of Zagreb (Figs. 2.1-2.2; ISIDe Working Group, 2007; Tomljenović et al., 2008; Grünthal et al., 2012; Stucchi et al., 2013; Geolab Pasaia.org). The mainshock was preceded the day before by two foreshocks at 05:28 and 06:49 (UTC time), with Mw 5.2 and 4.8, respectively.

The seismic sequence came nine months after the Zagreb earthquake, a mainshock of Mw 5.5 that was followed by a largest aftershock of Mw 4.9, both occurred on March 22, between 4 and 7 km north-northwest of Zagreb (CSEM-EMSC, emsc-csem.org) (Figs. 2.1-2.2). In the last two centuries the same area was affected by three moderate earthquakes: on December 18, 1861 (Mw 5.4), on February 11, 1883 (Mw 5.1), and on October 8, 1909 (Mw 5.7) (Stucchi et al., (2013) (Fig. 2.2). The Mw 6.4 Petrinja earthquake occurred at the boundary of the two main geological provinces of Croatia: the Dinarides mountain belt and the Pannonian Basin (Fig. 2.1; Tomljenović and Csontos, 2001; Schmid et al., 2008). The Dinarides, a wide NW-SE striking fold-and-thrust belt stretching from southwestern Slovenia to Montenegro along the Adriatic coast of Croatia and inland, are the result of the Alpine collision between the Eurasian and Adriatic tectonic plates (e.g., Anderson and Jackson, 1987; Battaglia et al., 2004; Stipcevic et al., 2011; Stipcevic et al., 2020). The most prominent structures of the Dinarides are NW-SE trending folds and thrusts exposed along the SW margin of the Pannonian Basin, a wide depression located in the interior of the arcuate Carpathian mountain chain. The latter joins the Alps to the west and the Dinarides to the southwest. The Croatian sector of the Pannonian Basin is limited to the southwest by the Sava sub-basin, a NW-SE oriented tectonic depression showing an asymmetrical shape, with a gentle slope to the SW and a steep NE flank (Ustaszewski et al., 2014). Here, the post-rift sediments are represented by the lower Pannonian (i.e., lower Tortonian) marly limestones, upper Pannonian (i.e., upper Tortonian) and lower Pontian (i.e., lower Messinian) turbidite sandstones as well as upper Pontian and

Pliocene deltaic and alluvial depositional systems (Pavelić et al., 2018; Pavičić et al., 2019). All these sedimentary units have been deformed by strike-slip tectonics and are characterized by positive flower structures that are nowadays still active and seismogenic (Kastelic et al., 2013; Carafa and Kastelic, 2014). This geodynamic framework originated from the cessation of normal faulting in the Pannonian Basin and the ongoing counter clockwise rotation of the Adriatic microplate around a pole located in the Western Alps. This dynamic resulted in inversion tectonics dominated by thrusting and strike-slip faulting along the basin margins (e.g., Bada et al., 1999; Scognamiglio et al., 2006). The Petrinja earthquake reflects this geodynamic setting, as the focal mechanism suggests a roughly N-S, horizontal maximum compression (Fig. 2.2). The fault plane solution includes nearly vertical southeast and southwest striking nodal planes. In the Sava sub-basin, active strike-slip fault systems including both NW-SE and NE-SW oriented faults are reported in the literature (Tomljenović and Csontos, 2001).

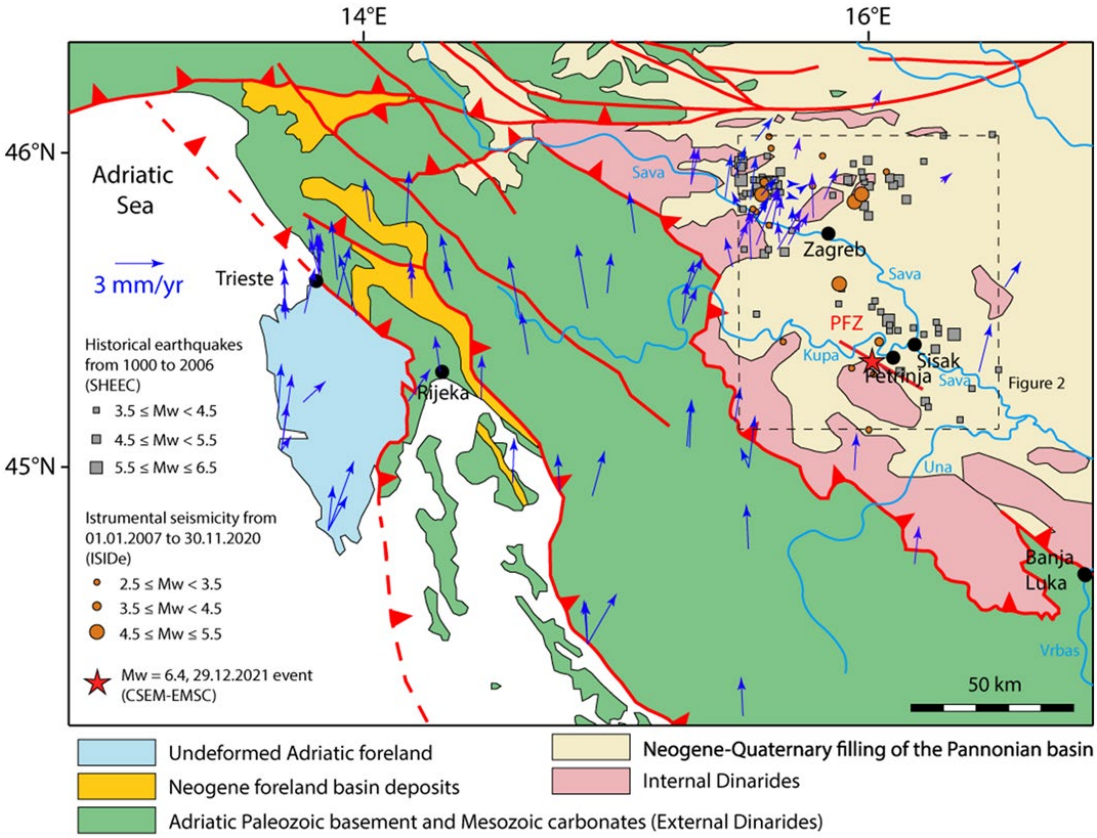

Figure 2.1 Geodynamic setting of the study area within the Dinarides-Pannonian Basin framework (modified after Tomljenović and Csontos, 2001). The location of the main fault belonging to the Petrinja Fault Zone is marked as PFZ. Blue arrows display horizontal vector motion of permanent Global Navigation Satellite System (GNSS) stations in the "European fixed" reference frame (Geolabpasaia.org). Dashed box shows the location of Fig. 2.2 with epicentres of historical earthquakes from 1000 to 2006 (grey squares) selected from Grünthal and Wahlström (2012) and Stucchi et al. (2013) and instrumental seismicity from 01.01.2007 to 30.11.2020 selected from ISIDe Catalogue. The epicentre of the Mw 6.4 event of 29.12.2020 is shown for reference (red star).

Thanks to the flying of the Sentinel 1A radar satellite of ESA (European Space Agency) over the area struck by the earthquake already on December 30 (ascending orbit 146), it was possible to compute an InSAR imaging of the ground deformation caused by the earthquake very soon after the event, allowing to constrain the region where ground effects were mostly to be expected. The scenes utilized for the interferogram formation shown in Fig. 2.2 were acquired on December 18 (slave) and 30 (master). The processing was carried out with the SNAP toolbox of ESA and the SNAPHU software for phase unwrapping. The observed deformation field in the line of sight (LOS) direction shows on the NW side a maximum shortening of the distance from the satellite of ca. 36 cm, and a lengthening of the same distance reaching a

maximum of ca. 33 cm centred in the area of Petrinja (east of the ruptured fault). The deformation pattern imaged by the InSAR, considered the ENE-oriented direction of recording, is interpretable as a right-lateral, north-westward slip of the region west of the Petrinja Fault Zone. The fringe geometry has served here basically to direct our field observations toward the areas of highest linear deformation, where tectonic ground ruptures were most likely to be present, and subsequently to compare the InSAR-imaged deformed region with the distribution and size of geological coseismic effects observed in the field.

As observations of coseismic surface effects are of considerable scientific importance, it is necessary to carry out the surveys as soon as possible. As a matter of fact, surface effects may be erased by degradation of fault scarps or by road/infrastructure repair, as well as overprinted by postseismic afterslip (Civico et al., 2018; Stemberk et al., 2019; Corradetti et al., 2020). The engineers of Croatian Water Management Department started the survey of surface effects immediately after the main shock, while a working group represented by eight researchers of different Italian institutions (University of Camerino, ISPRA, CNR, DPC) began surveying the ground coseismic effects on 10 January 2021, working 8 hours a day per person for the following 8 days. In this report (Map and Dataset) we present earthquake surface ruptures along a ca. 10 km wide (across strike), right-lateral strike-slip shear zone that we term Petrinja Fault Zone (PFZ). Mapping was carried out using both field observations and aerial surveys using a drone and relative photogrammetry elaborations. By integrating our observations with available seismological and geodetic data, we also provide an interpretation and a discussion of the fault ruptures associated with the Mw 6.4 mainshock.

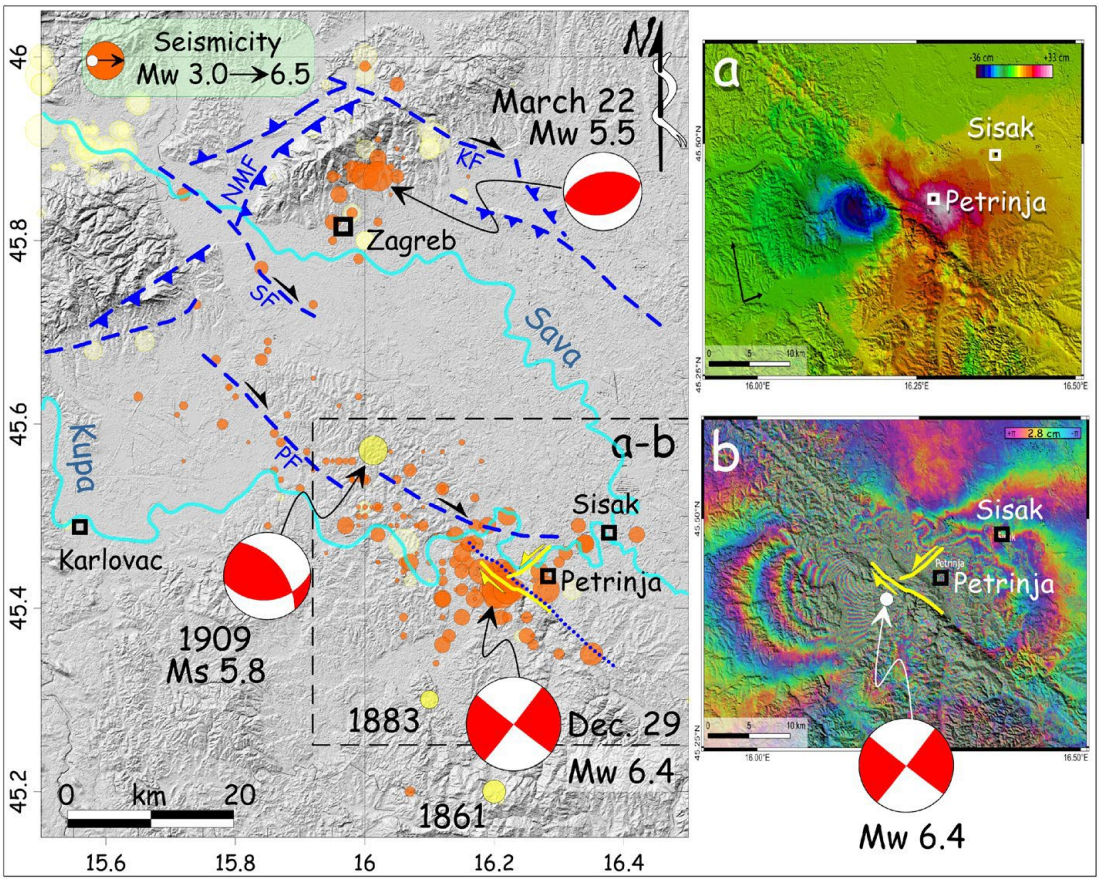

Figure 2.8 Shaded relief map (from ASTER GDEM data) of the area affected by the 2020 seismic sequence (orange epicenters, EMSC data; www.emsc-csem.org). Yellow epicenters, historical seismicity (Grünthal and Wahlström, 2012). Blue dashed lines, main Quaternary active faults (mod. from Tomljenović et al., 2008); NMF, north Medvednica; SF, Sava; KF, Kasina. PF, Pokuplje fault (Herak and Herak, 2010). Blue dotted line, buried fault in the 1: 100,000 scale Official Geological Map of Croatia (Pikija, 1987). Yellow lines, coseismic surface faulting related to the 29 December 2020 Petrinja earthquake. The focal mechanism of the Kupa Valley earthquake in 1909 is from (Herak and Herak, 2010). Those of 2020 are from (Scognamiglio et al., 2006). Panel A is an interferometric imagery (Sentinel-1A Ascending orbit, 20201224-20201230) showing surface motion associated with the 29 December 2020 Mw 6.4 earthquake. Below: Each fringe represents a shift of approximately 2.8 cm along the satellite's line of sight (LOS), which is oriented from WSW to ENE; above: actual displacement in cm along the LOS, in blue are the areas with a component of motion toward the satellite (WSW-ward) and in red areas that have moved away. This implies a right-lateral slip in the order of several tens of cm.

2.2 METHODS AND DATA RECORDS

The description of surface coseismic effects is very important in earthquake geology, as it provides a unique opportunity to observe short-term time scale deformation. These observations allow a much more robust interpretation of the long-term time

scale geological features for seismic and surface faulting hazard evaluation purposes. Data collected in our survey may contribute to update and integrate the worldwide database aimed at assessing fault displacement hazard (Villani et al., 2018). Furthermore, the geometry, kinematics, and amount of displacement of fault ruptures propagated from depth during an earthquake constrain the modelling of seismic sources based on inversion of geophysical datasets (e.g., strong motion recordings, GPS time-series and InSAR images).

An Unmanned Aerial Vehicle (UAV) was used as a complementary tool of the traditional field work. We performed aerial Structure from Motion (SfM) photogrammetry, collecting large numbers of overlapping photos to construct 3D, digital, virtual outcrop models (VOMs; (Tavani et al., 2014; Pitts et al., 2020; Jablonska et al., 2021) using Agisoft Metashape software, following the workflow outlined by (Pitts et al., 2017). Digital geologic interpretations and structural data extraction were made using the Virtual Reality Geologic Studio software (VRGS).

Our surveying, which has led to the recognition and mapping in the epicentral area of the most significant surface ruptures, their geometry, kinematics, and associated displacement, is summarized in a concise dataset (Tab. 1) and map (Fig. 2.3).

The dataset presented in the Supplementary Material is a text file consisting of 222 records organized into 14 fields. Each record describes a single observation point. The fields have a name and a short name, and are described as follows:

1. NUMBER (short name: No);

2. DATE (short name: Date);

3. LATITUDE (short name: Lat);

4. LONGITUDE (short name: Long);

5. OBSERVATION (short name: Obs): five categories are defined: “Coseismic shear fracture” (ground break displaying a perceivable shear offset of the ground surface, i.e. >1 cm); “Coseismic open fracture” (ground break with no perceivable shear offset, i.e. << 1 cm); “Coseismic sliding” (generic landslide of ascertained coseismic origin);

“Coseismic sand boil” (sand volcanism phenomena related to liquefaction induced by the earthquake); “Sinkhole” (ground collapse caused by the earthquake);

6. TYPE OF SUBSTRATUM (short name: Sub): nature of the substratum where the coseismic effect was observed;

7. STRIKE (short name: Strike);

8. DIP DIRECTION (short name: Dip dir);

9. DIP ANGLE (short name: Dip);

10. LENGTH (short name: Len): length measured in meters of a rupture or sliding surface;

11. OPENING (short name: Ope): aperture of a rupture or sliding surface measured in centimetres, orthogonal to the fracture walls;

12. OFFSET (short name: Off): net displacement of a coseismic rupture measured in centimetres;

13. RAKE (short name: Rak): the angle of the slip lineation on the fault plane measured in degrees (in the 0°-180° range);

14. VECTOR (short name: Vec): the trend (range 0°-360°) and plunge (range 0°-90°) of the slip lineation in degrees, measured with respect to the North and the horizontal, respectively.

No	Date	Lat	Long	Obs	Sub	Strike [deg]	Dip dir [deg]	Dip [deg]	Len [m]	Ope [cm]	Off [cm]	Rak [deg]	Vec [deg]
1	14/01/21	45.4241	16.2226	coseismic shear fracture	soil	296	26	85	60	5	36	10	297/10
2	14/01/21	45.4241	16.2225	coseismic shear fracture	soil	290	36	85	8	4	36		
3	11/01/21	45.424	16.2226	coseismic shear fracture	road	162	252	89	15	8	10		
4	11/01/21	45.4241	16.2231	coseismic open fracture	road	323			15				
5	11/01/21	45.4241	16.223	coseismic open fracture	road	346			15				

Tab. 2.1 Examples of records extracted from the dataset.

2.3 SURFACE RUPTURE DESCRIPTION

The major, long-term, morphotectonic feature in the epicentral area of the Petrinja earthquake is the elongated NW-SE trending ridge that develops between the Kupa river, to the north, and the village of Blinja, to the south, for a length of about 30 km (Fig. 2.4). This ridge culminates at about mid-length with the Cepelis Peak (415 m a.s.l.) and is affected by rivers deeply carved into the southern, uplifted block. Streams flowing across the ridge reaching their outwash at the foot of its NW flank appear to be locally diverted, changing their direction from orthogonal to parallel to the western slope or even dammed by fault activity.

The 29 December mainshock, whose epicentre was close to the town of Petrinja (Fig. 2.2), produced surface coseismic effects mostly distributed in the area between Petrinja and Sisak (Fig. 2.3). The coseismic effects consisted of primary surface ruptures, that are those directly related to the slip along the earthquake fault, and other coseismic effects induced by ground shaking. The latter have left an overall modest signature in the landscape, both permanent (e.g., landslides, sinkholes) and ephemeral (sand boil associated with liquefaction phenomena). Notably, we also observed several coseismic effects aligned along a NE-SW oriented fault that is marked as buried in the geological map at scale 1:100,000 (Pikija, 1987).

2.4 PRIMARY EFFECTS

The pattern of primary surface ruptures depicts a fault system including two sets of coseismic shear fractures (Fig. 2.2). The NW-SE-trending shear fractures are characterized by right-lateral strike-slip offset reaching a maximum value of 36 cm (Fig. 2.3b). On the other hand, the NE-SW-trending shear fractures are characterized by left-lateral strike-slip offsets of up to 10 cm (Fig 3c).

Southwest to Petrinja, an almost continuous NW-SE pattern of primary coseismic surface ruptures was observed for an end-to-end extent of about 15 km along a pre-existing fault zone, here named the Župić Fault (Fig. 2.3a, b). Along this trend, in the vicinity of the village of Župić, we mapped more than 2 km of almost continuous coseismic surface rupture, characterised by >20 cm mean right-lateral horizontal offset. The local largest offset, up to 36 cm, was observed along the national road 37. Here the coseismic reactivation of the fault produced a right-lateral offset of the roadside scarp surface along a 120°N striking, steeply NE dipping fault plane (observation point No. 1 in Fig. 2.3a; Fig. 2.5a, b). The rupture could be followed across the road, where it attained an approximate N-S strike (i.e., roughly perpendicular to the road direction, which most probably controlled the rupture propagation in the asphalt); we observed a right-lateral offset of 10 cm, accompanied by an opening of 8 cm. The rupture joined a fault plane in a quarry located ca. 180 m to the SE, which was reactivated as well (observation point No. 22 in Fig. 2.3; Fig. 2.5c), where poorly lithified Pliocene shallow marine calcareous deposits outcrop, showing a right-lateral offset of ∼15 cm along a 134°N striking, sub-vertical fault plane (Fig 2.6a, b). Shear fractures associated with this fault were observed also to the NW (observation points No. 109-118 in Fig. 2.3) and SE of it (observation points No. 31-43 and 44-74 in Fig. 2.3), characterized by a right-lateral offset in the range of 2 to 4 cm and accompanied by several open fractures having approximately the same orientation. At these observation points, as well as at the observation points No. 81-86 (Fig. 2.3), the lack of markers on the road made it difficult or impossible to measure any strike-slip offset. In some cases, it was possible to measure the shear offset by observing the geometry of the fracture and the relative extensional and compressional jogs (see the supplementary photo archive included in the database for the extensive

documentation on the observed shear and open fractures). Other minor shear fractures with a right-lateral offset of 1 to 2 cm were seen across a road immediately to the NE of the Župić Fault (observation points 87-94 and 95-108). Moreover, 10 km NE of the Župić fault (observation points No. 173-176), a ~300 m long right-lateral shear zone was identified in the alluvial plain of the Kupa river. This shear zone was characterized by en echelon open fractures with intervening mole tracks (see Fig. 2.8 and photos included in the database).

Between Petrinja and Sisak, along the alluvial plain of the Kupa river, a NE-SW pattern of primary surface ruptures was also mapped for an end-to-end extent of about 8 km. This feature is here named Kupa Fault (Fig. 2.5d, e). It is important to note that these coseismic effects are aligned along a NE-SW striking fault which is marked as buried in the 1: 100,000 scale Official Geological Map of Croatia (Pikija, 1987).

The main coseismic surface ruptures along the Kupa Fault consisted of shear fractures displaying >5 cm left-lateral horizontal offset, observed along the national road 37 (Fig. 2.5d, e; observation points No. 128-138), as well as shear fractures and en echelon open fractures displaying >10 cm left-lateral horizontal offset detected along the alluvial plain of the Kupa river (Figs. 2.5d and 2.7a, b; observation points No. 139-159). Here, fractures were generally associated with sand boils produced by liquefaction phenomena, which damaged the banks and the dam along the Kupa river (Fig. 2.7e, f). In this area, the assessment of the amount of the left-lateral offset associated with the NE-SW oriented shear fractures was permitted by the presence of both cut roots and trees located across these fractures (Fig. 2.5d).

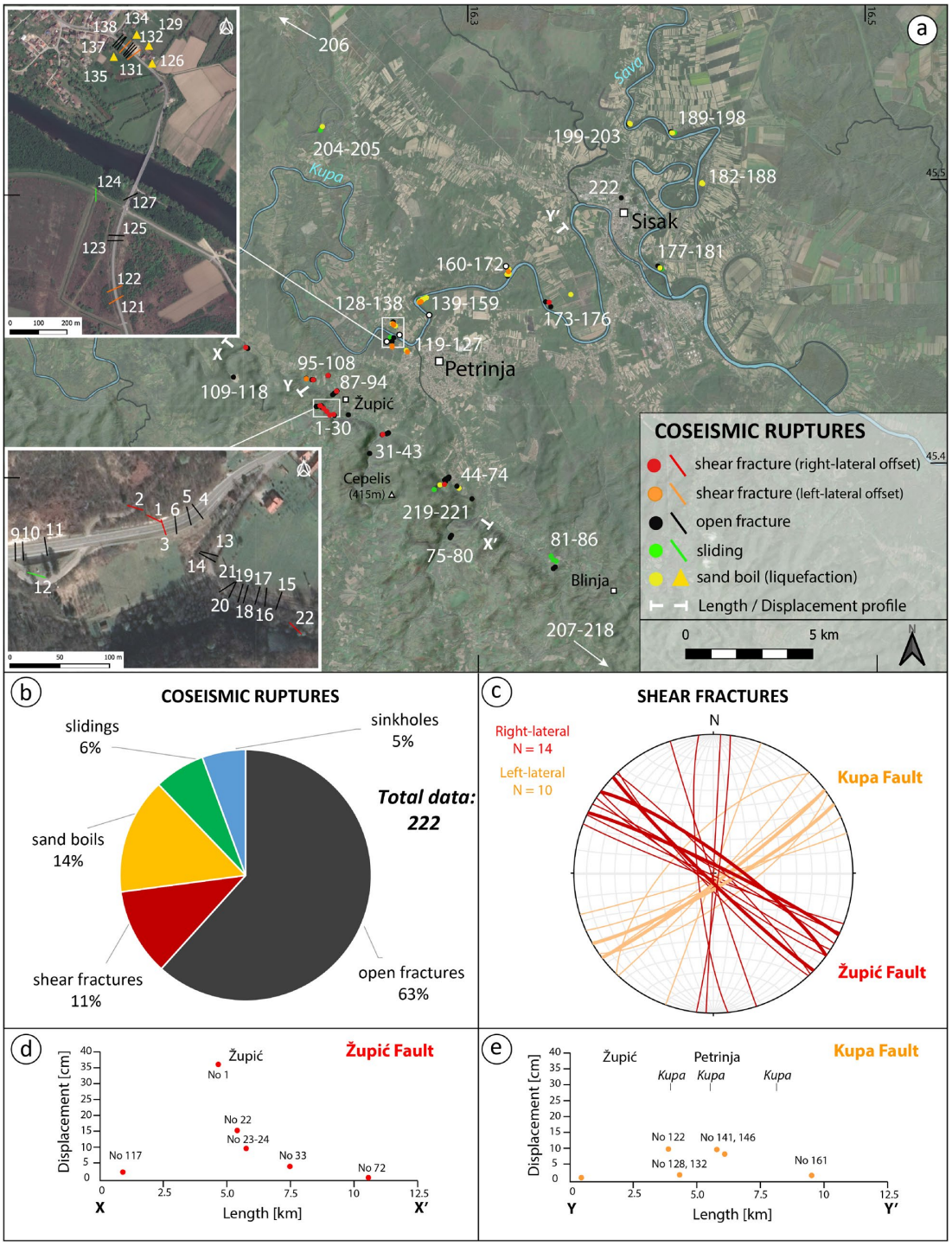

Figure 2.9. (a) Map of the surface ruptures measured in the epicentral area of the Petrinja earthquake. The numbers refer to the "No" of records present in the database. Below are displacement/length profiles for the Župić (b) and Kupa (c) Faults, as well as pie diagrams showing the relative proportion of the main types of measured coseismic ruptures (d) and coseismic fractures (e).

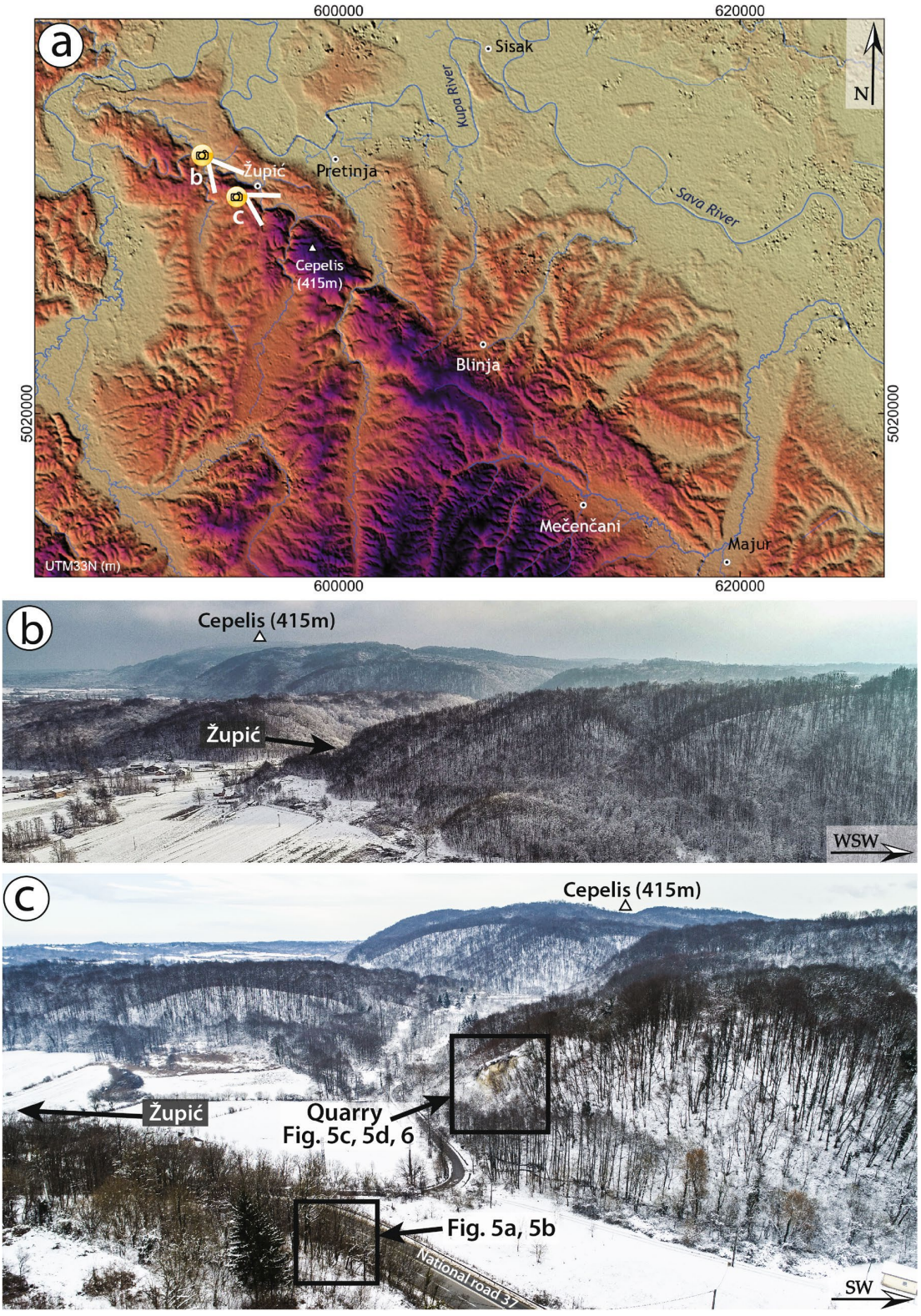

Figure 2.10 (a) Digital Elevation Model (EU-DEM v1.1, 25 m resolution) of the epicentral area of the 29 December 2020 Petrinja earthquake. The direction of the panoramic views of (b) and (c) are also indicated; (b) Panoramic view of the Župić area showing a portion of the ridge NW of Župić and the south-eastern ridge in the background (photo acquisition date 12/01/2021); (c) Panoramic view of the Župić south-eastern ridge area showing the locations of Fig. 2.5 and 2.6 (photo acquisition date 14/01/2021).

2.5 SECONDARY EFFECTS

Coseismic surface effects related to ground shaking, permanent or ephemeral (e.g., landslides, sinkholes and sand boils), were identified in the epicentral area between Petrinja and Sisak (Fig. 2.3). In particular, sand liquefaction was widespread along the NE-SW oriented fault zone inside the alluvial plain of the Kupa River (Fig. 2.7a, d). These phenomena were often clearly associated with surface ruptures represented by shear fractures and en echelon open fractures. Immediately NW of Petrinja, both surface rupture and liquefaction phenomena (i.e., sand boil) had seriously damaged the banks and the dam along the Kupa river (Fig. 2.7e, f), making it necessary to build an outermost embankment to contain the potential floods.

Landslides mainly matched pre-existing gravitational movements and induced large fractures in the roads. Rockfall and debris fall occurred in quarry crowns and in correspondence of steep scarps (Fig. 2.7b). The largest one occurred in a quarry close to the Hrastovica village, with a total volume exceeding 70 cubic meters, and single rock blocks up to 2-4 cubic meters. Small landslides were mapped by (Tomljenović, 2021) on the slope next to the parish church in the village of Viduševac and along the road Kravarsko - D. Hruševac. Minor landsliding was also present along the river embankments as a result of seismic shaking and consequent liquefaction (Fig. 2.7f). The seismic vibration also induced the compaction of the artificial fillings and embankments, causing the formation of differential settlements and fractures (Fig. 2.7e).

The very moderate evidence and the limited occurrence of gravitative movements triggered by the earthquake can be related to the low energy of the relief, as the epicentral zone is mainly located in the plain of the Kupa river; furthermore, the mountains south-east of Petrinja are characterized by a smooth morphology, without evident strong changes in slope, except for the escarpment running about NW-SE in the Župić area (Fig. 2.3).

Collapses and opening of small sinkholes in the ground have been described by the inhabitants in the urban area of Petrinja, but we were unable to document this effect as

the holes had been filled with debris soon after their formation. A man (Edison Tomas) now living in Župić told us that some holes had already opened 4-5 hours before the main shock in the road close to the house of his daughter in Petrinja with a depth reaching 6 meters.

In the Mečenčani area (see Fig. 2.4), about 20 km southeast of Petrinja, the most impressive effect was represented by the opening of about 30 sinkholes (observation points No 207-218 in Fig. 2.3; Fig. 2.4). The sinkholes had different dimensions, from one to tens of meters in diameter (Fig. 2.3; Fig. 2.7c) and were several meters deep. All the sinkholes appeared filled by water up to a depth of about 3 meters from the surface, which is the level of the water table in the alluvial deposits. According to the narration of the locals, the collapses occurred after the earthquake, with a delay from a few hours to a few days.

The observation of aerial and satellite images clearly shows that in many cases the areas prone to the sinkhole collapses were already recognizable before the event. Following this approach, many potential sinkholes could be additionally identified by an aerial (drone) survey of the plain in order to identify the sectors of higher hazard. In any case, this preliminary analysis needs to be complemented with geophysical prospecting to complete the mapping of the zones most prone to such highly hazardous phenomenon.

Finally, two likely cases of hydrological anomaly were spotted in the area close to the village of Hrastovica, SE of Petrinja, where a copious flow of water with sand sprung up from the garage of a house and a nearby geyser-similar water fountain with a height of 50-70 cm produced a strong increase of the flow rate of the drainage ditch (observation points No. 219-221 in Fig. 2.3). Similar geyser-like effects occurred at Brest Popupsky springing from a water well (observation point No. 126 in Fig. 2.3).

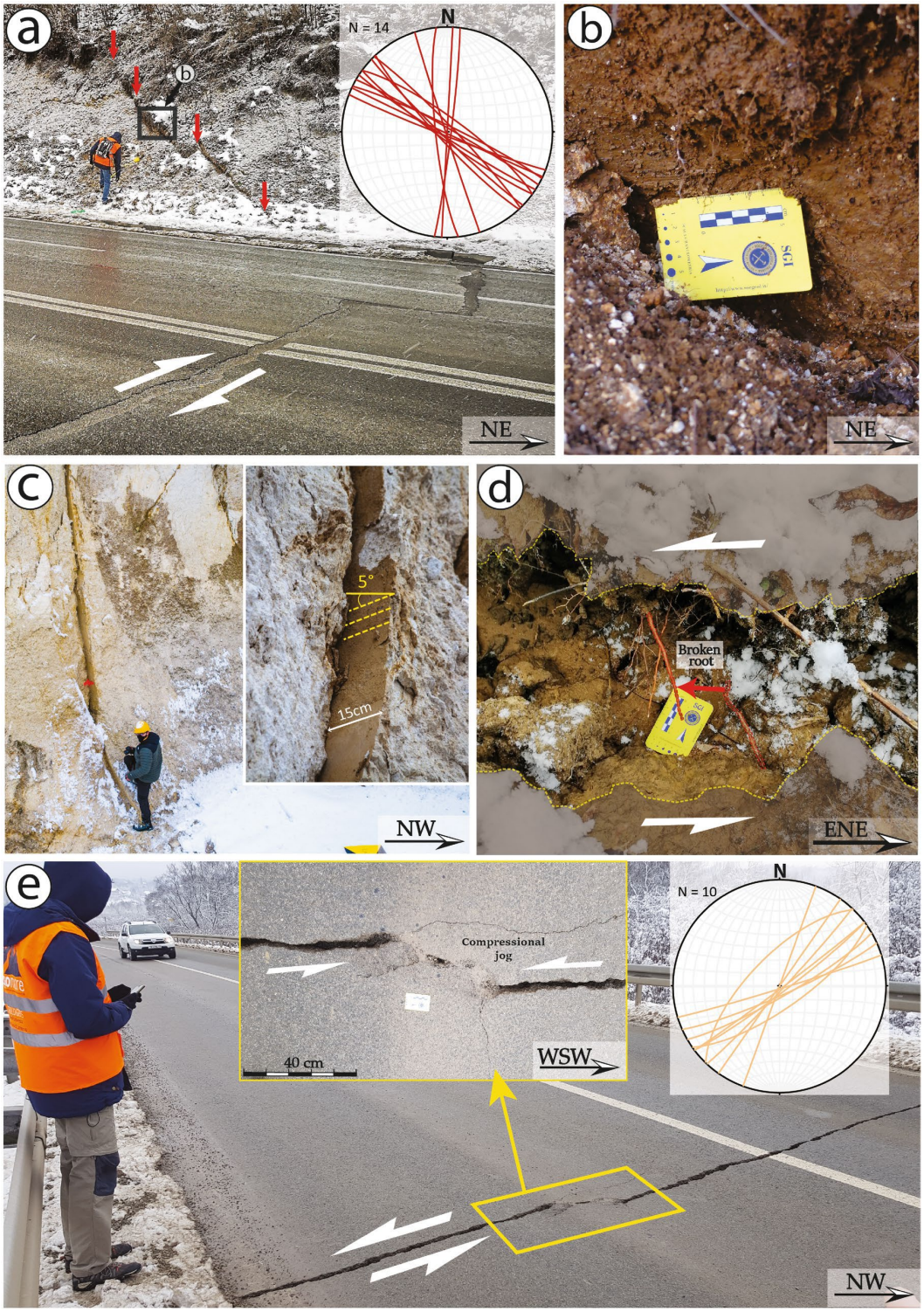

Figure 2.11 Examples of NW-SE to N-S oriented right-lateral strike-slip surface faulting (a-c) and NE-SW to E-W oriented left-lateral strike-slip surface faulting (d-e): (a) coseismic rupture with right-lateral offset near the village of Župić (No 1, 14/01/2021) and lower-hemisphere, equal-area projection of the overall coseismic ruptures with right-lateral offset; (b) close-up of slickenlines on the fault plane (13/01/2021); (c) evidence of right-lateral surface faulting on bedrock (No 22, 11/01/2021), the inset is a close-up of the fault plane showing 15 cm horizontal offset with slickenlines (rake=5°); (d) Broken and displaced root (No 149, 13/01/2021) showing 8 cm left-lateral offset; (e) coseismic rupture in paved road

near the village of Brest Pokupski (No 121, 12/01/2021) showing 5 cm left-lateral offset and lower-hemisphere, equal-area projection of the overall coseismic ruptures with left-lateral offset. The inset shows a close-up of compressional jog. The numbers (No 1) refer to the observation points (indicated in Fig. 2.3) of the records in the database, while the dates refer to the photo acquisition.

2.6 DISCUSSION

The recognition of coseismic effects in the aftermath of an earthquake is fundamental for individuating primary surface faulting and its structural arrangement. Understanding the relationship between the seismic source at depth and its primary evidence at surface creates the basis for using surface active faults to contribute foreseeing which structure will rupture next. This work also provides new data on surface coseismic faulting in strike-slip domains, which is not a common event in the Alpine-central Mediterranean area.

Coseismic surface faulting of the 2019 earthquake is represented by both aligned and en echelon fault segments, defining the main Župić and Kupa Faults, which display a typical shear zone structural pattern near the town of Petrinja (here named the Petrinja Fault Zone or PFZ). Geometrically, an idealized shear zone consists of six principal elements: R and R' conjugate shears, T tension fractures, P shears, and X and Y shears, which are all oriented at well-defined angles to the general trend of the shear zone, called the Principal Displacement Zone or PDZ (Fig. 2.8b). R and R' shears form a conjugate Riedel shear set (Tchalenko, 1970). Y and X shears, showing opposite senses of movement, define a 'conjugate' set characterised by different angular relationships (i.e., the maximum compression axis is parallel to the bisector of the obtuse angle – rather than the acute angle – between Y and X shears; for this reason, we use the inverted commas for this 'conjugate' set, to distinguish it from typical conjugate faults such as R and R' shears). Previous studies have shown that R and R' shears, T tension fractures and P shears (mole tracks) may form simultaneously along pre-existing strike-slip faults during large-magnitude earthquakes (e.g., Angelier et al., 2004; Tondi et al., 2005; Lin and Chiba, 2017). On the other hand, X shears forming as 'conjugate' faults to the Y faults within coseismic surface rupture zones are not well known to date. The coseismic development of X shears has only recently been reported

as part of the surface ruptures produced by the 2014 Yutian Mw 6.9 (Tibetan) earthquake (Li et al., 2016); however, their kinematic nature and formation mechanisms remain unclear. Therefore, the coseismic 'conjugate' fault system described in this study represents a rare case demonstrating the simultaneous activation of X and Y shear faults during an earthquake. Coseismic surface deformation associated with the Petrinja earthquake also includes en echelon tension cracks (T fractures) and mole tracks (or P shears) associated with strike-slip faulting (Fig. 2.8a and b). Changes in the orientation of the various structures are a function of the magnitude and localization of the shear strain, reflecting the different stages in the evolution of the strike-slip shear zone (e.g., Ahlgren, 2001; Katz et al., 2004; Aktar et al., 2007; Tondi et al., 2020).

The InSAR imaging of the deformation field (Fig. 2.1) is in good agreement with the field observations, both in terms of concentration of effects – which are most evident where the InSAR shows the highest displacement – and in terms of type of displacement expected for a dominantly dextral-slip event. The InSAR imaging of the deformation was particularly helpful to locate the fault and assess its sense of displacement. On the other hand, the related offsets could not be accurately quantified by this elaboration. The deformation pattern of Figure 2.2A points to a total strike-slip dextral displacement of about 70 cm for the two blocks across the Župić Fault. However, the InSAR-derived displacement evaluated directly on the fault trace is of about 30 cm. This discrepancy is a commonly observed feature (Livio et al., 2016), testifying for a near surface distributed deformation that often accommodates a substantial part of the actual fault slip. Our field measurements of right-lateral offset along the Župić Fault, reaching a maximum value of 36 cm (Fig. 2.3b), are therefore fully consistent with the InSAR data. Moreover, the InSAR-derived deformation pattern clearly defines two domains characterised by a different behaviour within the SE-slipping, northeastern block of the Župić Fault. These two domains are separated by the map trace of the Kupa Fault, this being consistent with its left-lateral coseismic motion (Fig. 2.3c). Since in general the north-south component of the displacement is not resolved by InSAR due to the orientation of the satellite orbits, left-lateral slip along the Kupa Fault is mainly marked by horizontal components of motion in the E-W direction. Such a motion results in an east-ward displacement of the block east of

the fault, and a west-ward motion of the block west of it. While the former adds to the general east-ward movement of the northeastern block of the Župić Fault, the latter subtracts to it, thus consistently explaining the observed displacement field.

Consistently with the focal mechanisms of the December 29 mainshock, and also of the March 22, 2020, and of the 1909 event, our field investigations and the analytic results of coseismic 'conjugate' shear structures reveal that the direction of the principal compressive stress is horizontal and roughly N-S trending in the study area. Coseismic surface ruptures occurred along the PFZ, which represents the Principal Displacement Zone or PDZ in Fig. 2.8b. Accordingly, we suggest that coseismic 'conjugate' faulting during the 2020 Petrinja earthquake was mainly controlled by the pre-existing, active strike-slip PFZ within the framework of the present tectonic stress associated with the ongoing motion of Adria with respect to the Eurasian Plate. Roughly N-S convergence across the plate boundary, marked by the NW striking Dinaride chain, is recorded by horizontal vector motion of permanent GNSS stations (Fig. 2.1). This motion resulted in partitioning of the deformation into dominant thrusting in the Adriatic frontal part of the Dinarides (Macchiavelli et al., 2012) and belt-parallel dextral strike-slip faulting in its interior (including the area of the present study), as it is typical in regions of oblique plate convergence (Authemayou et al., 2006).

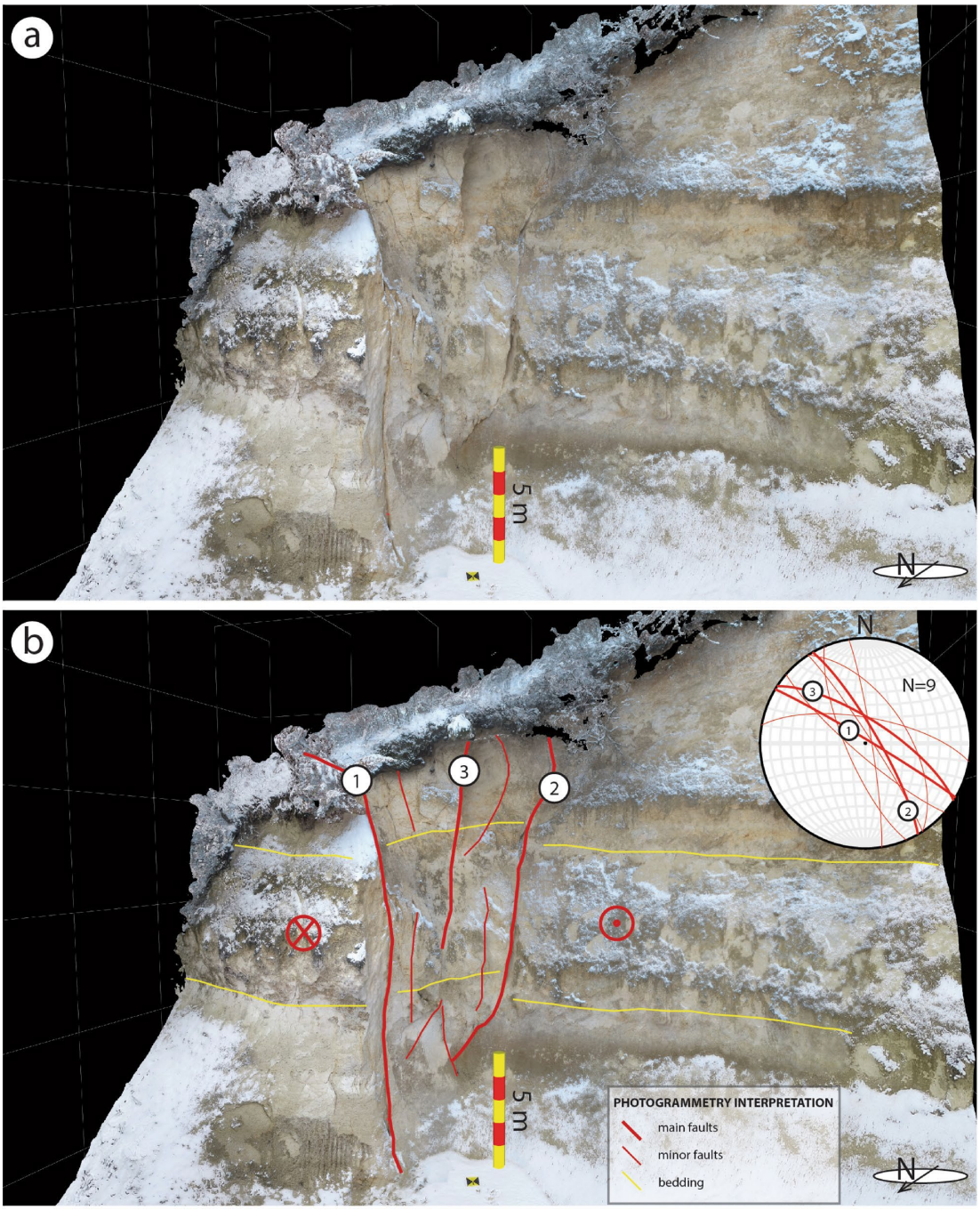

Figure 2.12 (a) Virtual outcrop model of the Župić Fault exposed in a quarry in poorly-lithified Pliocene shallow marine calcareous deposits (see also Fig. 2.5c). (b) Geologic interpretation and structural data extracted from the VRGS software, depicts a positive flower structure composed of three main fault planes.

2.7 CONCLUSIONS

Following the 29 December 2020, Mw 6.4 Petrinja earthquake, a complex surface faulting pattern was observed and mapped in the field along the causative PFZ. Based on our study of the co-seismic shear structures, we can draw the following conclusions:

1. The co-seismic shear structures were produced by this earthquake along the pre-existing right-lateral strike-slip PFZ, and they are mainly characterized by Y and X shears, tension cracks (T fractures), and mole tracks (P shears).

2. The 'conjugate' fault structures comprise two sets of coseismic shears that are striking NW-SE and NE-SW. The NW-SE-trending structure represents a Y shear with right-lateral strike-slip displacement of up to 40 cm, including left-stepping en echelon tension cracks (T) and mole tracks (P). On the other hand, the NE-SW-trending structure represents a X shear with left-lateral displacement of up to 20 cm, including right-stepping en echelon cracks (T) and mole tracks (P), which are concentrated in a zone of < 5 m around individual rupture zones.

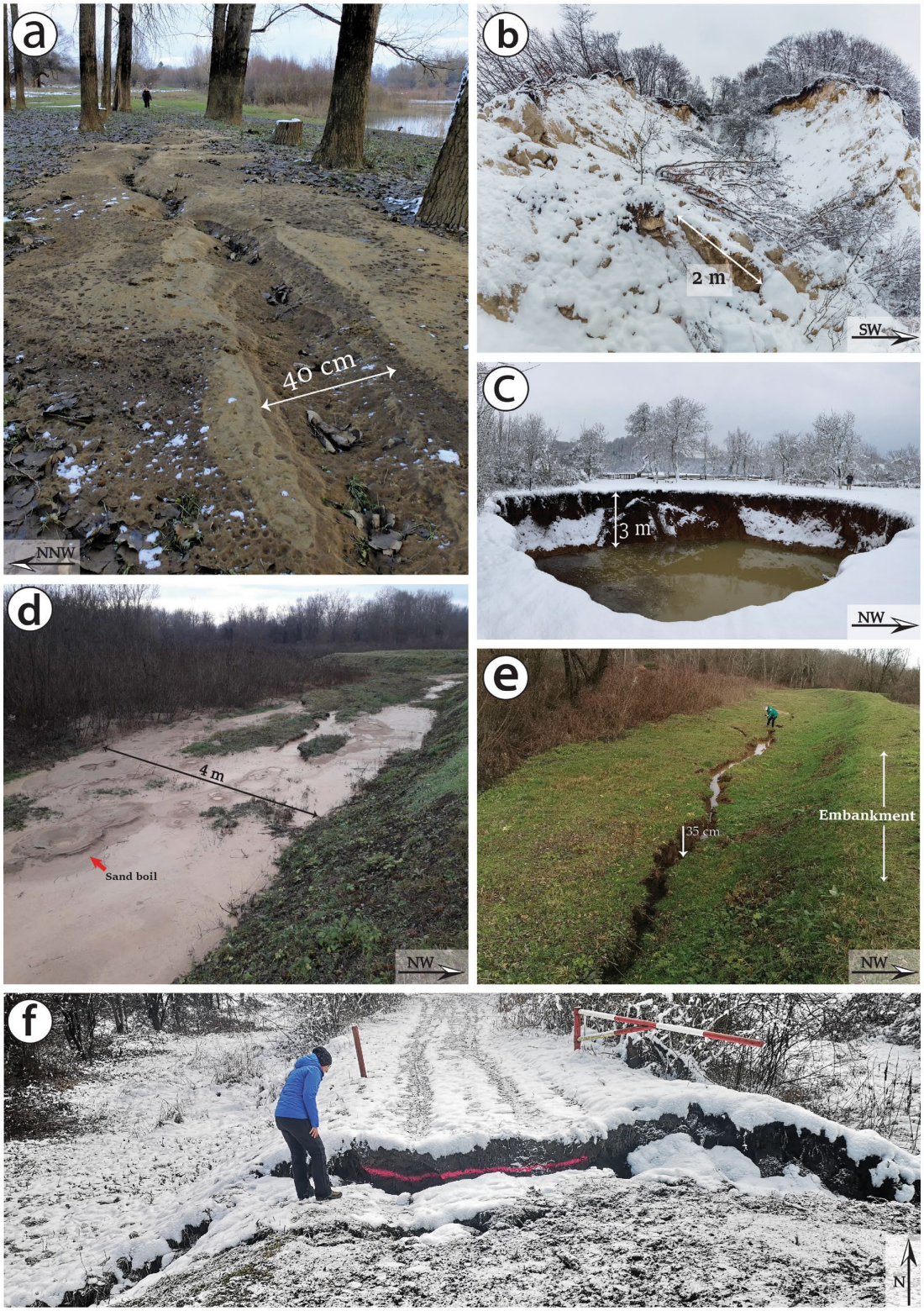

Figure 2.13 Examples of sliding, rockfall, fracture, sinkhole, and sand volcanism in the epicentral area of the Petrinja earthquake. (a) (15/01/2021) and (d) (5/01/2021) Examples of sand boil associated with liquefaction phenomena occurred in the valley of the Kupa river (No 165, 166, 205). (b) The earthquake triggered some rockfalls along the crown of the quarry close to the village of Hrastovica (No 64, 12/01/2021). (c) The largest sinkhole opened in the Mečenčani area with a diameter of about 20 meters (No 212, 14/01/2021). (e) Large fracture

connected to the sinking of the river dam induced by liquefaction below (No 204, 5/01/2021). (f) Failure of river embankment induced by liquefaction (No 189, 14/01/2021). The numbers (No 1) refer to the observation points of the records in the dataset indicated in Fig. 2.3 and the dates refer to the photo acquisition.

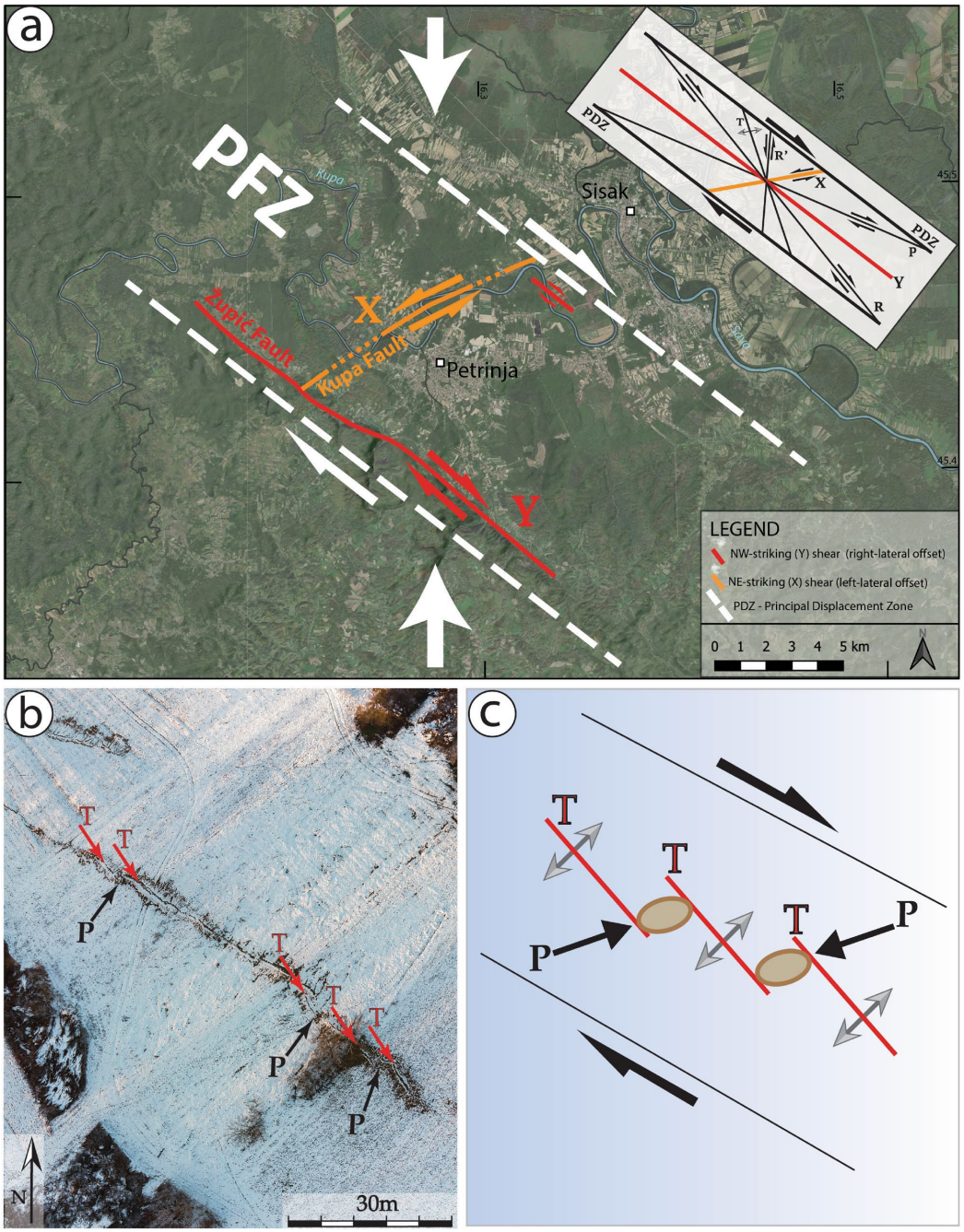

Figure 2.14. Diagrams showing the main active faults activated during the 29 December 2020 Petrinja earthquake. (a) The Petrinja Fault Zone (PFZ) is a ca. 10 km wide right-lateral strike-slip shear zone composed by "conjugate" faults in which the Župić and the Kupa Faults represent (Y) and (X) shears, respectively. The inset shows the structural features of an idealized shear zone. (b) Tension cracks (T) and mole tracks (P) are developed coseismically within the NW-striking (Y) and NE-striking (X) shears (observation points No 173-176 in Fig.

2.3, photo acquisition date 13/01/2021). The NS oriented arrows indicate the horizontal maximum compression based on geological data, geophysical observations (Bada et al., 1999) and the field data obtained in this study. (c) Simplified sketch of Fig. 2.8b.

Our findings suggest that the coseismic 'conjugate' Y and X faulting is mainly controlled by the pre-existing, active PFZ within the framework of the ongoing northward 'push' of the Adria Plate along the margins of the Pannonian Basin. The regional geodynamic setting of partitioned transpression results in active thrusting in the outer Dinarides and dominant strike-slip faulting in the interior of the belt, as it occurs in the epicentral area of the 29 December 2020, Mw 6.4, Petrinja earthquake.

The mapped pattern of coseismic fault ruptures is relevant for improving the assessment of the seismic and surface faulting hazard of this region, beside the danger related to landslides, liquefaction and sinkholes. More in general, the prompt, accurate mapping of the coseismic ruptures associated with this moderate magnitude earthquake contributes to improve our understanding of earthquake faulting processes and to better forecast the impact of the more energetic earthquakes expected in the Alpine-Dinarides-Albanides orogen, where the knowledge regarding such phenomena is still modest.

Acknowledgements

Thoughtful and constructive comments by two Anonymous Reviewers, as well as by Editorial Board Member Yuji Yagi, are gratefully acknowledged. We would like to thank the Italian Embassy in Zagreb for the kind support to the mission in the field. This work was partly supported by the FAR Unicam project “Novel Approach for Seismic Hazard Analysis - NoHard", responsible Emanuele Tondi.

Data Availability

All data generated or analysed during this study are included in this published article (and its Supplementary Information files).

Funding

Funding was provided by University of Camerino, Italy (No. STI000104) and Institute of Geosciences and Earth Resources, National Research Council, Firenze, Italy.

References

Ahlgren, S.G. The nucleation and evolution of Riedel shear-zones as deformation bands in porous sandstone. *Journal of Structural Geology*, **23(8)**, 1203-1214, DOI: 10.1016/S0191-8141(00)00183-8 (2001).

Aktar, M., Karabulut, H., Ozalaybey, S., Childs, D. A conjugate strike-slip faults within the extensional tectonics of Western Turkey. *Geophysical Journal International*, **171(3)**, 1363-1375, DOI: 10.1111/j.1365-246X.2007.03598.x (2007).

Anderson, H. & Jackson, J. Active tectonics of the Adriatic Region. *Geophysical Journal International*, **91**, 3, 937–983. https://doi.org/10.1111/j.1365-246X.1987.tb01675.x (1987).

Angelier, J., Bergerat, F., Bellou, M., Homberg, C. Co-seismic strike-slip fault displacement determined from push-up structures: the Selsund Fault case, South Iceland. *Journal of Structural Geology*; **26(4)**, 709-724, DOI: 10.1016/j.jsg.2003.07.006 (2004).

Authemayou, C. *et al*. Late Cenozoic partitioning of oblique plate convergence in the Zagros fold-and-thrust belt (Iran). *Tectonics*, **25**, TC3002. https://doi.org/10.1029/2005TC001860fin (2006).

Bada, G., Horváth, F., Gerner, P., Fejes, I. Review of the present-day geodynamics of the Pannonian basin: progress and problems. *Journal of Geodynamics*, **27**, 4-5, 501-527. https://doi.org/10.1016/S0264-3707(98)00013-1 (1999).

Battaglia, M., Murray, M.H., Serpelloni, E., Bürgmann, R. The Adriatic region: An independent microplate within the Africa-Eurasia collision zone. *Geophysical Research Letters*, **31**, 1-4, doi: 10.1029/2004GL019723 (2004).

Carafa, M.M.C. & Kastelic, V. Earthquake rates inferred from active faults and geodynamics: the case of the External Dinarides. *Bollettino di Geofisica Teorica ed Applicata*, **55-1**, 69-83. DOI:10.4430/bgta0112 (2014).

Civico, R.& the Open EMERGEO Working Group. Surface ruptures following the 30 October 2016 Mw 6.5 Norcia earthquake, central Italy. *Journal of Maps*, **14**, 151-160, DOI: 10.1080/17445647.2018.1441756 (2018).

Corradetti, A., Zambrano, M., Tavani, S., Tondi, E., Seers, D.T. The impact of weathering upon the roughness characteristics of a splay of the active fault system responsible for the massive 2016 seismic sequence of the Central Apennines, Italy. *GSA Bulletin*, https://doi.org/10.1130/B35661.1 (2020.)

CSEM-EMSC. emsc-csem.org last access on: 29.01.2021.

Geolab Pasaia. geolabpasaia.org/gnss/agi/maps/EU-DenseVelocities.html#8/45.333/15.520 last access on: 29.01.2021

Grünthal, G. and Wahlström, R. The European-Mediterranean Earthquake Catalogue (EMEC) for the last millennium. *Journal of Seismology*, **16**, 535-570, DOI: https://doi.org/10.1007/s10950-012-9302-y (2012).

Herak, D. & Herak, M. The Kupa Valley (Croatia) Earthquake of 8 October 1909--100 Years Later. *Seismological Research Letters*, **81(1)**, 30-36. DOI: 10.1785/gssrl.81.1.30 (2010).

ISIDe Working Group. Italian Seismological Instrumental and Parametric Database (ISIDe). Istituto Nazionale di Geofisica e Vulcanologia (INGV). DOI: https://doi.org/10.13127/ISIDE (2007).

Jablonska, D. *et al*. 3D outcrop modelling of large discordant breccia bodies in basinal carbonates of the Apulian margin, Italy. *Marine and Petroleum Geology*, **123**, 104732 (2021)

Kastelic, V. *et al.*Seismogenic sources in the Adriatic Domain. *Marine and Petroleum Geology*, **42**, 191-213. https://doi.org/10.1016/j.marpetgeo.2012.08.002 (2013).

Katz, Y., Weinberger, R., Aydin, A. Geometry and kinematic evolution of Riedel shear structures, Capitol Reef National Park, Utah. *Journal of Structural Geology*, **26(3)**, 491-501, DOI: 10.1016/j.jsg.2003.08.003 (2004).

Li, H. *et al*. Co-seismic surface ruptures associated with the 2014 Mw 6.9 Yutian earthquake on the Altyn Tagh Fault, Tibetan plateau. *Bulletin of the Seismological Society of America*, **106(2**), DOI: 10.1785/0120150136 (2016).

Lin, A., Chiba, T. Coseismic conjugate faulting structures produced by the 2016 Mw 7.1 Kumamoto earthquake, Japan. *Journal of Structural Geology*, **99**, 20-30, http://dx.doi.org/10.1016/j.jsg.2017.05.003(2017).

Livio, F., Serva, L., Gürpinar, A., Locating distributed faulting: contributions from InSAR imaging to probabilistic fault displacement hazard analysis (PFDHA). *Quatern. Int.* http://dx.doi.org/10.1016/j.quaint.2016.09.034 (2016).

Macchiavelli, C. *et al*. Applying the Multiple Inverse Method to the analysis of earthquake focal mechanism data: new insights into the active stress field of Italy and surrounding regions. *Tectonophysics*, **580**, 124-149, doi: 10.1016/j.tecto.2012.09.007 (2012).

Markušic, S., *et al*. The Zagreb (Croatia) M5.5 Earthquake on 22 March 2020. *Geosciences*, **10**, 252, 1-21. doi:10.3390/geosciences10070252 (2020.)

Pavelić, D. & Kovačić, M. Sedimentology and stratigraphy of the neogene rift-type north Croatian Basin (Pannonian Basin System): A review. *Marine and Petroleum Geology*, **91**, 455–469. DOI: 10.1016/j.marpetgeo.2018.01.026 (2018).

Pavičić, I., Rukavina, D., Matoš, B., Tomljenović, B. Interpretation of the tectonic evolution of the western part of the Sava Depression: structural analysis of seismic attributes and subsurface structural modeling, *Journal of Maps*, **15-2**, 733-743. DOI: 10.1080/17445647.2019.1663374 (2019).

Pikija, M. Geological map, scale 1:100,000, sheet Sisak L 33-93. *Federal Geological Office*, Beograd, 1987 (in Croatian) (1987).

Pitts, A.D. *et al*. Integrating traditional field methods with emerging digital techniques for enhanced outcrop analysis of deep water channel-fill deposits. *Mar. Petrol. Geol.*, **87** https://doi.org/10.1016/j.marpetgeo.2017.05.001 (2017).

Pitts, A.D. *et al*. Sedimentological and stratigraphic signature of the Plio-Pleistocene tectonic events in the Southern Apennines, Italy: the Calvello-Anzi Basin case study. *Mar. Petrol. Geol*., **116**, 104198. https://doi.org/10.1016/j.marpetgeo.2019.104198 (2020).

Schmid, S.M. *et al*. The Alpine-Carpathian-Dinaridic orogenic system: correlation and evolution of tectonic units (with Supplementary material). *Swiss Journal of Geosciences*, **101**, 139–183. https://doi.org/10.1007/s00015-008-1247-3 (2008).

Scognamiglio, L., Tinti, E., Quintiliani, M. Time Domain Moment Tensor [Data set]. Istituto Nazionale di Geofisica e Vulcanologia (INGV), https://doi.org/10.13127/TDMT (2006).

Stemberk, J. *et al*.Strain monitoring of active faults in the central Apennines (Italy) during the period 2002–2017. *Tectonophysics*, **750**, 22-35, DOI:10.1016/j.tecto.2018.10.033 (2019.)

Stipcevic, J. *et al.* Crustal Thickness Beneath the Dinarides and Surrounding Areas from Receiver Functions. *Tectonics*, **37**, 1-15. https://doi.org/10.1029/2019TC005872 (2020).

Stipcevic, J., Tkalcic, H., Herak, M., Markusic, S., Herak, D. Crustal and uppermost mantle structure beneath the External Dinarides, Croatia, determined from teleseismic receiver functions. *Geophysical Journal International*, **185**, 1103–1119, doi: 10.1111/j.1365-246X.2011.05004.x (2011).

Stucchi, M. *et al.* The SHARE European Earthquake Catalogue (SHEEC) 1000–1899. *Journal of Seismology*, **17**, 523–544, https://doi.org/10.1007/s10950-012-9335-2 (2013).

Tavani, S. *et al.* Building a virtual outcrop, extracting geological information from it, and sharing the results in Google Earth via OpenPlot and Photoscan: an example from the Khaviz Anticline (Iran). *Comput. Geosci.*, **63**, 44–53 (2014).

Tchalenko, J.S. Similarities between shear zones of different magnitudes. *Geological Society of America Bulletin*, **81**, 1625-1640, DOI: 10.1130/0016-7606(1970)81[1625:SBSZOD]2.0.CO;2 (1970).

Tomljenović, B. & Csontos, L. Neogene–Quaternary structures in the border zone between Alps, Dinarides and Pannonian Basin (Hrvatsko zagorje and Karlovac Basins, Croatia). *International Journal of Earth Sciences*, **90**, 560–578. https://doi.org/10.1007/s005310000176 (2001).

Tomljenović, B., Csontos, L., Márton, E. & Márton, P. Tectonic evolution of the northwestern Internal Dinarides as constrained by structures and rotation of Medvednica Mountains, North

Croatia. *Geological Society, London, Special Publications*, **298**, 145-167. DOI: http://doi.org/10.1144/SP298.8 (2008).

Tomljenović, B., Stipčević, J., Sečanj, M. Izvješće o zabilježenim pojavama kosezmičkih povrsinških deformacijana na području Pokuplja i Banovine nastalih potresnom serijom od 28.12. 2020. do 5.01.2021. https://www.rgn.unizg.hr/hr/izdvojeno/2790-izvjesce-o-zabiljezenim-pojavama-koseizmickih-povrsinskih-deformacija-na-podrucju-pokuplja-i-banovine-nastalih-potresnom-serijom-od-28-12-2020-do-5-01-2021 (2021).

Tondi, E. *et al*. The Campotosto linkage fault zone between the 2009 and 2016 seismic sequences of central Italy: Implications for seismic hazard analysis. *GSA Bulletin*, https://doi.org/10.1130/B35788.1 (2020).

Tondi, E., Piccardi, L., Cacon, S., Kontny, B., Cello, G. Structural and time constraints for dextral shear along the seismogenic Mattinata Fault (Gargano, southern Italy). *Journal of Geodynamics*, **40**, 134-152. DOI: 10.1016/j.jog.2005.07.003 (2005).

Ustaszewski, K., Herak, M., Tomljenovic, B., Herak, D., Matej, S. Neotectonics of the Dinarides–Pannonian Basin transition and possible earthquake sources in the Banja Luka epicentral area. *Journal of Geodynamics*, **82**, 52-68. http://dx.doi.org/10.1016/j.jog.2014.04.006 (2014).

Villani, F. *et al.*, A database of the coseismic effects following the 30 October 2016 Norcia earthquake in Central Italy. *Sci Data*, **5**, 180049, https://doi.org/10.1038/sdata.2018.49 (2018)

CHAPTER 3: New Methodological Approach in The Evaluation of Faults Interaction: Insights From The Central Apennine Fault System

G. Valentini[1,2], T. Volatili[1], P. Galli[3,4], E. Tondi[1,2]

1. School of Science and Technology - Geology Division, University of Camerino, Italy.
2. Istituto Nazionale di Geofisica e Vulcanologia (INGV), Sezione di Sismologia e Tettonofisica, Camerino, Italy
3. Dipartimento Protezione Civile, Rome, Italy
4. Consiglio Nazionale delle Ricerche, Istituto di Geologia Ambientale e Geoingegneria, Rome, Italy

Bulletin of Geophysics and Oceanography Vol. 64, n. 4, pp. 387-404; December 2023
DOI 10.4430/bgo00428

New methodological approach in the evaluation of fault interaction: insights from the central Apennines fault system

G. VALENTINI[1,2], T. VOLATILI[1], P. GALLI[3,4] AND E. TONDI[1,2]

[1] *School of Science and Technology, Geology Division, University of Camerino, Camerino, Italy*
[2] *Istituto Nazionale di Geofisica e Vulcanologia, Sezione di Sismologia e Tettonofisica, Camerino, Italy*
[3] *Dipartimento Protezione Civile, Roma, Italy*
[4] *Consiglio Nazionale delle Ricerche, Istituto di Geologia Ambientale e Geoingegneria, Roma, Italy*

(Received: 23 November 2022; accepted: 12 July 2023; 26 September 2023)

ABSTRACT The central Apennines host several normal active faults, which are distributed along the Central Apennine Fault System (CAFS), known for generating dozens of earthquakes, of moderate to high magnitudes, in the last thousand years. The latest events caused by this system occurred in the epicentral area of Colfiorito in 1997 (M_w 6.0), L'Aquila in 2009 (M_w 6.2), and at the border between the Marche, Umbria, and Lazio regions in 2016 (M_w 6.6), this latter a catastrophic event with hundreds of victims and extensive damages. Thereafter, significant interest arose in the study of fault behaviour in the axial zone of the central Apennines. This work proposes a new methodological approach to studying fault interaction within the framework of the CAFS seismic cycle, modelling faults with a more complex geometry characterised by an elliptical outline, which better describes the actual shape of a fault at depth. All the destructive earthquakes ($M_w > 6.0$) that occurred in the last thousand years were taken into account, and the static stress between the causative fault and adjacent one was calculated. The results demonstrate how the newly modelled faults critically affect Coulomb stress transfer compared to planar and rectangular fault modelling usually adopted by previous authors.

Key words: active normal faults interaction, Coulomb stress transfer, fault modelling, seismic cycle, Central Apennines Fault System.

Abstract

The central Apennines hosts several normal active faults which are distributed along the CAFS (central Apennine fault system), known for generating dozens of earthquakes with moderate to high magnitudes in the last thousand years. The latest events caused by this system occurred in the epicentral area of Colfiorito in 1997 (Mw 6.0), L'Aquila in 2009 (Mw 6.2), and the catastrophic events in 2016 (Mw 6.6) at the border among Marche, Umbria and Latium regions, resulting in hundreds of victims and extensive damages. Thereafter, a relevant interest in studying fault behavior in the axial zone of the central Apennines arose. This work proposes a new methodological approach to the study of faults interaction within the framework of the CAFS seismic cycle, modeling faults with a more complex geometry characterized by an elliptical outline, which better describes the actual shape of a fault at depth. All the destructive earthquakes (Mw > 6.0) that occurred in the last thousand years were taken into account and the static stress between the causative fault and the adjacent one was calculated. The results demonstrate how the newly modeled faults critically affect the Coulomb stress transfer compared to the planar and rectangular fault modeling usually adopted by previous authors.

3.1 INTRODUCTION

The Central Apennine Fault System (CAFS in Cello et al., 1997) is composed of several active normal to oblique faults that caused several destructive earthquakes during the last millennium. According to seismic catalogues (CPTI15; Rovida et al., 2022) 15 seismic events with $5.8 \leq Mw \leq 7.0$ in central Italy (since 1279 CE) can be associated with CAFS-related structures. Seismicity appears to be concentrated in 3 distinct time-windows: in the 12th-13th and 17th-18th centuries and between the end of the 20th and today. The most recent seismic events struck the axial zone of the central Apennine fold-and-thrust belt between 1979 (Mw 5.8 Valnerina sequence) and 2016-2017 (Mw 6.5 Amatrice- Norcia-Visso sequence; Chiaraluce et al., 2017) also involving the northern area of the CAFS and its southern border (1997, Mw 6.0 Colfiorito-Sellano and 2009, Mw 6.2 L'Aquila sequences, respectively) (Amato et al.,1998; Cello et al.,1998; Tondi, 2000; Vittori et al., 2000; Chiarabba et al., 2009; Chiaraluce et al., 2011; Vannoli et al.,2012 and references therein) causing severe damages and hundreds casualties, leading to awaken interest in the study of the seismic behavior of these seismogenic structures.

The Apennines host the CAFS in their central portion, extending 100 km in a NW-SE direction and 50 km from W to E. In this system, several segmented surface expressions of seismogenic sources outcrop and have been precisely mapped (Barchi et al., 2000; Galadini and Galli, 2000; Tondi, 2000; Tondi et al., 2021). Furthermore, numerous paleoseimological analyses (Galli et al., 2008; Galli, 2020; Galli et al.,2022) conducted on trenches along faults provided useful information about their past activity.

Nowadays, one of the main research objectives in the field of earthquake geology is to understand the mechanisms that influence recurrence intervals. By studying the interaction between neighboring faults, it is possible to estimate which fault is the most prone to slip. Although several factors can influence fault activity, such as fluid circulation, climate-controlled changes in surface loads or elastic strain energy accumulation (Oskin et al., 2008; Hetzel and Hampel, 2005; Brodsky and van der Elst, 2014, Gold et al., 2017; Wedmore et al., 2017), static and dynamic stress transfer play a crucial role in triggering fault ruptures. In particular, the rapid propagation of seismic

waves produces short-time changes in dynamic stress, while static stress transfer is a permanent variation of the stress condition in the crust around a causative fault affecting also faults far from the source (Gomberg & Jonson, 2005; Velasco et al., 2008; Toda et al., 2012). Since we are investigating stress transfer over an entire millennium, static Coulomb stress transfer (CST) within the CAFS is of primary importance.

In this study we reconstructed the CAFS seismic cycle (Tondi and Cello, 2003; Fig. 3.1b) considering the 3 time-windows of seismicity over the last millennium and investigated the role of CST in promoting or inhibiting ruptures of neighboring faults. Furthermore, considering the importance of fault geometry in influencing the result, we propose a new strike-variable and ellipse-shaped three-dimensional model as input for the CST simulation.

3.2 THE CENTRAL APENNINE FAULT SYSTEM (CAFS)

The Italian central Apennines are dissected by several NW–SE trending normal to oblique faults developed coherently to the current extensional regional stress field. Since Late-Quaternary, central Apennines were subject to a NE–SW-oriented minimum horizontal compressive stress producing large sub-parallel extensional faults that, in some cases, overprint older compressive structures inverting the kinematic consistent with the formation of the fold and thrust belt (Cello et al. 1997). This structural framework accounts for surface evidence of normal faulting along a very large area extending from Colfiorito (CAFS northern edge) to L'Aquila, usually bordering the eastern side of tectonic basins infilled by Pleistocene to Holocene deposits. The slickensides outcropping in almost the entire CAFS demonstrate the recent fault activity, often displaying kinematic indicators consistent with the current stress field. According to the empirical relationship between length and magnitude proposed by Galli et al. (2008), the expected magnitude of the CAFS faults varies within a range of Mw 5.7 to Mw 7.0. The surface length of the faults indeed ranges from a few kilometers up to 44 km (e.g. Gran Sasso Fault, Galli et al., 2022), with an average dip angle of approximately 57 degrees. The CAFS has been studied

extensively in the recent decades by several authors and the fault scarps have been mapped in detail providing valuable data for the seismic hazard assessment. For the sake of modeling, in this work only the main fault traces associated to the studied seismogenic sources have been considered, although the superficial expression of these deep seismogenic structures may be represented by multiple ruptures at surface. These structures generated several large earthquakes over the last thousand years, as recorded by the Italian historical catalogs, which are among the most complete and back-in-time extended seismic compilations worldwide. Historical data, supported by hundreds of paleoseismological surveys, allowed to acquire a large amount of reliable data on the recent activity of the CAFS.

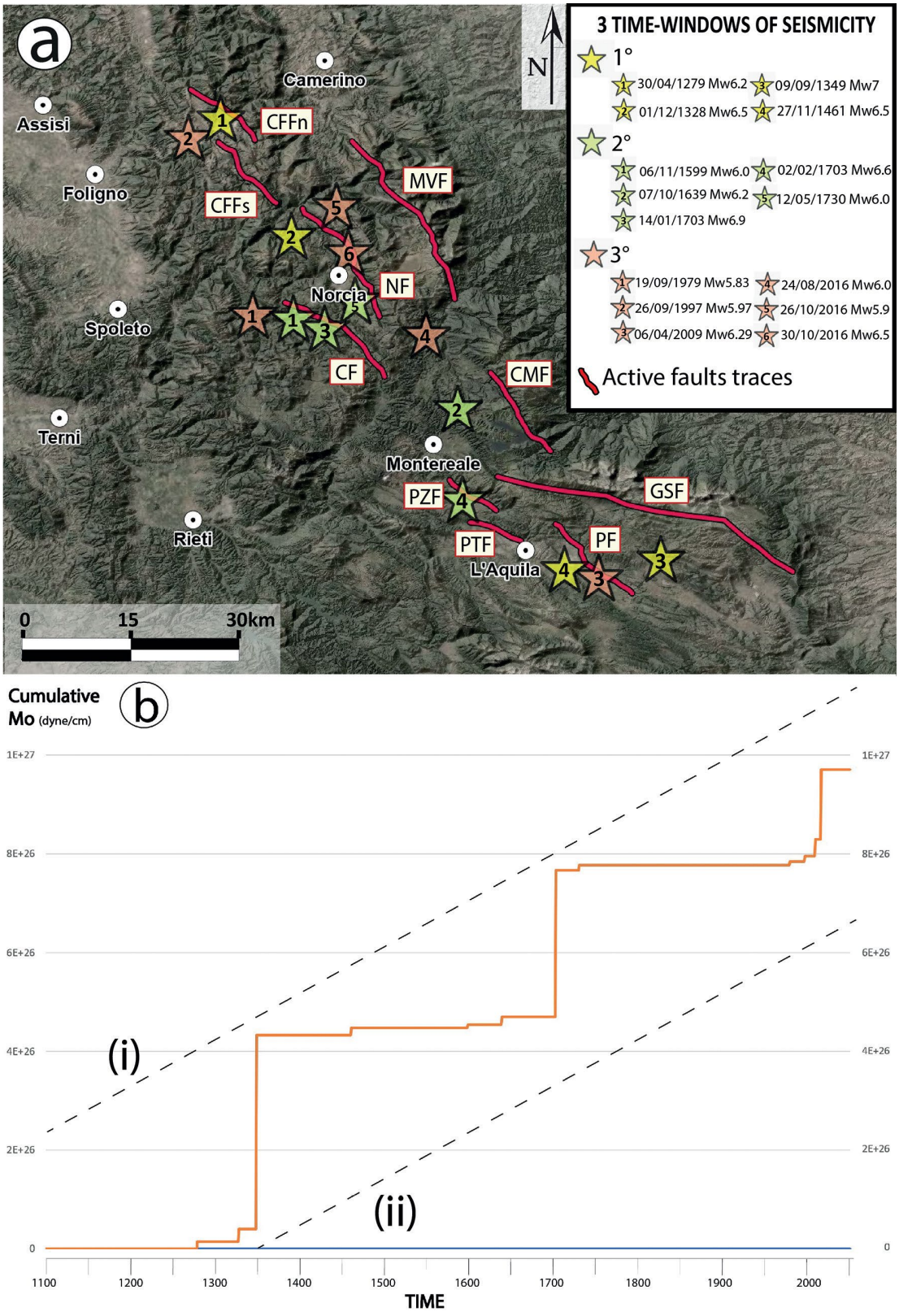

Figure 3.1 a) Map of the 15 seismic events with 5.8 ≤ Mw ≥ 7.0 in the CAFS area since 1279CE. Main active fault traces on the topographic surface are also shown in red (CFFn – Colfiorito Fault nord; CFFs - Colfiorito Fault south; MVF – Monte Vettore Fault; NF – Norcia Fault; CF – Cascia Fault; CMF – Campotosto Fault; GSF – Gran Sasso Fault; PZF

– Pizzoli Fault; PF – Paganica Fault; PTF – Pettino Fault) (Tondi, 2000; Galderisi and Galli, 2020; Tondi et al., 2020; Galli et al., 2022 and references therein). b) CAFS cumulative seismic moment (dyne/cm) as a function of time. Dashed lines show the hypothetical course of the seismic cycle if the system had been (i) ''energy-predictable'' and (ii) ''time-predictable'' (Shimazaki and Nakata, 1980; Tondi and Cello, 2003).

3.3 METHODS

3.3.1 SEISMIC DATA AND CAUSATIVE FAULTS

In this study, a total of 15 earthquakes have been considered and their parameters summarized in table 1. Specifically, 9 historical earthquakes (CPTI15 seismic catalogue) and 6 instrumental ones (ISIDe Working Group, 2007; Italian Seismological Instrumental and Parametric Database. https://doi.org/10.13127/ISIDE) have been selected with Mw≥6.0 and Mw≥5.8, respectively. Different magnitude thresholds between historical and instrumentals datasets were adopted to overcome the likely overestimation of the estimated magnitude for historical events (Vannucci et al., 2021 and references therein). Once all the historical earthquakes were selected based on magnitude, an additional strategy was adopted to overcome the issue of overestimation: the catalogs provide an error for each magnitude, and for calculation purposes, we subtracted this error from the magnitude indicated in the catalog. For the seismic event of 1349 CE, the data in the catalog has been replaced with the recent revision by Galli et al. (2022), who identified the source of this devastating earthquake attributing a magnitude Mw=7.

Year	Month	Day	EpicentralArea	Lat	Lon	Io	Mw	ErrorMw	TMw	SOURCE
1279	4	30	Umbria-Marche Apennines	43.093	12.872	9	6.20	0.16	Mdm	CPTI15
1328	12	4	Valnerina	42.857	13.018	10	6.49	0.28	Mdm	CPTI15
1349	9	9	Abruzzo	42.334	13.613	10	7.00	ND	Mdm	Galli et al., 2022
1461	11	27	L'Aquila	42.308	13.543	10	6.50	0.46	Mdm	CPTI15
1599	11	6	Valnerina	42.724	13.021	9	6.07	0.24	Mdm	CPTI15
1639	10	7	Laga Mountains	42.639	13.261	9-10	6.21	0.15	Mdm	CPTI15
1703	1	14	Valnerina	42.708	13.071	11	6.92	0.1	Mdm	CPTI15
1703	2	2	L'Aquila	42.434	13.292	10	6.67	0.11	Mdm	CPTI15
1730	5	12	Valnerina	42.753	13.120	9	6.04	0.1	Mdm	CPTI15
1979	9	19	Valnerina	42.73	12.956	8-9	5.83	0.1	InsO	CPTI15
1997	9	26	Umbria-Marche Apennines	43.014	12.853	8-9	5.97	0.07	InsO	CPTI15/ISIDe
2009	4	6	L'Aquila	42.309	13.510	9-10	6.29	0.07	InsO	CPTI15/ISIDe
2016	8	24	Laga Mountains	42.698	13.233	10	6.00	0.07	InsO	CPTI15/ISIDe
2016	10	26	Valnerina	42.904	13.090		5.90	0.07	InsO	CPTI15/ISIDe
2016	10	30	Valnerina	42.83	13.109	11	6.50	0.07	InsO	CPTI15/ISIDe

Table 3.3 List of historical (Mw≥6) and instrumental (Mw≥5.8) seismic events from 1279 to 2016 caused by CAFS (from CPTI15; Rovida et al., 2022 and ISIDe seismic catalogues; ISIDe Working Group, 2007, Italian Seismological Instrumental and Parametric Database. https://doi.org/10.13127/ISIDE). Mdm: Macroseismic from Intensity Data. InsO: Instrumental.

A causative fault has been associated to each studied earthquake after a detailed scrutiny of fault-related data present in literature (i.e., paleoseismological, structural, macroseismic). Secondly, its fault trace with a resolution depending on the CAFS scale have been elaborated in a Geographic Information System, GIS (refer to Fig. 3.1a). All the constructed lineaments are supported by robust field-based constrains from literature (Galli and Galadini,1999; Tondi,2000; Galadini and Messina, 2001; Messina et al.,2002; Tondi and Cello,2003; Galli et al.,2005; Galli et al.,2011; Galli et al.,2016; Galli et al.,2018; Galli et al.,2019; Galderisi and Galli, 2020; Tondi et al., 2020; Galli et al.,2022 and references therein). The fault dataset (Tab. 2) was compiled with the following fields: i) fault name, ii) dip angle, iii) rake (using the Aki and Richards (1980) conventions), iv) dip direction, and v) length.

Fault	Surface lenght (Km)	Max subsurface length (Km)	Dip angle	Dip direction	Rake
COLFIORITO NORD	8.9	19	42	230	-80
COLFIORITO SUD	12.8	17	40	236	-83
GRAN SASSO	44.4	60	63	208	-95
PAGANICA	16.6	25	56	230	-97
CASCIA	19.5	27	65	230	-98
CAMPOTOSTO	8.4	12	51	249	-86
NORCIA	22.9	31	37	243	-98
VETTORE	34.4	54	36	240	-98
PETTINO	7.6	10	63	200	-95
PIZZOLI	6.6	9	56	226	-97

Table 3.4 List of causative faults belonging to the CAFS with the related parameters. The "Max subsurface length" refers to the length of the major axis of the ellipse. If not available from the literature, we assumed the length from standard geometric relationship as described in section 3.2.

We estimated the seismic moment released by historical earthquakes by extrapolating it from the Hanks and Kanamori (1979) formula. The equation used is:

M0=10^[(3/2)*(Mw+10.73)]

where M0 is the seismic moment and Mw is the moment magnitude. Then we compared seismic energy released during the main time-windows of seismicity that clustered in the CAFS area to better constrain the spatiotemporal evolution of the CAFS seismic cycle.

3.3.2 COULOMB STRESS TRANSFER (CST) AND FAULT MODELING

We propose a novel approach to model seismogenic sources for CST calculation purposes, aimed to reduce uncertainties on fault interaction. This approach adopts as a cornerstone the hypothesis that the most reliable approximation of 2D-fault geometry is an ellipse (Barnett et al., 1987; Walsh and Watterson,1987; Gupta and Scholz, 2000). This concept is strictly related to the variation in displacement that ranges from the maximum at the center of the fault to zero at the elliptical tip-line loop. Furthermore, faults are commonly modelled as planar geometries in Coulomb calculations but, as demonstrated by Mildon et al. (2016), Coulomb stress transfer is highly sensitive to strike-variable geometries of the receiver faults. Since a realistic CAFS base model is of paramount importance in reducing calculation errors, we adopted a new strike-variable and ellipse-shaped three-dimensional model as input file for the CST simulations.

To do so, we used "3-D Faults" (Mildon et al., 2016) MATLAB code. To test the efficiency and the effective influence of this new model in terms of CST results, we performed calculations on both planar-rectangular faults and strike-variable and elliptic faults. We used the same receiver and source faults but two different geometric model to find and quantify differences.

We performed CST simulations within each seismic sequence respecting the real rupture conditions of the earthquake (e.g., partial or entire rupture, slip distribution).

We conducted CST calculations assuming that when an earthquake occurs on a fault, the Coulomb stress can be transferred to the surrounding faults. The failure of the latter will be promoted if the Coulomb stress change is positive or inhibited if it is negative (King et al., 1994). The change in the Coulomb stress depends on the distance between the receiver fault and the source fault, on their position, geometry, kinematics and slip of the source fault. The CST was calculated with the following equation, using the software "Coulomb 3.4" (Lin and Stein, 2004; Toda et al., 2005):

$$\Delta CST = \Delta\tau s + \mu\Delta\sigma n$$

where ΔCST is the variation of the Coulomb Stress Transfer, $\Delta\tau$s is the change of the shear stress, μ is the friction coefficient and $\Delta\sigma$n is the change of the normal stress.

The input file was created by modeling the faults in the elastic-half space as linear elements with variable strike, dividing them into 0.5-km-long rectangular elements along strike. The choice of this very fine mesh lattice over the usual use of kilometric mesh yields a precise evaluation of the variation of the Coulomb stress by applying the various fault geometries, to the detriment of the computational time employed. For this purpose, the use of the "Faults 3D" code (Mildon et al 2016) allowed us to generate 3d strike-variable faults from fault traces and to create a slip distribution for each fault. Keeping the friction coefficient constant, we used the function of the code that calculates the Coulomb stress for each individual rake, using the parameters specified in the input file for each of the rectangular elements comprising the fault surface.Where possible, the actual slip of the earthquake was replicated reproducing the coseismic slip distribution occurred along the fault surface (only for recent earthquakes with a large amount of slip data). In turn, for the lesser-known earthquakes, a simple bull's eye slip distributions calibrated on the relative seismic moment released was assumed, setting the location of maximum slip at the center of the fault plane. When the width of the faults was not indicated in the examined bibliography, it was derived from standard geometric relationships (Gupta and Scholz, 2000) assuming a 1.5 aspect ratio (length/width). Whereas, the fault maximum depth was set like the thickness of the seismogenic layer (≈ 15 km; Gasparini et al., 1985; Chiarabba and De Gori, 2016) in case of fault with an exceeding lengt.

3.4 RESULTS

CAFS SEISMIC CYCLE

The cumulative seismic moment released during the last 1000 years was similar in the 3 main time-windows separated by ca. 300-350 years of time gap as hypothesized by Tondi and Cello (2003) who determined the seismic cycle using the calculation of the cumulative coseismic slip derived from the decomposition of the seismic moment. We instead used the cumulative seismic moment directly.

The graph in figure 3.1b shows how most of the seismic energy released in the last millennium can be associated with three distinct "steps", one between 1300 CE and 1400 CE, one around 1700 CE and one corresponding to the latest events, from 1979 to 2016. Assuming that a millennium is a long enough time span to define the seismic cycle, it is possible to speculate that the time interval separating the release periods of most of the seismic energy is about 300-350 years. On the other hand, the quantity of energy released is not constant among the three time windows of seismicity. The seismic moment released by the first time window of seismicity is the highest (Mo=4.47E+26 dyne/cm), whereas the sum of the seismic moments released in the second and third time windows are 3.29E+26 dyne/cm and 1.93E+26 dyne/cm, respectively.

FAULT MODELING

The adoption of strike-variable and elliptic-shaped faults in static CST modeling revealed significant differences in terms of amount of transferred stress and stress patterns on the receiver faults compared to the classical planar and rectangular faults. In particular, the effect of ellipticity in increasing lateral extension of the fault surfaces at about half of their maximum depth considerably reduces the distance between neighboring faults, increasing the degree of interaction and, consequently, the amount of static Coulomb stress transferred to the tips of the receiving faults located along strike of the source faults (Fig. 3.3). We also found differences in the stress pattern generated on laterally sub-parallel faults that experience a larger decrease in stress. The intersection between the elliptical fault plane and the topographic surface defines the trace of the fault in map view, whereas the corresponding length is not the real length of the fault in depth, which is longer on average by 36.25% for ellipses with a geometric ratio of 3:2 between major and minor axe (Fig. 3.2). This consideration is consistent with the areal distribution of the instrumental hypocenters of the aftershocks and foreshocks that extend well beyond the tip of the causative fault, outlining rather precisely the real extent of the fault in depth that roughly coincides with the modeling we have carried out.

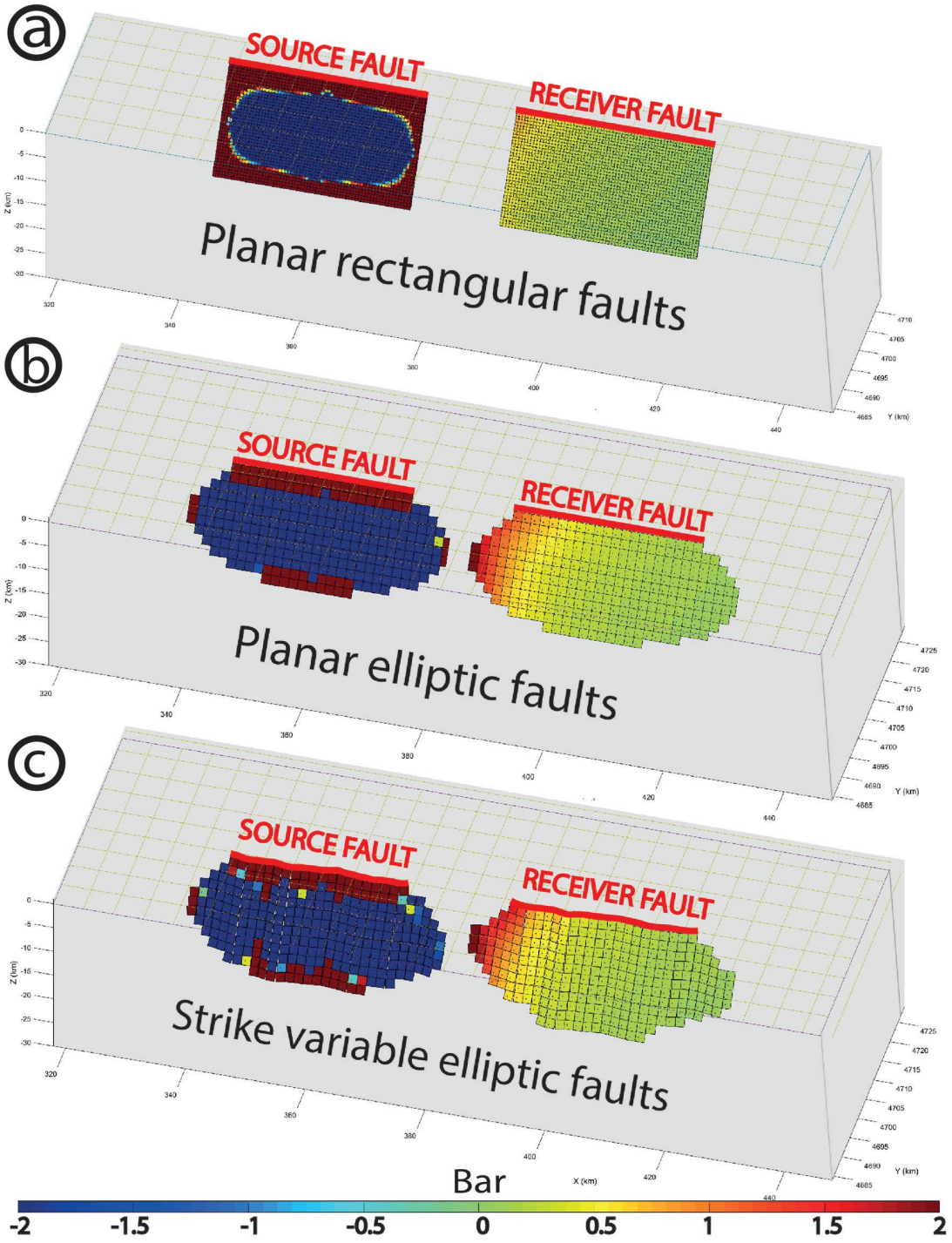

Figure 3.2 Simulations to test the influence of different fault models on CST. With a planar rectangular model (a), the receiver fault is negligibly influenced, whereas with elliptical faults (b) the receiver fault tip shows higher stress values. By further adding the effect of the variable strike (c), a more heterogeneous stress pattern is noted on the receiver fault.

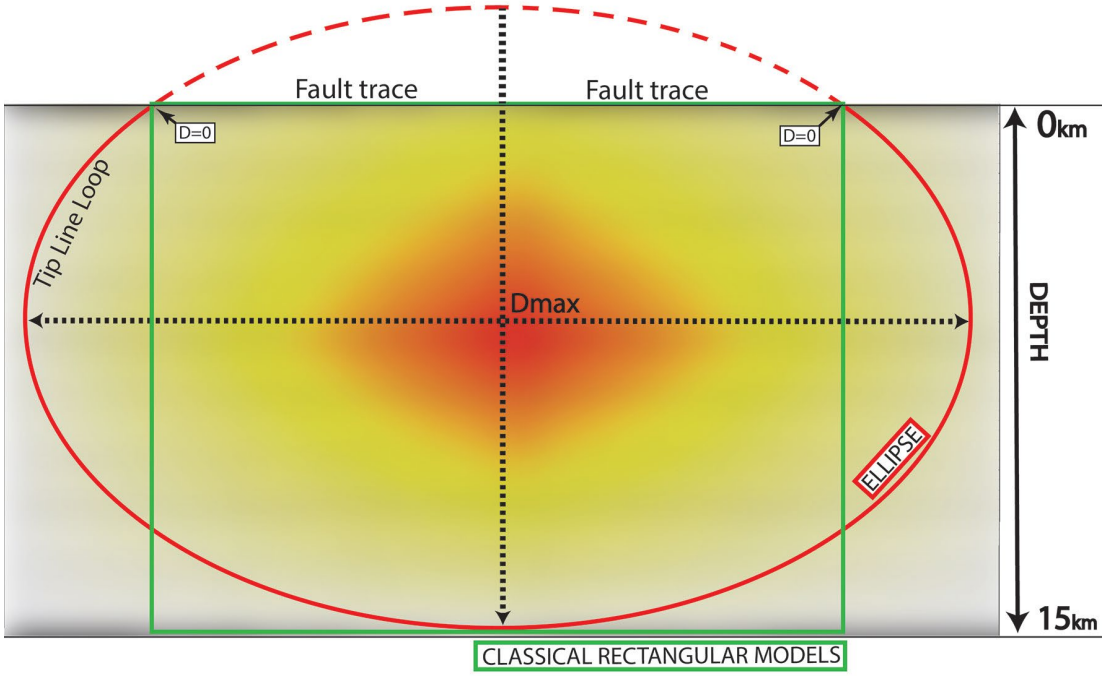

Figure 3.3 Comparison between the elliptical tip line loop of the fault (in red) and the commonly adopted rectangular shape (in green). The dashed part of the ellipse indicates the hypothetical continuation of the perimeter above the topographical surface. Center-to-perimeter faded colors show the ideal variation of displacement on the fault surface, maximum in the center and zero along the tip line loop.

3.5 COULOMB STRESS TRANSFER (CST)

The results regarding the modeling of the CST are encouraging, highlighting how this new methodology can make significant differences compared to the classical methodology. We tested the method on several faults for some of the most interesting historical earthquakes, trying to understand how the surrounding faults were affected. We found a good agreement between the spatiotemporal evolution of CAFS earthquake sequence and the permanent static stress transferred to the nearby faults. Faults falling into the stress shadows were inhibited in their reactivation after a strong earthquake generated by the adjoining source fault. Conversely, fault segments subject to increased stress ruptured in shorter times than their characteristic return time or faults surfaces partially affected by stress increase subsequently showed partial ruptures only on the positively stressed fault tip. Below are some examples of the results obtained.

3.5.1. COLFIORITO 1279 VS NORCIA 1328

The oldest earthquake considered in this work is that of April 30, 1279 CE which roughly struck the same area affected by the events of 1997. This sequence was sourced by the Colfiorito fault system, composed by two main structures (Colfiorito north and Colfiorito south faults, CFFn and CFFs respectively in Fig. 3.4 and Fig. 3.5), with an en-echelon geometrical relationship with a dextral step-over (Galli and Galadini, 1999). According to Galli and Galadini (1999), the 1279 earthquake is probably a twin of the 1997 one, and would have activated the same fault segments, corresponding in this work to the Colfiorito north and Colfiorito south faults. Therefore, we modeled the simultaneous activation of both faults (Fig. 3.4c). The effect of the individual and contemporaneous activation of the two segments were analysed in order to assess the CST for the following scenarios: i) Colfiorito north as source fault (Fig. 3.4a); ii) Colfiorito south as source fault (Fig. 3.4b); iii) simultaneous activation of both faults (Fig. 3.4c). In all three cases, the magnitude of the event remained constant, and only the slip pattern was changed to adapt the magnitude to the different source faults.

The receiver fault is the Norcia fault, which subsequently activated in 1328 CE. The aim is to understand the influence that the 1279 CE Colfiorito earthquake on the the Norcia fault in 1328 CE.

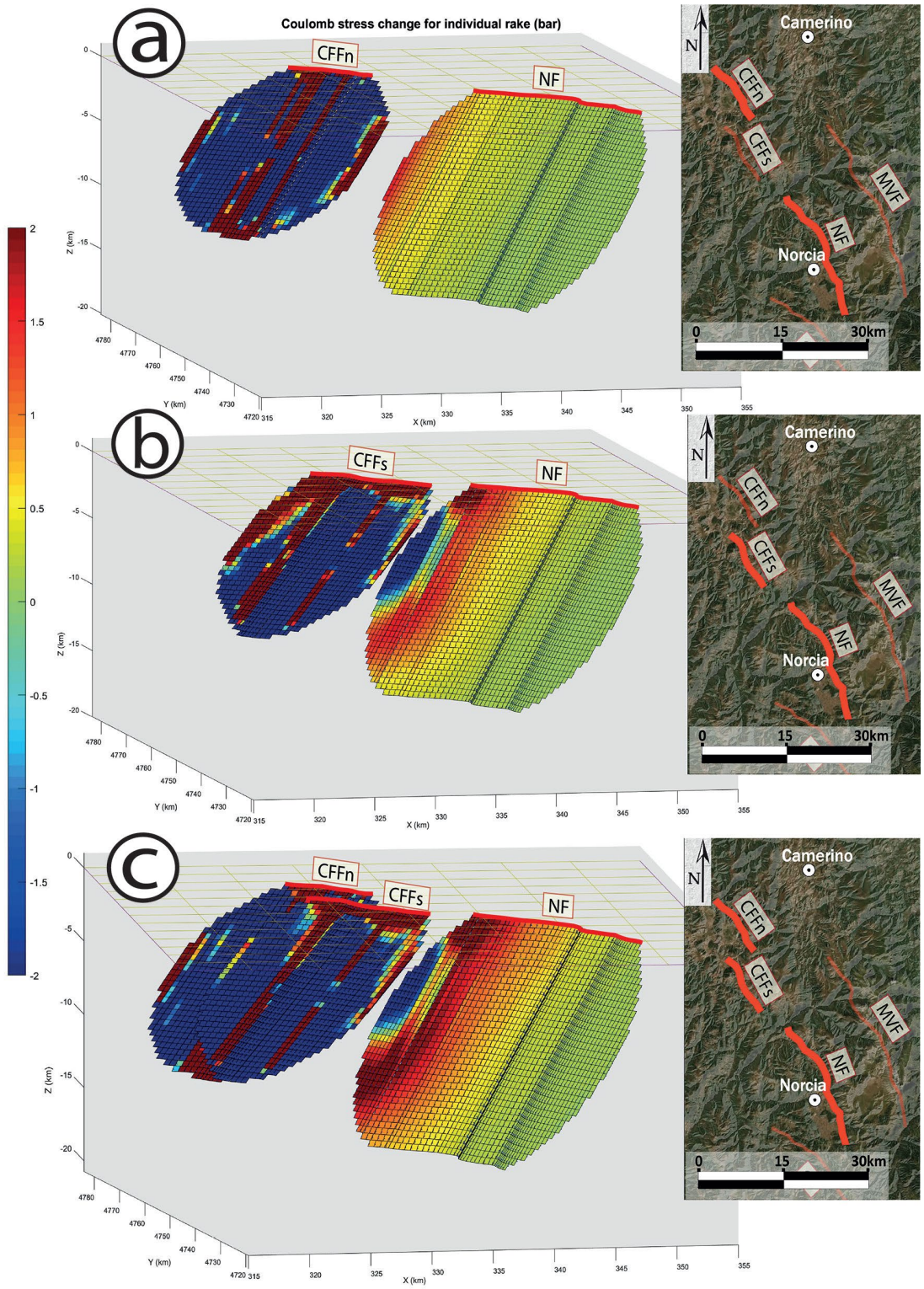

Figure 3.4 CST on the Norcia fault (NF) caused by the slip of the a) Colfiorito north fault (CFFn), b) Colfiorito south fault (CFFs) and c) simultaneous activation of both faults. The pictures on the right side show the fault location in map view.

The results of this calculation demonstrate how the mutual position of the faults influences the CST. The three faults, distributed from NW to SE along the same axis, sharing a similar strike demonstrate fault tips very close to each other (Fig. 3.5). In the scenario, considering only the Colfiorito North fault as causative fault, only the northern tip of the Norcia fault would be positively loaded by CST (Fig. 3.4a), with a stress increase of about 1.8 bar in a very small area. The slip on the Colfiorito south fault, on the other hand, would have produced a more pronunced and heterogeneous CST pattern, partially influenced by the stress shadow area. In this case, in fact, the northern tip of the Norcia fault and the southern tip of the Colfiorito south fault partially overlap at depth, creating a small zone of stress reduction in correspondence with the northern tip of the Norcia fault. The rest of the northern half of the receiver fault is positively stressed by a maximum of 2.2 bar. Finally, in the last case, considering the simultaneous activation of Colfiorito north and south faults (Fig. 3.4c and Fig. 3.5), the pattern is similar to the previous scenario but with much higher values of CST, reaching even 3 bars of positive stress in a large area.

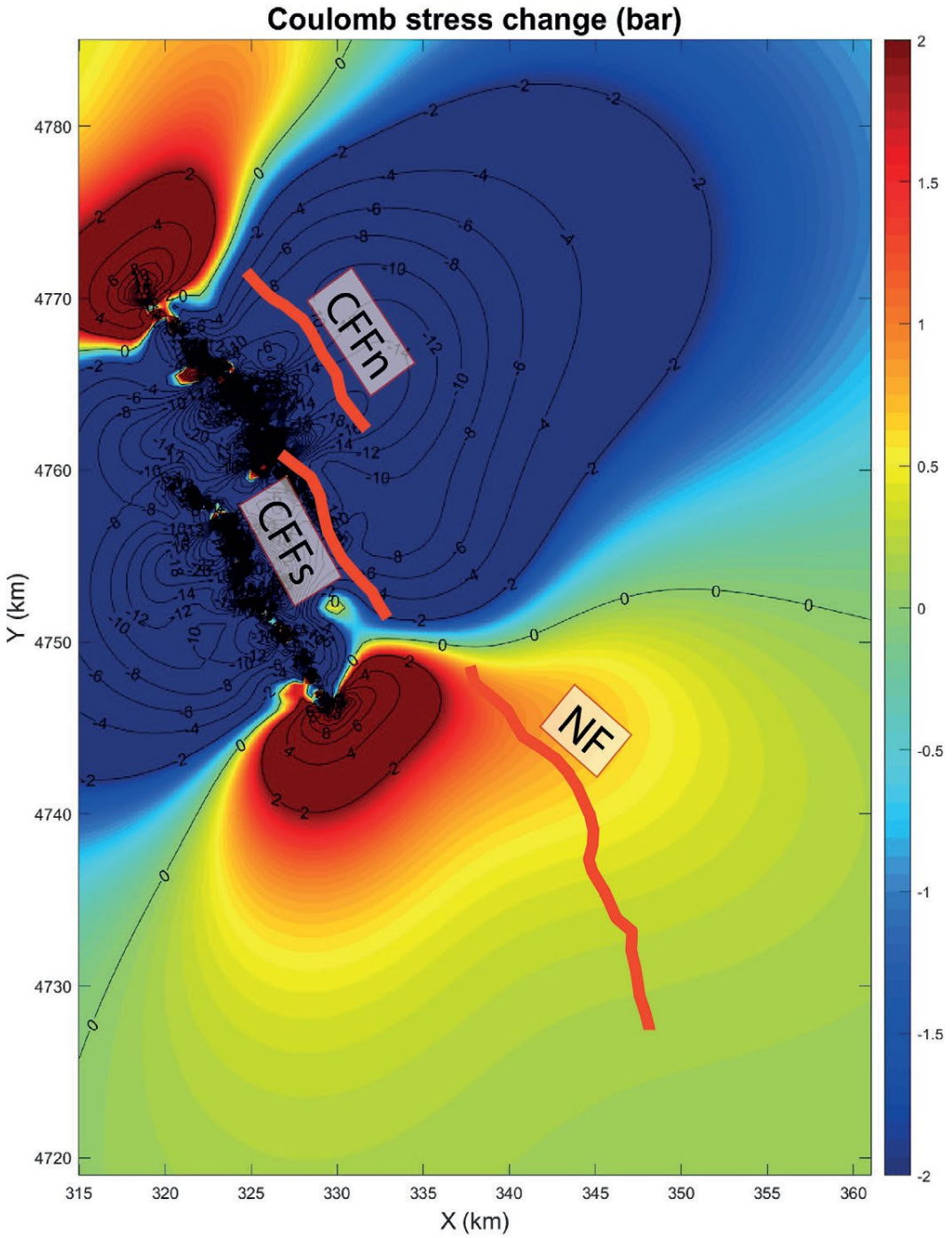

Figure 3.5 Map view of the spatial distribution of the CST caused by the simultaneous activation of Colfiorito north and South faults, the calculation was performed on a plane at 7.5km depth.Contour lines of equal stress variation on the receiver fault are drawn in black (numbers are stress in bars). The red traces are the surface traces of the faults (CFFn-Colfiorito north fault, CFFs- Colfiorito south fault, NF-Norcia fault)

3.5.2. NORCIA 1328 VS CASCIA 1599

Here we calculate the effect of the 1328 CE Norcia event (see Galli et al., 2005; 2018) on the Cascia fault system (Cascia plus Mt. Alvagnano faults), activated in 1599, i.e., 271 years later (Galli et al., 2019). On December 4th, 1328 CE a Mw 6.5 earthquake struck an area between Marche and Umbria regions, causing extensive damage and numerous casualties in Norcia. The distribution of the highest intensity datapoints suggests that part of the Norcia fault system was its causative structure (Galli et al., 2005; 2018). The eastern Norcia fault system borders the Quaternary Campi and Norcia basins, extending from the northwest to the southeast at surface for about 23 km. It is worth noting that in the late Middle Ages, central Apennines experienced two additional earthquakes, but rather far from Norcia, the first in 1349 CE in the Gran Sasso area (Galli et al., 2022), the second in 1461 CE on the Paganica fault (Chiarabba et al., 2009). The next earthquake took place near Cascia in 1599 CE, with a magnitude Mw 6.0 (Galli et al., 2019). This event attracted our attention as a possible candidate for the calculation of the stress transfer for the following reasons:

i) The extreme proximity to the Norcia fault;

ii) The partial overlap between the tips of the two faults.

iii) The Cascia earthquake is located between two Norcia earthquakes (1328 CE and 1703 CE), so it is possible to calculate the mutual stress transfer;

iv) The other two earthquakes after 1328 CE struck an area very distant from Norcia, resulting in a negligible CST effect on the faults.

The Cascia faults (i.e., Cascia plus Mt. Alvagnano faults) are over 19 km long, with a strike similar to the Norcia faults and an overlap step of about 5-10 km. The results of the CST from the Norcia fault to the Cascia fault during the 1328 CE earthquake are illustrated in Fig. 3.6. The causative fault undergoes an overall significant decrease in stress except along vertical strips of the fault surface where there is a sudden change in strike, that is, along the fault bends. There, the CST increases by 2-6 bars, and a similar increase is also found in narrow portions of the northern and southern fault tips. The receiver fault experiences a heterogeneous stress transfer pattern, with an evident

negative stress lobe in its northern half at a depth greater than 4km. In this stress shadow zone, there is a decrease in stress up to 6 bar. The same amount of negative stress occurs at the center of the fault but closer to the topographic surface, up to a depth of 2 km, while the remaining fault surface is subjected to a positive stress that reaches 2.5 bar. Furthermore, the CST pattern was modeled in map view at 7.5 km depth (Fig. 3.6), which correspond to the most representative distribution of the stress transfer in the surrounding area. Here, the two stress shadow lobes are much more extensive than the positively stressed ones.

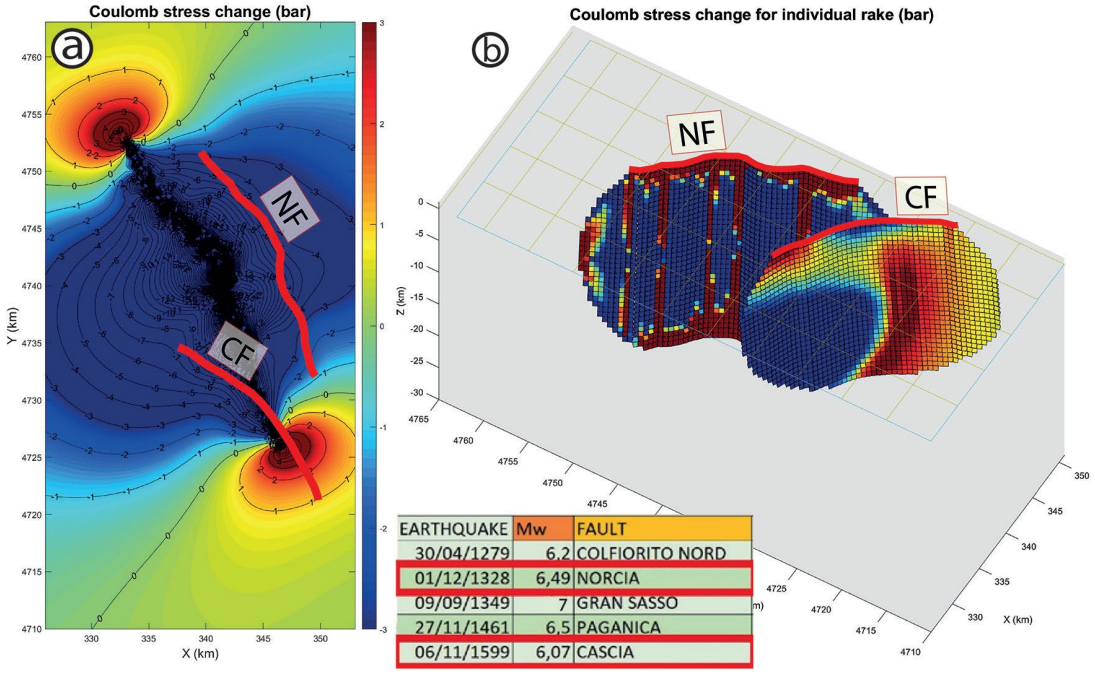

Figure 3.6 CST on the Cascia fault (CF) following the 1328 Mw6.49 seismic event caused by the slip on the Norcia fault (NF). a) Plan view of the spatial distribution of the CST on a plane at 7.5km depth. Contour lines of equal stress variation on the receiver fault are drawn in black (numbers are stress in bars). The red traces are the surface traces of the faults. b) 3D view of the CST on fault surfaces.

3.5.3. CASCIA 1599 VS NORCIA 1703

We previously calculated the effect in terms of CST caused by the activation of the Norcia fault on the Cascia fault. Guided by the interest in modeling the opposite case, we modeled the 1599 CE (Total seismic moment =1.42e+25 dyne/cm - Mw6.07) earthquake that occurred on the Cascia fault against the Norcia fault, which reactivated about a century later, in 1703 CE, together with the Cascia fault themselves (Galli et

al., 2021). This example is useful to understand if there are differences between the receiver faults placed in the hanging wall of the causative fault or in the footwall. In fact, these two faults overlap for several kilometers, and both dip to the southwest. The results of this calculation show the Cascia fault (causative) subject to negative stress except on the tips and in the superficial and deep extremes. This stress release is released in the surrounding crust and affects the Norcia fault, especially in correspondence with the bends. In Fig. 3.7 it is possible to observe how the red areas (positive stress) on the Norcia fault correspond to the bends better visible in Fig. 3.7a. The zone covered by stress shadow is also clearly visible, affecting the overlap zone of the two faults, subtracting stress from the southern and superficial half of the Norcia fault. The northern tip, on the other hand, seems to have been negligently affected by the reactivation of the Cascia fault.

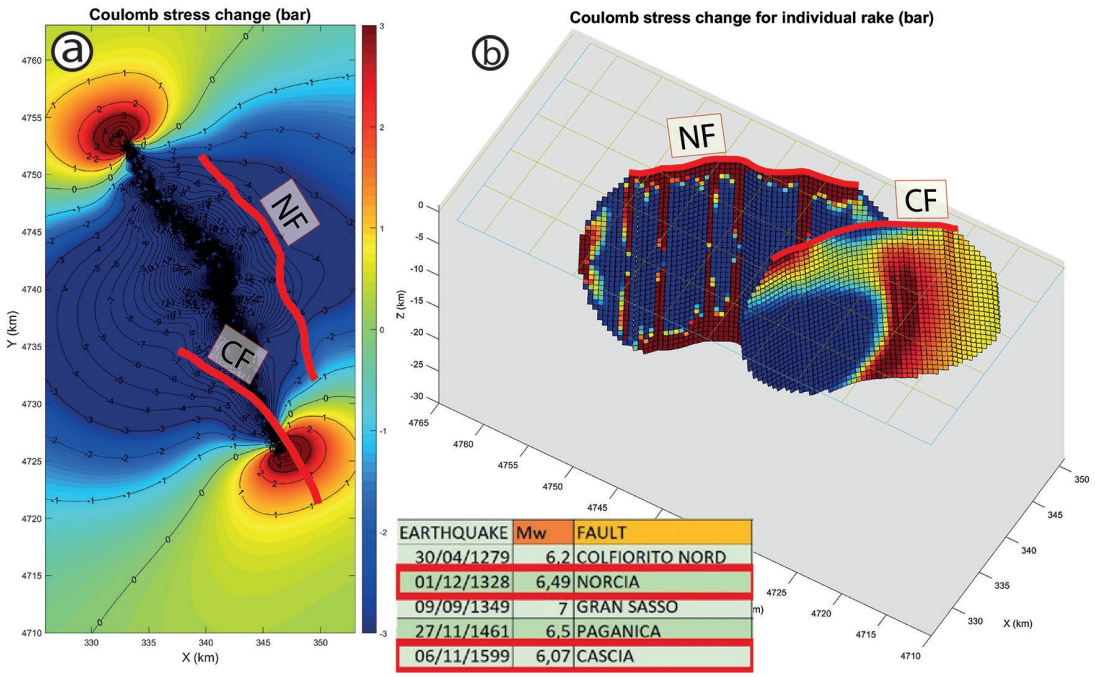

Figure 3.7 CST on the Cascia fault (CF) following the 1328 Mw6.49 seismic event caused by the slip on the Norcia fault (NF). a) Plan view of the spatial distribution of the CST on a plane at 7.5km depth.Contour lines of equal stress variation on the receiver fault are drawn in black (numbers are stress in bars). The red traces are the surface traces of the faults. b) 3D view of the CST on fault surfaces.

3.6 DISCUSSION

In this work, a new methodology for the evaluation of the interaction phenomena of neighboring faults is applied to the active faults of the central Apennines (The Central Apennines Fault System - CAFS in Cello et al., 1997). The choice of the aforementioned fault system is due to the good knowledge of the size, geometry and kinematics of the active faults, both for the several geological (i.e. structural and paleoseismological) and seismological available data, the last deriving from earthquakes occurred in recent decades (Rovida et al., 2019).

In the last 1000 years, the area experienced three major periods of seismic moment release (Fig. 3.1b, after Tondi and Cello 2003). The energy released during the first seismicity window (around 1300 CE) is about 1.35 times greater than the second one and 2.31 times greater than the third one. This is consistent with the magnitude overestimation of historical earthquakes documented by Vannucci et al. (2021), likely linked to the intrinsic difficulties in estimating the magnitude based on macroseismic data. These uncertainties may lead to an overestimation of the seismic moment generated by pre-instrumental events, therefore causing an imbalance in the previous comparison of cumulative seismic moments among the three time windows of seismicity. To minimize this issue, we subtracted the catalog error, therefore aligning the data with more recent and instrumentally recorded events. By doing so, the estimation of the seismic moment for each sequence can be considered mutually comparable. The energy released during the last millennium has gradually decreased going from the first to the last seismicity window, the decrease stands at 1.18E+26 dyne/cm between the first and the second and 1.36E+26 dyne/cm between the second and the third. The difference in the energy released between seismic periods also affects the correspondence among the depicted seismic cycle and the two dotted lines (i, ii) in figure 3.1b, that show the trend of a hypothetical seismic cycle if it is energy (i) and time (ii) predictable. Considering the most recent seismic events of 2009 and 2016 and taking into account the error attributed to the moment magnitude of each selected instrumental and historical earthquake (Vannucci et al., 2021), the CAFS seismic cycle seems to have lost the predictable character described by Tondi and Cello (2003). In hypothesizing the possible causes that determined this heterogeneity

among the three steps of the seismic cycle, it is worth considering the individual seismogenic sources belonging to the CAFS that released the greatest amount of energy in each of the three seismic windows. During the first seismic window the energy released by the Gran Sasso fault system unequivocally dominates (Galli et al., 2022). The second step of the seismic cycle is largely given by the earthquake of 1703 CE (Mw=6.92) which involved the entire Norcia fault system, (Tondi, 2000; Galli et al. 2018). Finally, a large part of the seismic energy released during the last seismicity window is attributed to the Mt. Vettore fault (Villani et al., 2018).

The intent to make the three-dimensional models of active faults more realistic has prompted us to reconsider the simplifications assumed in previous modeling for calculating the CST. We tested a new model that, in addition to the variable strike, considers the elliptical shape of the faults in three dimensions. For the sake of modeling we considered a ratio between the major axis and the minor axis of the ellipse of 3:2 (Gupta and Scholz, 2000), a simplification that derives from the absence of certain data on the areal extension in depth of the active faults analyzed, but which seems to have a correspondence with the extension beyond the tips of the aftershocks and foreshocks. If we assume a fault aspect ratio (length/width) equal to 1.5 the major axis of the ellipse is approximately 36.25 % longer than the surface fault trace. This is consistent with the related aftershocks distribution. So far, the elliptical shape of the fault was not considered in the calculations of the CST and seems to be influential especially in loading or unloading the tip of parallel faults.

This new fault geometry further affects the extent and shape of the stress shadow produced by the causative fault, which can impart negative stress to normal faults located both across strike and partially overlapping the causative fault. The effect of the variable strike is appreciable when the bends are quite drastic, creating a pattern with vertical bands more or less stressed than the surrounding areas. Mildon et al. (2016) demonstrated that alterations in the fault strike exert the most substantial influence on Coulomb stress transfer. A mere 10-20° shift in strike is adequate to elicit a change in stress from positive to negative. It is noteworthy that the faults with the most significant stress discrepancies are the faults that exhibits prominent bends. If, however, the positively stressed vertical bands take place on the causative fault's

surface and it ruptures entirely without any partial activation, then the stress accumulation bands should be deemed insignificant in terms of triggering future earthquakes. That is because the rest of the fault's surface has already dissipated all the previously accumulated stress, leaving those narrow positive stress bands inadequate to cause a new main shock. Nevertheless, it would be intriguing to explore the potential correlation between these positive stress zones and the occurrence of subsequent aftershocks to confirm a possible relationship. However, the simplistic assumption remains that these bends continue in depth with the same geometry as on the surface. Another simplification concerns the slip pattern, which we have often assumed as bullseye shaped due to the absence of slip data on historical earthquakes. In fact, we have noticed a large variation in the stress imparted to the receiving faults as the slip pattern of the causative faults varies.

The influence of this new pseudorealistic model has been tested both on imaginary faults positioned in different spatial relationships, and on real faults, using three historical earthquakes as examples (Colfiorito 1279 CE, Norcia 1328 CE, Cascia 1599 CE). This new methodology has been applied to these case studies to test its feasibility, effectiveness, and improvements compared to the methodology used so far.

The calculation of the CST generated by the 1279 CE Colfiorito earthquake was also useful to develop the methodology for modeling two different faults with simultaneous activation. It is not certain that both faults (CFFn and CFFs) contributed to the 1279 CE earthquake, but this is the more likely hypothesis as argued by Galli and Galadini (1999). The analysis of the effect of the single activation of each of the two faults showed how the neighboring faults can be influenced in the case of a future activation of a single segment. The similarity between the stress pattern on the Norcia fault after the activation of the CFFs alone and after the simultaneous activation of both CFFn and CFFs is remarkable, with a conspicuous difference in the CST values the latter showing a much wider range of bars, and a more limited stress shadow, while the positively stressed zone has higher values. This testifies the importance played by systems with en-echelon geometrical relationship, therefore by the partial overlapping of the tips which, in the case of normal faults, generates a negative stress zone on the receiver fault.

This feature is also common to the second example analyzed (Norcia earthquake, 1328 CE), in this case the stress shadow on the receiving fault (Cascia fault) is wider due to the greater overlap area. Furthermore, the slip on the source fault is greater than the slip of the previous Colfiorito example, this generates a much more accentuated stress reduction zone, with values reaching 6 bars. Although half of the Cascia fault seems to be inhibited, 271 years later this structure generated an earthquake with a magnitude Mw=6. This could be due to the long period between the two earthquakes which could have "recharged" the fault with interseismic stress loading. Another theoretically acceptable explanation could be the split of the fault into two segments, the southern one called Mount Alvagnano Fault (MAF) in Galli et al. (2019), and the northern one which is the Cascia Fault (CF). Having two different strikes, these two segments accumulated the stress differently, MAF stored positive stress and CF negative stress. Subsequently, in 1599 CE, the southern (positively stressed) segment may have been activated, transmitting static and dynamic stress to the northern segment, generating an instantaneous cascade effect.

In turn, the Cascia fault in 1599 CE transferred Coulomb stress to the Norcia fault, but only in restricted and defined portions of the fault. The effect of the bends along NF had a significant role in delimiting the positively stressed zones, while an extensive stress shadow is visible on the southern portion. This does not explain the massive reactivation of the Norcia fault during the 1703 CE, which involved also the Cascia segments (Cascia and Alvagnano faults in Galli et al. (2019)) and the Upper Aterno Valley faults soon after. These multiple events could be the result of the combined action of static and dynamic stress transfer, but also of the underground fluid migration or other factors influencing fault activity. In this case, in fact, the CST alone is not enough to justify the activation of so many structures.

In some cases, the link between CST and subsequent reactivation of the receiving fault (with positive stress change values) is not clear. In fact, the variation in static stress is not the only influencing factor in the dynamics of fault activation, there are other factors that should be taken into consideration. Dynamic stress transfer, for instance, can affect in the short term after a rupture, due to the passage of seismic waves. But what we certainly should implement in the applicability of this methodology is to also

calculate the contribution of the interseismic stress accumulation controlled by the aseismic creep in the viscous lower crust.

3.7 CONCLUSIONS

In this work, the seismic cycle of Tondi and Cello (2003) has been revised and updated in light of the most recent seismic events that hit the central Apennines in 2009 and 2016. Three time windows of seismicity have been identified, separated by 300-350 years of time gap. A new methodology was then proposed to analyze the spatiotemporal evolution of seismicity, considering the contribution of the CST on fault interactions. The intent was to create an innovative methodology capable of minimizing simplifications in the fault modeling. The introduced elliptical geometry of the studied faults resulted in huge changes of the static stress transfer.

Specifically, three historical CAFS-related seismic events, Colfiorito 1279 CE, Norcia 1328 CE, and Cascia 1599 CE, were examined to test this new methodology, which led to the following conclusions:

The first simulation on the 1279 CE Colfiorito earthquake highlighted the importance of the position of the causative faults respect to the receiving fault in building the stress pattern. The simultaneous activation of multiple segments increases the amount of stress transferred to the receiving fault but has little influence on its pattern. The 1279 CE earthquake, according to our calculations, promoted the subsequent reactivation of the Norcia fault ca.50 years later.

The second simulation, carried out on the Norcia fault activated in 1328 CE, demonstrated that in some cases, the classic CST is not a sufficient triggering fractor, and in these cases, the contribution of other additional factors such as the interseismic stress loading or the dynamic coseismic stress transfer could be considered influential. The Cascia fault, activated 271 years later, is in fact subjected to an extensive stress shadow that covers the northern half of the fault, while the southern one is positively stressed. The complete reactivation of this fault in 1599 could therefore be explained by the dynamic stress transfer from the southern to the northern portion during this

seismic event, or by the change in the stress state of the fault during the interseismic period.

The last simulation was performed on the Norcia fault after the reactivation of the Cascia fault in 1599 CE. It is noticed that the variable strike of the receiving fault has a marked influence on the stress distribution, but this alone is not sufficient to explain the subsequent massive reactivation in 1703 CE of the Norcia, Cascia and part of the Upper Aterno Valley faults. Therefore, other mechanisms not considered in this work may have played a relevant role.

The efficiency of this novel approach to the analysis of the seismic cycle and the influence of Coulomb static stress transfer have been tested on historical seismic activity. The presented workflow may be adopted in advanced future applications in estimating active fault rupture susceptibility, perhaps integrating additional multidisciplinary data from research branches studying other factors which may influence fault activity (e.g. fluid pressure, regional stress, interseismic stress accumulation in the viscous lower crust etc.). Important implications of this new methodology are desirable in the context of the seismic hazard assessment for the implementation of advanced and integrated strategies on seismic risk reduction and disaster management.

References

Aki K. and P. G. Richards; 1980: Quantitative Seismology, 2nd ed., edited by J. Ellis, Univ. Sci. Books, New York.

Amato A., Azzara R., Chiarabba C., Cimini G. B., Cocco M., Di Bona M., Margheriti L., Mele F., Selvaggi G., Basili A., Boschi E., Courbolex F., Deschamps A., Gaffet S., Bittarelli G., Chiaraluce L., Piccinini D. and Ripepe M.; 1998: The 1997 Umbria-Marche, Italy, earthquake sequence: A first look at the main shocks and aftershocks. Geophysical Research Letters, 25(15), 2861-2864.

Barchi M., Galadini F., Lavecchia G., Messina P., Michetti A. M., Peruzza L., Pizzi A., Tondi E. and Vittori E.; 2000: Sintesi delle conoscenze sulle faglie attive in Italia Centrale: parametrizzazione ai fini della caratterizzazione della pericolosità sismica. GNDT-Monografie

Barnett J. A., Mortimer J., Rippon J. H., Walsh J. J. and Watterson J.; 1987: Displacement geometry in the volume containing a single normal fault. AAPG Bulletin, 71(8), 925-937.

Brodsky E. E. and N. J. van der Elst; 2014: The uses of dynamic earthquake triggering. Annu. Rev. Earth Planet. Sci., 42, 317–339, DOI 10.1146/ annurev-earth-060313-054648

Cello G., Deiana G., Mangano P., Mazzoli S., Tondi E., Ferreli L., Maschio L., Michetti A.M., Serva L. and Vittori E.; 1998: Evidence for surface faulting during the September 26, 1997, Colfiorito (Central Italy) earthquakes. Journal of Earthquake Engineering, 2(2), 303-324.

Cello G., Mazzoli S., Tondi E. and Turco E.; 1997: Active tectonics in the central Apennines and possible implications for seismic hazard analysis in peninsular Italy. Tectonophysics, 272(1), 43-68.

Chiarabba C., Amato A., Anselmi M., Baccheschi P., Bianchi I., Cattaneo M., Cecere G., Chiaraluce L., Ciaccio M. G., De Gori P., De Luca G., Di Bona M., Di Stefano R., Faenza L., Govoni A., Improta L., Lucente F. P., Marchetti A., Margheriti L., Mele F., Michelini A., Monachesi G., Moretti M., Pastori M., Piana Agostinetti N., Piccinini D., Roselli P., Seccia D., Valoroso L.; 2009: The 2009 L'Aquila (central Italy) MW6.3 earthquake: Main shock and aftershocks. Geophysical Research Letters, 36(18).

Chiarabba C. and De Gori P.; 2016: The seismogenic thickness in Italy: constraints on potential magnitude and seismic hazard. Terra Nova, 28(6), 402-408.

Chiaraluce L., Di Stefano R., Tinti E., Scognamiglio L., Michele M., Casarotti E., Cattaneo M., De Gori P., Chiarabba C., Monachesi G., Lombardi A., Valoroso L., Latorre D. and Marzorati S.; 2017: The 2016 central Italy seismic sequence: A first look at the mainshocks, aftershocks, and source models. Seismological Research Letters, 88(3), 757-771.

Chiaraluce L., Valoroso L., Piccinini D., Di Stefano R. and De Gori P.; 2011: The anatomy of the 2009 L'Aquila normal fault system (central Italy) imaged by high resolution foreshock and aftershock locations. Journal of Geophysical Research: Solid Earth, 116(B12).

Galadini F. and Galli P.; 2000: Active tectonics in the central Apennines (Italy)–input data for seismic hazard assessment. Natural Hazards, 22(3), 225-268.

Galadini F. and Messina P.; 2001: Plio-Quaternary changes of the normal fault architecture in the central Apennines (Italy). Geodinamica Acta, 14(6), 321-344.

Galderisi A. and Galli P.; 2020: Coulomb stress transfer between parallel faults. The case of Norcia and Mt Vettore normal faults (Italy, 2016 Mw 6.6 earthquake). Results in Geophysical Sciences, 1, 100003.

Galli P. and Galadini F.; 1999: Seismotectonic framework of the 1997-98 Umbria-Marche (Central Italy) earthquakes. Seismological Res. Letters, 70 (4) 404-414

Galli P.; 2020: Recurrence times of central-southern Apennine faults (Italy): hints from palaeoseismology. Terra Nova, 32(6), 399-407.

Galli P., Galadini F. and Calzoni F.; 2005: Surface faulting in Norcia (central Italy): a "paleoseismological perspective". Tectonophysics, 403(1-4), 117-130.

Galli P., Galderisi A., Marinelli, R., Peronace E., Messina P. and Polpetta F.; 2019: A reappraisal of the 1599 earthquake in Cascia (Italian Central Apennines): Hypothesis on the seismogenic source. Tectonophysics, 774, 10.1016/j.tecto.2019.228287.

Galli P., Galderisi, A., Ilardo, I., Piscitelli, S., Scionti, V., Bellanova, J. and Calzoni, F.; 2018: Holocene paleoseismology of the Norcia fault system (Central Italy). Tectonophysics, 745, 154-169.

Galli P. A., Giaccio B., Messina P., Peronace E. and Zuppi G. M.; 2011: Palaeoseismology of the L'Aquila faults (central Italy, 2009, M w 6.3 earthquake): Implications for active fault linkage. Geophysical Journal International, 187(3), 1119-1134.

Galli P., Galadini F. and Pantosti D.; 2008: Twenty years of paleoseismology in Italy. Earth-Science Reviews, 88(1-2), 89-117.

Galli P., Galderisi A., Messina P. and Peronace E.; 2022: The Gran Sasso fault system: Paleoseismological constraints on the catastrophic 1349 earthquake in Central Italy. Tectonophysics, 822, 229156.

Galli P., Galderisi A., Peronace E., Giaccio B., Hajdas I., Messina P., Pileggi D. and Polpetta F.; 2019: The awakening of the dormant Mount Vettore fault (2016 central Italy earthquake, Mw 6.6): Paleoseismic clues on its millennial silences. Tectonics, 38(2), 687-705.

Galli P., Peronace E., Bramerini F., Castenetto S., Naso G., Cassone F. and Pallone F.; 2016: The MCS intensity distribution of the devastating 24 August 2016 earthquake in central Italy (MW 6.2). Annals of Geophysics, 59.

Galli P., Peronace E. and Messina P.; 2022: Archaeoseismic evidence of surface faulting in 1703 Norcia earthquake (Central Italian Apennines, Mw 6.9). Geosciences, 12(1), 14.

Gasparini C., Iannaccone G. and Scarpa R.; 1985: Fault-plane solutions and seismicity of the Italian peninsula. Tectonophysics 117, 59–78.

Gold R. D., E. Cowgill, J. R. Arrowsmith and A. M. Friedrich; 2017: Pulsed strain release on the Altyn Tagh fault, northwest China. Earth Planet. Sci. Lett., 459, 291–300, doi:10.1016/j.epsl.2016.11.024.

Gomberg J. and Johnson P.; 2005: Dynamic triggering of earthquakes. Nature, 437(7060), 830-830.

Gupta A. and Scholz C. H.; 2000: A model of normal fault interaction based on observations and theory. Journal of structural Geology, 22(7), 865-879.

Hanks T. C. and Kanamori H.; 1979: A moment magnitude scale. Journal of Geophysical Research: Solid Earth, 84(B5), 2348-2350.

Hetzel R. and A. Hampel; 2005: Slip rate variations on normal faults during glacial-interglacial changes in surface loads, Nature, 435, 81–84, DOI:10.1038/nature03562.

ISIDe Working Group; 2007: Italian Seismological Instrumental and Parametric Database (ISIDe). Istituto Nazionale di Geofisica e Vulcanologia (INGV). https://doi.org/10.13127/ISIDE

King G. C., Stein R. S. and Lin, J.; 1994: Static stress changes and the triggering of earthquakes. Bulletin of the Seismological Society of America, 84(3), 935-953.

Lin J. and Stein R. S.; 2004: Stress triggering in thrust and subduction earthquakes and stress interaction between the southern San Andreas and nearby thrust and strike-slip faults. Journal of Geophysical Research: Solid Earth, 109(B2).

Messina P., Galadini F., Galli P. and Sposato A.; 2002: Quaternary basin evolution and present tectonic regime in the area of the 1997–1998 Umbria–Marche seismic sequence (central Italy). Geomorphology, 42(1-2), 97-116.

Mildon Z. K., Toda S., Faure Walker J. P. and Roberts G. P.; 2016: Evaluating models of Coulomb stress transfer: Is variable fault geometry important?. Geophysical Research Letters, 43(24), 12-407.

Oskin M., Perg L., Shelef E., Strane M., Gurney E., Singer B. and Zhang X.; 2008: Elevated shear zone loading rate during an earthquake cluster in eastern California, Geology, 36(6), 507–510, DOI:10.1130/G24814A.1.

Pantosti D. and Boncio P.; 2012: Understanding the April 6th, 2009 L'Aquila earthquake-the geological contribution: an introductory note to the special issue. Italian Journal of Geosciences, 131(3), 303-308.

Rovida A., Locati M., Camassi R., Lolli B., Gasperini P. and Antonucci A.; 2022: Catalogo Parametrico dei Terremoti Italiani CPTI15, versione 4.0.

Shimazaki K. and Nakata T.; 1980: Time-predictable recurrence model for large earthquakes. Geophysical Research Letters, 7(4), 279-282.

Toda S., Stein R. S., Beroza G. C. and Marsan D.; 2012: Aftershocks halted by static stress shadows. Nature Geoscience, 5(6), 410-413.

Toda S., Stein R. S., Richards-Dinger K. and Bozkurt S. B.; 2005: Forecasting the evolution of seismicity in southern California: Animations built on earthquake stress transfer. Journal of Geophysical Research: Solid Earth, 110(B5).

Tondi E.; 2000: Geological analysis and seismic hazard in the central Apennines (Italy). Journal of Geodynamics, 29(3-5), 517-533.

Tondi E. and Cello G.; 2003: Spatiotemporal evolution of the Central Apennines fault system (Italy). Journal of Geodynamics, 36(1-2), 113-128.

Tondi E., Jablonská D., Volatili T., Michele M., Mazzoli S. and Pierantoni P. P.; 202: The Campotosto linkage fault zone between the 2009 and 2016 seismic sequences of central Italy: Implications for seismic hazard analysis. GSA Bulletin, 133(7-8), 1679-1694.

Vannoli P., Burrato P., Fracassi U. and Valensise G.; 2012: A fresh look at the seismotectonics of the Abruzzi (Central Apennines) following the 6 April 2009 L'Aquila earthquake (Mw 6.3). Italian Journal of Geosciences, 131(3), 309-329.

Vannucci G., Lolli B. and Gasperini P.; 2021: Inhomogeneity of macroseismic intensities in Italy and consequences for macroseismic magnitude estimation. Seismological Research Letters, 92(4), 2234-2244.

Velasco A. A., Hernandez S., Parsons T. O. M. and Pankow K.; 2008: Global ubiquity of dynamic earthquake triggering. Nature geoscience, 1(6), 375-379.

Villani F., Pucci S., Civico R., De Martini P. M., Cinti F. R. and Pantosti D.; (2018): Surface faulting of the 30 October 2016 Mw 6.5 central Italy earthquake: Detailed analysis of a complex coseismic rupture. Tectonics, 37(10), 3378-3410.

Vittori E., Deiana G., Esposito E., Ferreli L., Marchegiani L., Mastrolorenzo G., Michetti A.M., Porfido S., Serva L., Simonelli A.L. and Tondi E.; 2000: Ground effects and surface faulting in the September–October 1997 Umbria–Marche (Central Italy) seismic sequence. Journal of Geodynamics, 29(3-5), 535-564.

Walsh J. J. and Watterson J.; 1987: Distributions of cumulative displacement and seismic slip on a single normal fault surface. Journal of Structural Geology, 9(8), 1039-1046.

Wedmore L. N. J., Faure Walker J. P., Roberts G. P., Sammonds P. R., McCaffrey K. J. W. and Cowie P. A.; 2017: A 667 year record of coseismic and interseismic Coulomb stress changes in central Italy reveals the role of fault interaction in controlling irregular earthquake recurrence intervals. Journal of Geophysical Research: Solid Earth, 122(7), 5691-5711.

Acknowledgements

We would like to acknowledge Dr. Zoë Mildon and Dr. Manuel-Lukas Diercks for their kind assistance in using the "3D-Faults" MATLAB code. This work was supported by the FAR Unicam project “Novel Approach for Seismic Hazard Analysis—NoHard", responsible Emanuele Tondi.

CHAPTER 4: Investigating the Last Millennium Coulomb Stress Transfer in the Central Apennine Fault System (CAFS)

G. Valentini[1,2]., T. Volatili[1], P. Galli[3,4] and E. Tondi[1,2]

[1]School of Science and Technology - Geology Division, University of Camerino, Italy.

[2]Istituto Nazionale di Geofisica e Vulcanologia (INGV), Sezione di Sismologia e Tettonofisica, Camerino, Italy.

[3]Dipartimento Protezione Civile, Rome, Italy.

[4]Consiglio Nazionale delle Ricerche, Istituto di Geologia Ambientale e Geoingegneria, Rome, Italy.

Corresponding author: Giorgio Valentini (giorgio.valentini@unicam.it)

Tectonics

RESEARCH ARTICLE

Investigating the Last Millennium Coulomb Stress Transfer in the Central Apennine Fault System (CAFS)

G. Valentini[1,2]., T. Volatili[1], P. Galli[3,4] and E. Tondi[1,2]

[1]School of Science and Technology - Geology Division, University of Camerino, Italy.

[2]Istituto Nazionale di Geofisica e Vulcanologia (INGV), Sezione di Sismologia e Tettonofisica, Camerino, Italy.

[3]Dipartimento Protezione Civile, Rome, Italy.

[4]Consiglio Nazionale delle Ricerche, Istituto di Geologia Ambientale e Geoingegneria, Rome, Italy.

Key Points:

- The study examines the static stress transfer of 9 seismic events dating from 1279 to present in the Central Apennine Fault System (CAFS).
- The CST analysis demonstrates the key role of static stress transfer in fault activation and inhibition in central Italy.
- Innovative 3D model enhances CST accuracy in CAFS, revealing complex fault interactions and stress dynamics.

Correspondence to:
1,2 G. Valentini
giorgio.valentini@unicam.it

Received 29 Feb 2024

Abstract

The Central Apennine Fault System (CAFS) is an active tectonic region of significant importance, witnessing numerous destructive seismic events over the last millennia. Although numerous studies have underscored the role of Coulomb Stress Transfer (CST) in initiating some of the most catastrophic earthquakes, investigations focusing on its specific influence within the Central Apennine Fault System (CAFS) are limited. This research delves into a thoroughly examination of the effects of CST on both historical and instrumental seismic events of significant magnitude associated with the CAFS.

We selected 9 seismic events for the CST investigation, dating from 1279 to present. Beyond analyzing the static stress transfer for each individual seismic event, the cumulative CST of recent instrumental earthquakes was also examined to provide a comprehensive overview of the current stress scenario. Leveraging an innovative approach, faults were modeled adopting a variable strike three-dimensional elliptical shape, ensuring enhanced calculation accuracy.

Significant findings emerge from the analysis: CST has played a pivotal role in either activating or inhibiting the faults of the CAFS over the centuries. Several examined instances showcase fault reactivation following increased transferred stress within relatively short time frames, while others highlight the inhibitory effect of stress shadows.

Deepening our understanding of CST not only illuminates the role of fault interactions in past earthquake occurrences but also offers valuable insights into forecasting potential future seismic sequences. This awareness is vital in crafting targeted seismic risk mitigation strategies, thereby safeguarding local communities from the profound consequences of earthquakes.

Plain Language Summary

Over the last millennium, the Central Apennine Fault System (CAFS) in Italy has witnessed devastating earthquakes. This research delves into how Coulomb Stress Transfer (CST) has influenced these earthquakes, either activating or inhibiting faults. By analyzing nine seismic events from 1279 to the present, we found that the static stress transferred among faults played a pivotal role. Utilizing an innovative 3D model to represent the faults, we gained a better understanding of how they interact with each other and how stress is distributed in the surrounding crust. Some earthquakes increased stress on certain faults, leading to their reactivation within relatively short periods, while others created "stress shadows" that calmed seismic activity. This knowledge not only helps us understand past earthquakes but also which faults are currently more prone to causing earthquakes, thus improving seismic risk mitigation strategies to protect local communities. This study sheds light on the complex interactions among faults in the Central Apennines, offering valuable insights that can assist in planning and preventing future seismic disasters.

Abstract

The Central Apennine Fault System (CAFS) characterizes an active tectonic region of significant importance, witnessing numerous destructive seismic events over the last millennia. Although numerous studies have underscored the role of Coulomb Stress Transfer (CST) in initiating some of the most catastrophic earthquakes, investigations focusing on its specific influence within the CAFS are limited. This research delves into a thorough examination of the effects of CST on both historical and instrumental seismic events of significant magnitude associated with the CAFS.

We selected 9 seismic events for the CST investigation, dating from 1279 CE to present. Beyond analyzing the static stress transfer for each individual seismic event, the cumulative CST of recent instrumental earthquakes was also examined to provide a comprehensive overview of the current stress scenario. Leveraging an innovative approach, faults were modeled adopting a variable strike three-dimensional elliptical shape, ensuring enhanced calculation accuracy. Significant findings emerge from the analysis: CST has played a pivotal role in either activating or inhibiting the faults of the CAFS over the centuries. Several examined instances showcase fault reactivation following increased transferred stress within relatively short time frames, while others highlight the inhibitory effect of stress shadows. Examining the differences in seismic moment release across 3 seismicity windows (the first one between 1300 and 1400, the second around 1700, and the last one from 1979 to 2016) reveals distinct periods of higher seismicity in the past millennium. The latter shows the lowest cumulative seismic moment, suggesting a potential seismic gap equivalent to a Mw 6.67 earthquake. Deepening our understanding of CST illuminates the role of fault interactions in past earthquake occurrences, offering valuable insights into forecasting potential future seismic sequences. This awareness is vital in crafting targeted seismic risk mitigation strategies, thereby safeguarding local communities from the profound consequences of earthquakes.

Plain Language Summary

Over the last millennium, the Central Apennine Fault System (CAFS) in Italy generated devastating earthquakes. This research delves into how Coulomb Stress Transfer (CST) has influenced the occurrence of these earthquakes, either activating or inhibiting faults as demonstrated by numerous CST studies on major earthquakes worldwide (e.g., the San Andreas Fault, Japanese megathrusts, North Anatolian Fault). By analyzing 9 seismic events from 1279 CE to the present, we found that the static stress transferred among faults played a pivotal role. Utilizing an innovative 3D model to represent the faults, we gained a better understanding of how they interact with each other and how stress is distributed in the surrounding crust. Some earthquakes increased stress on certain faults, leading to their reactivation within relatively short periods, while others created "stress shadows" that calmed seismic activity. This knowledge not only helps us understand past earthquakes but also which faults are currently more prone to causing earthquakes, thus improving seismic risk mitigation strategies to protect local communities. This study sheds light on the complex interactions among faults in the central Apennines, offering valuable insights that can assist in planning and preventing future seismic disasters.

4.1 INTRODUCTION

The Central Apennine Fault System (CAFS, sensu Cello et al., 1997) is characterized by strong seismic activity (6.0<Mw<7.0). The CAFS is an integral component of a complex mosaic of active fault systems spanning the Apennine range, extending over 130 km between the intramontane, tectonic basins of Colfiorito and L'Aquila (Fig. 1). Since the Early Pleistocene, the central Italian Apennines have been subjected to an extensional tectonic regime oriented from northeast to southwest, leading to the formation of mainly NW-SE striking normal faults. In certain contexts, these have modified and overprinted pre-existing compressive structures, aligning with the genesis of the fold and thrust orogenic belt (Cello et al., 1997). This structural arrangement is composed of normal-oblique faulting, typically associated with the eastern margins of tectonic basins filled with sediments from the Late Pliocene-Early Pleistocene to Holocene (Cello et al., 1995, 1997; Boncio and Lavecchia, 2000; Tondi, 2000; Boncio et al., 2004; Iezzi et al., 2019; Tondi et al., 2021). The predominant NW-SE orientation of the CAFS fault planes mirrors the current stress field. The entire CAFS region displays evidence of Quaternary tectonic activity, as supported by several paleoseismological investigations (Blumetti, 1995; Galadini and Galli, 2003; Galli et al., 2005; 2008; 2011; 2018; 2020; 2022; 2023; Falcucci et al., 2015; Iezzi et al., 2023) and by the occurrence of strong, crustal seismic events (CPTI15, 2023). Relying on the empirical relationship between fault length and magnitude outlined by Galli et al. (2008), the magnitude of the largest faults of the CAFS may range between Mw 5.7 and Mw ~7.0. These faults, with lengths ranging from a few kilometers to as long as 44 km, (e.g. the Gran Sasso Fault: Galli et al., 2022), exhibit an average dip of ca. 55°. Several researchers have driven the detailed mapping of the fault scarps and the segmented surface traces of the CAFS, providing invaluable data for seismic risk assessments (Barchi et al., 2000; Galadini and Galli, 2000; Morewood & Roberts, 2000; Tondi, 2000; Roberts & Michetti, 2004; Papanikolaou et al., 2005; Papanikolaou & Roberts, 2007; Roberts, 2008; Faure Walker et al., 2009; 2010; Faure Walker et al., 2012; Wilkinson et al., 2015; Mildon et al., 2016a; Mildon et al., 2017; Tondi et al., 2021; Galli et al., 2022). However, in this study, we focus on the primary fault traces associated with the seismogenic sources, even though the surface expressions of these

structures might be more articulated, with a segmented geometry, at a smaller observation scale.

Seismic and paleoseismic catalogs (CPTI15; Rovida et al., 2022; Galli et al., 2008) allow to infer that 15 earthquakes with magnitudes Mw≥5.8 that occurred in central Italy since 1279 AD can be attributed to the CAFS. Historical records highlight three distinct periods of strong seismic activity: the 12th-13th, 17th-18th, and 20th centuries onwards (Valentini et al., 2023). In the last few decades seismic occurrences were documented in the central Apennines, affecting the whole CAFS region, starting from the northernmost Colfiorito-Sellano sequence (1997, Mw 6.0) to the southernmost L'Aquila sequence (2009, Mw 6.2) (Amato et al.,1998; Cello et al., 1998; Galli and Galadini, 1999; Tondi, 2000; Vittori et al., 2000; Chiarabba et al., 2009; Chiaraluce et al., 2011; Vannoli et al., 2012). These seismic events resulted in substantial damage, leading to many casualties and displacing countless residents (Camassi et al., 1997; Galli et al., 2009).

The main challenge of this study is to understand how static stress transfer between the faults of the CAFS has influenced seismic sequences over the past 750 years and how it might affect future seismicity. Among the various mechanisms that can inhibit or promote fault rupture (Oskin et al., 2008; Hetzel and Hampel, 2005; Brodsky and van der Elst, 2014, Wedmore et al., 2017), Coulomb Stress Transfer (CST) played a key role in the past and likely continue to do so in the future, affecting earthquake recurrence time (Harris and Simpson, 1992; Reasenberg and Simpson, 1992; King et al., 1994). King et al. (1994) demonstrated that part of the stress generated by a seismic event can be transferred to neighboring faults adjacent to the causative fault. Specifically, for faults with normal-to-oblique kinematics, the stress at the center of the causative fault (and generally at the slip zones) decreases instantaneously, transferring towards the fault tips and surrounding crust. This assumption has led many researchers (e.g., Nostro et al., 2005; Mildon et al., 2016, 2017; Wedmore et al., 2017; Wang et al., 2018; Improta et al., 2019; Mildon et al., 2019; Pino et al., 2019; Galderisi and Galli, 2020) to examine the interaction among the faults of the central Apennines, given the presence of numerous active fault systems that have been activated over the last millennium, as evidenced by extensive historical catalogs. Additionally, previous studies have analyzed the cumulative CST on historical or instrumental seismic events

outside the CAFS (e.g. Marchandon et al., 2021; Asayesh et al., 2018). However, the present study diverges in two fundamental aspects from previous research. The first one is related to the fault modeling approach; an elliptical geometry of the fault was factored into the CST calculations, and it appears to be particularly impactful in either increasing or decreasing stress at the ends of adjacent fault planes (Valentini et al., 2023). The second factor is the targeted analysis of CST on subsequently activated faults at potentially interactive distances and positions to isolate the effect of CST among earthquakes occurring in close spatiotemporal proximity. This study aims to analyze each considered earthquake individually and its effect in terms of CST on the subsequently activated fault. Here, a detailed analysis following step-by-step the CAFS seismic cycle progression to measure the influence of static stress culminates in an analysis of the cumulative stress derived from recent instrumental events.

Once the CST for each of the analyzed historical and instrumental earthquakes has been calculated, we seek to answer an intriguing scientific question that arose in a previous study (Valentini et al., 2023). The authors identify three prominent periods where most of the seismic moment was released. The initial phase spans from 1300 CE to 1400 CE, followed by a surge around 1700 CE, and the most recent phase extends from 1979 to 2016 with 300-350 years intervals. However, the scale of the released seismic moment varies across these distinct seismic periods. In the first seismicity window the cumulative seismic moment is approximately 1.35 times greater than in the second phase and about 2.31 times that of the third phase. Therefore, we hypothesize the existence of a notable seismic gap in the ongoing historical period. Should this gap exist, it implies the need for a seismic event large enough to bridge this gap. Studies regarding the connection between seismic gaps and CST have been provided by numerous authors who have demonstrated their direct correlation in various seismic regions worldwide (e.g. Stein et al., 1997; Stein, 1999; Shan et al., 2013; Xiong et al., 2017; Asayesh et al., 2020; Dong et al., 2022; Alkan et al., 2023). Therefore, CST calculation proves to be a valuable tool for understanding seismic sequences and potential seismic gaps, as well as providing insights into the most slip-prone causative faults. Finally, we will examine which faults could potentially bridge this seismic gap, in light of the CST analysis and the distribution of seismicity over the last millennium.

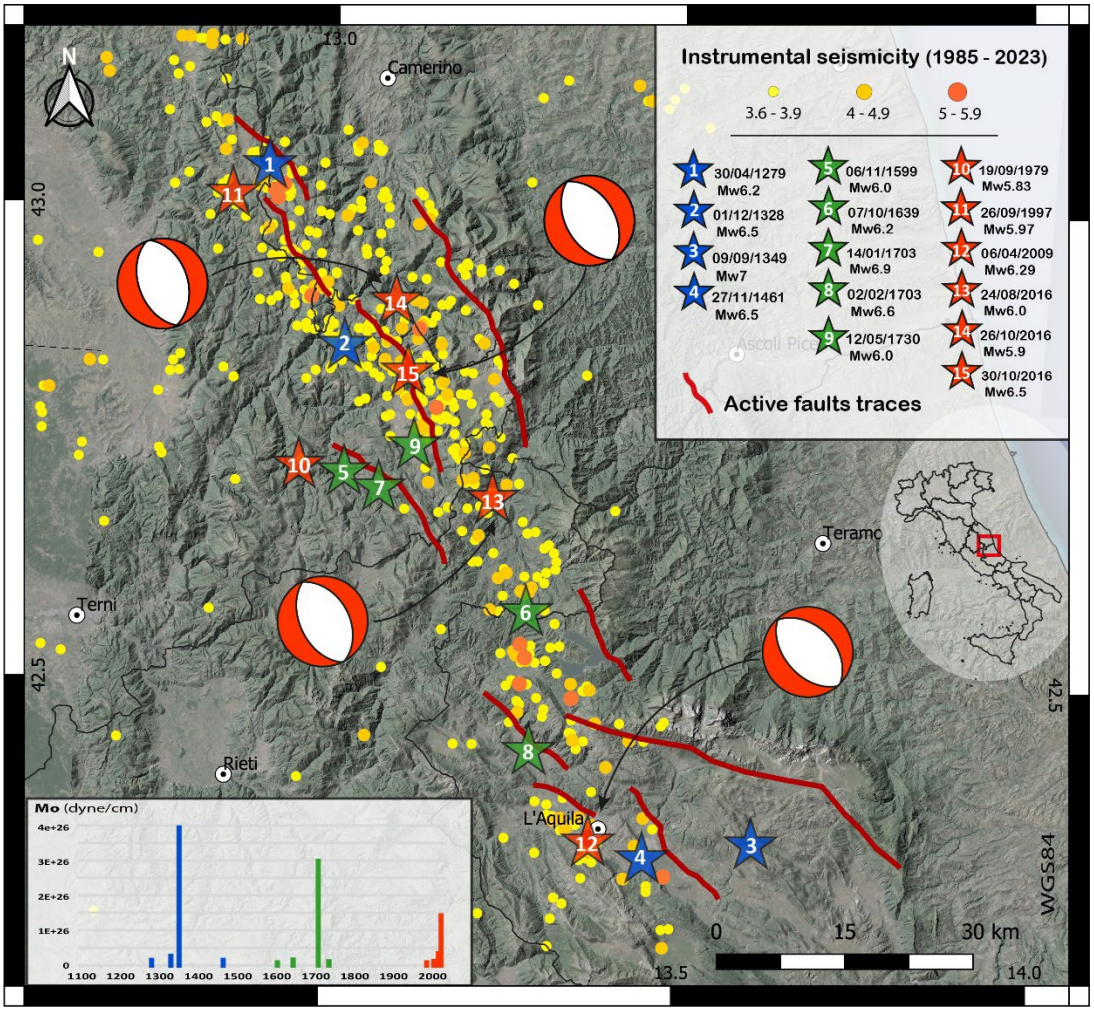

Figure 4.1 Map of the 15 seismic events with 5.8 ≤ Mw ≥ 7.0 in the CAFS area since 1279CE. Main active fault traces on the topographic surface are also shown in red (CFFn – Colfiorito Fault nord; CFFs - Colfiorito Fault south; MVF – Monte Vettore Fault; NF – Norcia Fault; CF – Cascia Fault; CMF – Campotosto Fault; GSF – Gran Sasso Fault; MF – Marine Fault; PF – Paganica-San Demetrio Fault; PTF – Pettino Fault) (Tondi, 2000; Galderisi and Galli, 2020; Tondi et al., 2020; Galli et al., 2022 and references therein). Modified after Valentini et al. (2023). Focal mechanism solutions are from Time Domain Moment Tensor (TDMT), INGV Data set (Scognamiglio et al., 2006).

4.2 SEISMICITY AND FAULT DATA

The initial step in our methodology involved the development of a basemap using a Geographic Information System (GIS). The database was populated with both tectonic and seismological information, serving dual purposes: firstly, for the selection of

seismic events to be analyzed, and secondly, as the foundation for subsequent computational tasks.

Upon a comprehensive review of the available data, seismic events were selected for analysis based on their spatiotemporal proximity to subsequent events. The three-dimensional fault modeling, geared towards Coulomb stress calculations, was performed following the approach developed in Valentini et al., (2023). This approach considers the elliptical geometry of the fault plane as the most realistic representation, favoring the accuracy of the results.

The CPTI15 catalog documents 15 seismic events that have occurred within the boundary of the region affected by the CAFS, all with Mw>6.0, spanning from 1279 CE to present day. By evaluating both the magnitude and the proximity to other fault that ruptured shortly after the primary event, we have chosen to focus on 9 of these earthquakes in relation to the Coulomb stress transfer (CST). The comprehensive list of these earthquakes, along with their specific attributes, is presented in Table 1, highlighting the ones selected for the CST analysis. For the multiple 1349 CE event we updated the catalogue parameters on the basis of the recent findings by Galli et al. (2022) who identified the seismogenic source of its northern mainshock, assigning a Mw ~7.

Subsequently, through a review of the available literature on faults, including paleoseismological analysis, geological structures, and macroseismic observations, we associated a causative fault for each earthquake event. Fault traces were mapped and digitalized using a Geographic Information System (GIS), as depicted in Fig.1. This process was grounded in robust and well-established data from original geological studies (Galli and Galadini,1999; Galadini and Galli, 2000; Barchi et al., 2000; Tondi, 2000; Galadini and Messina, 2001; Messina et al., 2002; Tondi and Cello,2003; Galli et al., 2005; Galli et al., 2010; Galli et al., 2011; Galli et al., 2016; Galli et al., 2018; Galli et al., 2019; Galderisi and Galli, 2020; Tondi et al., 2020; Galli et al., 2022 and references therein). Our fault database (Table 2) encompasses 6 fields such as: 1) fault name, 2) surface length, 3) subsurface length, 4) dip angle, 5) dip direction, 6) rake (using the Aki and Richards (1980) conventions).

Year	Month	Day	Epicentral Area	Lat	Lon	Io	Mw	ErrorMw	TMw	SOURCE
1279	4	30	Colfiorito	43.093	12.872	9	6.20	0.16	Mdm	CPTI15
1328	12	4	Valnerina	42.857	13.018	10	6.49	0.28	Mdm	CPTI15
1349	9	9	Gran Sasso	42.334	13.613	10	~7.00	ND	Mdm	Galli et al., 2022
1461	11	27	L'Aquila	42.308	13.543	10	6.50	0.46	Mdm	CPTI15
1599	11	6	Cascia	42.724	13.021	9	6.07	0.24	Mdm	CPTI15
1639	10	7	Laga Mountains	42.639	13.261	9-10	6.21	0.15	Mdm	CPTI15
1703	1	14	Valnerina	42.708	13.071	11	6.92	0.1	Mdm	CPTI15
1703	2	2	L'Aquila	42.434	13.292	10	6.67	0.11	Mdm	CPTI15
1730	5	12	Valnerina	42.753	13.120	9	6.04	0.1	Mdm	CPTI15
1979	9	19	Valnerina	42.73	12.956	8-9	5.83	0.1	InsO	CPTI15
1997	9	26	Colfiorito	43.014	12.853	8-9	5.97	0.07	InsO	CPTI15/ISIDe
2009	4	6	L'Aquila	42.309	13.510	9-10	6.29	0.07	InsO	CPTI15/ISIDe
2016	8	24	Laga Mountains	42.698	13.233	10	6.00	0.07	InsO	CPTI15/ISIDe
2016	10	26	Valnerina	42.904	13.090		5.90	0.07	InsO	CPTI15/ISIDe
2016	10	30	Valnerina	42.83	13.109	11	6.50	0.07	InsO	CPTI15/ISIDe

Table 4.1 List of historical (Mw≥6) and instrumental (Mw≥5.8) seismic events from 1279 to 2016 caused by CAFS (from CPTI15; Rovida et al., 2022 and ISIDe seismic catalogues). The seismic events selected for simulations are highlighted in green. "Lat" and "Lon" represent the coordinates of the epicenter, specifically Latitude and Longitude, respectively. "Io" denotes the epicentral intensity, and "Mw" refers to the moment magnitude along with the associated error ("ErrorMw"). The type of data used for calculating Mw is indicated in the "TMw" column: "Mdm" signifies that the data is derived from macroseismic intensities, while "InsO" indicates that the data is instrumental.

Fault	Surface length (Km)	Max subsurface length (Km)	Dip angle	Dip direction	Rake
COLFIORITO NORD	8.9	19	50	230	-80
COLFIORITO SUD	12.8	17	50	236	-83
GRAN SASSO	44.4	60	63	208	-95
PAGANICA-SAN DEMETRIO	16.6	25	56	230	-97
CASCIA	19.5	27	61	230	-66
CAMPOTOSTO	8.4	12	51	249	-86
NORCIA	22.9	31	59	243	-64
VETTORE	34.4	54	68	240	-80
PETTINO	7.6	10	63	200	-95
MARINE	6.6	9	56	226	-97

Table 4.2 List of causative faults belonging to the CAFS with related parameters from Barchi et al. (2000), Galli et al. (2010), ITHACA Working Group (2019), Galderisi and Galli (2020), Galli et al. (2022). "Surface length (Km)" and "Max subsurface length (Km)" have been respectively measured from the fault traces on the map and calculated based on the elliptical shape with a major to minor axis ratio of 3:2.

4.3 COULOMB STRESS TRANSFER ANALYSIS

Within the framework of our research, we have operated under the assumption that subsequent to seismic activity on a specific fault, Coulomb stress can propagate to neighboring faults. If this stress is positive, it might encourage fault rupture, whereas if negative, it could deter it (King et al., 1994). Numerous factors, including the distance between the causative fault and its neighboring one, their shapes, positions, dynamics, and the slip of the source fault, influence the Coulomb stress changes. Utilizing the "Coulomb 3.4" software, we derived the CST using the equation (Lin and Stein, 2004; Toda et al., 2005):

$$\Delta CST = \Delta\tau s + \mu \Delta\sigma n$$

In this equation, ΔCST represents changes in Coulomb Stress Transfer, $\Delta\tau s$ corresponds to changes in shear stress, while μ stands for the friction coefficient, and $\Delta\sigma n$ signifies changes in normal stress. We adopted a friction coefficient of 0.6, which is appropriate for normal faults in the Central Apennines. This value balances theoretical models and empirical observations (Anderson, 1951; Byerlee, 1978; Collettini et al., 2001; Fossen, 2016), making it suitable for CST analysis in this region

(e.g. Galderisi and Galli, 2020). We also tested different values for the friction coefficient between 0.2 and 0.8 (extreme values not suitable for the rheologies and tectonic regime of the CAFS) but did not obtain significantly different results in terms of CST patterns. We opted for default spatial parameters with a Poisson's ratio of 0.25 and a Young's modulus of 800,000 bar.

Regarding the three-dimensional portrayal of faults within CST calculations, we leaned on the methodology proposed by Valentini et al. (2023). We integrated a three-dimensional model featuring strike variations and an elliptical shape into our CST algorithm, believing that an accurate representation of the CAFS is pivotal to reducing potential computational inaccuracies. In advancing with the CST simulations, we endeavored to mirror the real seismic rupture dynamics, factoring in variables such as the slip distribution or the partial or entire rupture.

To ensure sharp graphical detail and enhanced bar value precision, we established a 1 km grid for the fault modeling. Faults, perceived in an elastic half-space, were outlined as lines with variable strike and segmented into 1 km units. This intricate segmentation proved to be a balanced choice between output detail and modeling duration, deviating from the more typical practice of using 2 km segments for CST modeling. Subsequently, using the "Faults 3D" Matlab tool (Mildon et al., 2016), we were able to construct 3D fault models, drawing from actual traces and determining a slip distribution for each fault. We chose to compute the Coulomb stress for each fault segment, maintaining a consistent friction coefficient. Where available, we used actual slip data for recent earthquakes taken from the models in the database of finite-fault rupture models of past earthquakes (SRCMOD – Mai and Thingbaijam, 2014). For less documented seismic events, we assumed a centered slip distribution, reminiscent of a bull's eye pattern, depending on the relative seismic moment. In instances where the fault width was not specified in the reviewed literature, we used standard geometric relationships (Gupta and Scholz, 2000) to determine it, basing our calculations on a 1.5 aspect ratio (length/width). For faults with an extended length, their maximum depth was aligned with the thickness of the seismogenic layer, approximately 15 km (Gasparini et al., 1985; Chiarabba and De Gori, 2016). To optimize CST data comprehension, we crafted three distinct representations. Initially, a traditional CST map was produced at a depth of 5 km, in plan view, providing an approximation of

CST distribution within the surrounding crust. This information was then translated to KML format for georeferenced visualization on Google Earth Pro®. Lastly, we crafted cross-sections perpendicular to fault strikes and developed a 3D model of the fault planes, obtaining the CST values for each 1 km fault segment, thus ensuring heightened precision in the assessment of stress for each individual segment.

4.4 RESULTS

Here we present the outcomes of CST calculations undertaken for nine historical and instrumental earthquakes. As aforementioned, our primary objective is to determine the potential correlation between subsequent seismic events triggered by CST and the extent to which this phenomenon influences the rupture of neighboring faults. The selected earthquakes, chosen based on their seismic moment and proximity (both spatial and temporal) to subsequently activated faults, include:

1) Colfiorito earthquake, Mw 6.2 (30/04/1279);

2) Gran Sasso earthquake, Mw ~7.0 (09/09/1349);

3) Norcia and Cascia earthquake, Mw 6.92 (14/01/1703);

4) Upper Aterno earthquake, MW 6.67 (02/02/1703);

5) Colfiorito earthquake, Mw 5.97 (26/09/1997);

6) Paganica earthquake, Mw 6.29, (06/04/2009);

7) Partial rupture at the southern tip of Mt. Vettore fault, Mw 6.00 (24/08/2016);

8) Partial rupture at the northern tip of Mt. Vettore fault, Mw 5.9 (26/10/2016);

9) Complete rupture of Mt. Vettore fault, Mw 6.5 (30/10/2016);

10) Cumulative CST generated by the 1997 Colfiorito, 2009 L'Aquila, and 2016 Vettore earthquakes.

Subsequent sections will delve into the specifics of how Coulomb stress transfers from the ruptured fault, "causative fault", to the afterwards activated fault, "receiver fault". It is worth noting that despite our calculations are based on the best available data,

there is still a significant lack of information regarding historical earthquakes (i.e., slip models, epicenter location, and magnitude), which implies an inherent uncertainty in the results obtained.

4.4.1 COLFIORITO EARTHQUAKE (M_W 6.20, 30/04/1279) VS NORCIA FAULT

We examined the 1279 CE earthquake that roughly occurred in the same region affected by the 1997 earthquake. This event was generated by the Colfiorito fault system, comprised of two primary structures: the Colfiorito north and south faults, here denoted as CFFn and CFFs. This fault system exhibits an en-echelon arrangement with a dextral step-over, as documented by Galli and Galadini (1999). According to these authors, the 1279 earthquake might share characteristics with the 1997 event, activating the same segments, especially Colfiorito north and south, which we modeled as a simultaneous rupture (Fig. 4.2a). Nearly half a century later, in 1328, the Norcia fault (*sensu* Galli et al., 2018; 2023) experienced a rupture, leading to a Mw 6.49 earthquake (12/4/1328). This fault lies a few kilometers southeast of the Colfiorito fault system and has a similar orientation. Given the spatial and temporal proximity between the two earthquakes, we designated the parameters of the Norcia fault as a receiver fault and estimated the stress transfer induced by the 1279 earthquake.

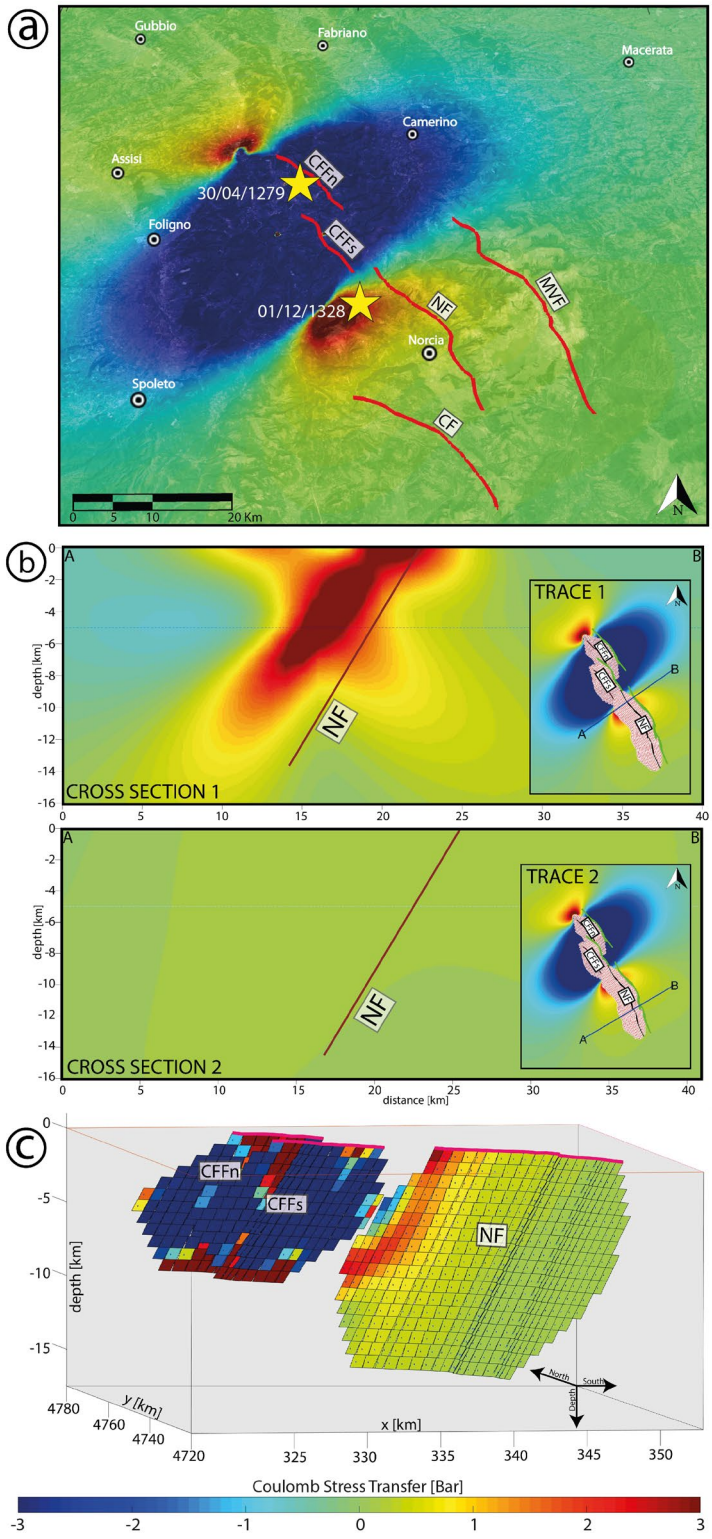

Figure 4.2 a) oblique view of the CST distribution on a plane located at a depth of 5 km. The causative faults are Colfiorito North and South, and the receiver fault is the Norcia Fault. b) Cross-sections perpendicular to the receiver fault (NF) one at the northernmost part of the fault, near the causative fault and the other at the southern portion of the Norcia fault. Note the difference in the CST pattern when moving just a few kilometers away from the causative

fault. c) 3D view of the causative and receiver faults. Note that the CST is calculated on each of the rectangles that make up the entirety of the faults.

This calculation considered planes with a dip direction of 243°, a dip angle of 59°, and a rake of -64°, as the Norcia fault. Our computational results in plan view (Fig. 4.2a) reveal two prominent zones of negative stress, extending in opposing directions, toward the northeast and southwest, neither of which envelopes the CAFS faults. In turn, one positive stress lobe emanating from the fault tips of the causative Colfiorito faults targets the north-westernmost part of the Norcia fault, inducing a stress increase of up to 2 bars. The positive stress on the Norcia fault tends to wane rapidly moving southwards. Consequently, the northern part of the Norcia fault is more prone to rupture than its southern counterpart, which appears almost wholly unaffected, as highlighted in the three-dimensional stress modeling (Fig. 4.2c). We constructed two parallel cross-sections, each approximately 40 km in length and perpendicular to the Norcia fault's orientation (Fig. 4.2b). The second section is located roughly 18 km southeast of the first, near the Colfiorito fault system. The stress distribution within the crust exhibits notable variance when transitioning from the source fault, showing peak values of more than 3 bars in the first section and a maximum of 0.2 bars in the second.

4.4.2 GRAN SASSO EARTHQUAKE (MW ~7.0, 09/09/1349) VS PAGANICA FAULT

The 1349 earthquake, which impacted the southern part of our study area, stands out as the strongest seismic event in the historical records we reviewed. Galli et al. (2022) ascertained that the causative fault for the northern mainshock of the 1349 seismic sequence was the Gran Sasso fault, a fault spanning 44 km. This earthquake, with a likely magnitude Mw ~7.0, damaged vast parts of central Italy, causing the partial collapse of some monuments in Rome. Given the fault segmented nature at the surface, we approached the seismic source as a unique, coherent unit. Over a century later, in 1461, a Mw 6.5 earthquake occurred in the hanging wall region of the Gran Sasso fault. This was attributed to the Paganica-San Demetrio fault (Galli et al., 2011), located roughly 10 km southwest of the Gran Sasso fault, representing thus a twin of

the 2009 L'Aquila event, which was also sourced by this fault. Despite the considerable temporal gap between the two events, our choice to designate the Paganica fault as the receiver fault hinges on its proximity to the Gran Sasso Fault, a region frequently subject to stress shadows in typical CST scenarios between parallel faults. Our hypothesis finds support in the CST results at a 5 km depth in plan view (Fig. 4.3a).

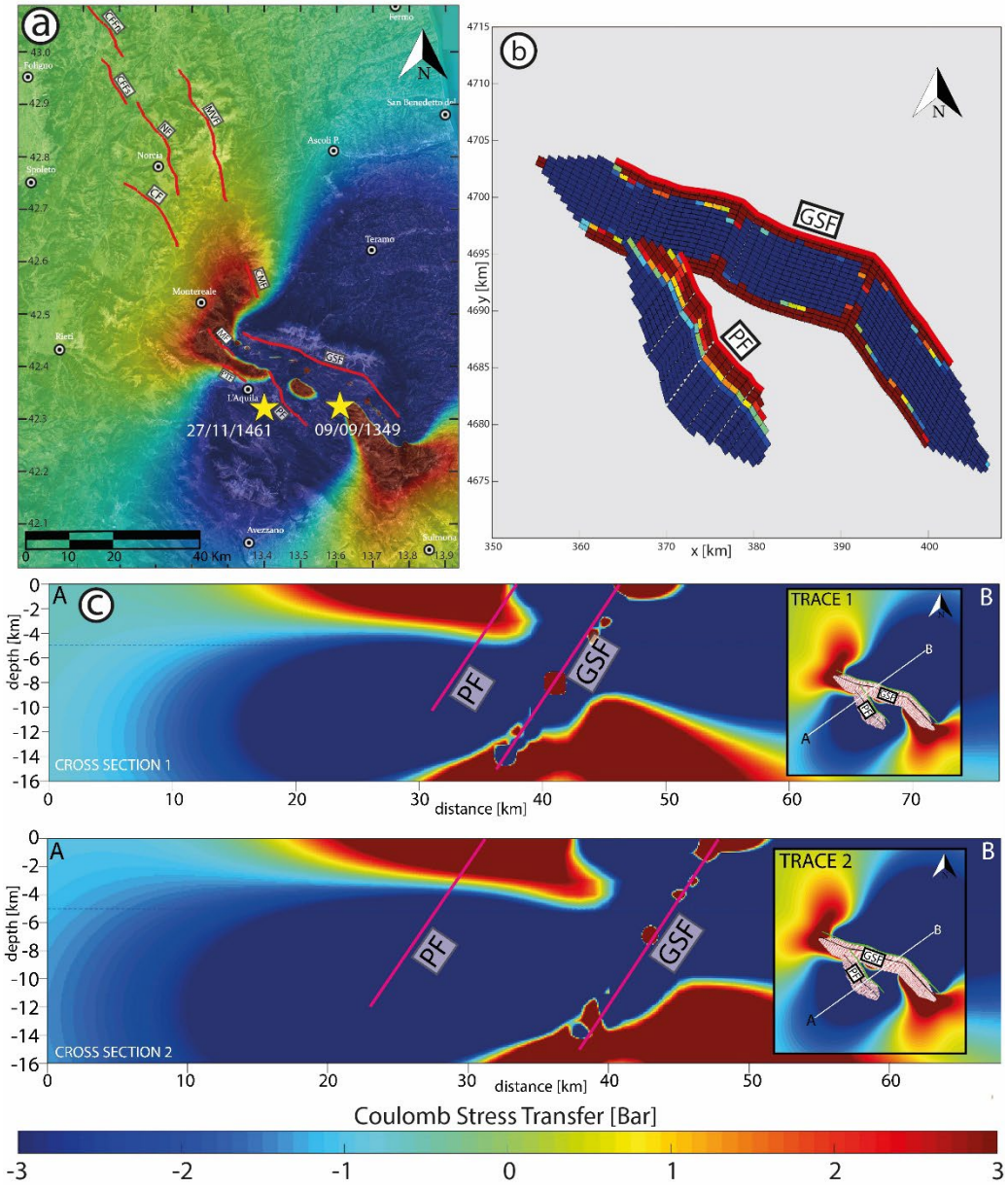

Figure 4.3 a) Plan view of the CST distribution on a plane located at a depth of 5 km. The causative fault is the Gran Sasso Fault, and the receiver fault is the Paganica Fault. b) 3D

view of the causative and receiver faults. Note that the CST is calculated on each of the rectangles that make up the entirety of the faults. c) Cross-sections perpendicular to the receiver fault (PF), one at the northernmost part of the fault and the other Cross-section at the southern portion of the Paganica fault.

A pronounced stress shadow extends perpendicularly southwest from the fault strike, with the Paganica fault situated within this pronounced zone of stress diminution. Northeastwards, the stress shadow influence is expansive, evidenced by the blue lobe stretching nearly 80 km directly from the causative fault, underscoring the far-reaching impact of an earthquake of such scale on the neighboring crust. As is common with normal faults, the positive stress lobes are considerably more confined. Twin red lobes, emanating from the Gran Sasso fault deep terminations, project southeast and northwest. These lobes, registering stress increases exceeding 5 bars, span over 30 km in both directions and widen northeast-southwest as one distances from the causative fault. The plan view further reveals a conspicuous concentration of positive stress between the Gran Sasso and Paganica faults. This cluster signifies the deep root of a positive stress lobe, originating from a 5 km depth and reaching the surface, as the cross-section in figure 4.3c displays. The plan view also shows positive stress lobes encompassing sections of the Marine, Pettino, and Campotosto faults. In contrast, the Paganica fault seems wholly enveloped in a stress shadow. Yet, cross-sectional analyses and 3D stress distribution (Fig. 4.3b) depictions on fault planes reveal that the Paganica fault's superficial segment experiences up to 5 bars of positive stress transfer throughout its length, from the surface down to 5 km. Notably, this stress distribution remains largely consistent along the fault's strike. The upper cross-sectional representation in figure 4.3c mirrors the lower one, positioned about 11 km further to the southeast. Conversely, the Gran Sasso fault exhibits a sharp stress reduction at the slip sites, typical of full fault ruptures where stress drops to nil. Nevertheless, the fault's extremities exhibit positive stress, as do the two marked bends dividing the fault into three segments with marginally distinct strikes. Additionally, it's worth noting that a minor positive stress magnitude (below 1 bar) reaches the southern extremities of the Monte Vettore, Norcia, and Cascia faults.

4.4.3 NORCIA AND CASCIA EARTHQUAKE (Mw 6.92, 14/01/1703) VS PAGANICA FAULT

The Norcia Fault System (NFS), which includes the Cascia fault and Mt. Alvagnano fault (here considered as part of the CF; see Galli et al., 2018; 2020), has been responsible for some of the most powerful earthquakes in the western Mediterranean. Extending over a distance of 30 km, the NFS is composed of multiple interconnected segments. Like other fault systems found in the Apennines, the individual segments of the NFS have the capacity to rupture either independently or collectively, resulting in earthquakes of moderate to high intensity. However, catastrophic events occur only when the entire system (Norcia faults plus Cascia faults) undergoes rupture, as witnessed by the Mw 6.9 earthquake on January 14, 1703 (Galli et al., 2022). Shortly after the strong earthquake in Norcia, on February 2, 1703, another devastating earthquake (Mw 6.7) struck the upper Aterno Valley, causing widespread destruction of the surrounding villages, including L'Aquila (MCS 9). This seismic event affected an extensive area located approximately 40 km southeast of the fault responsible for the earthquake on January 14. The close spatial and temporal proximity of these two earthquakes makes them ideal for studying the interaction between the fault systems involved, specifically in terms of CST. Following the study by Galli et al. (2011), the receiver faults considered in this analysis are the Marine Fault, Pettino Fault, and Paganica-San Demetrio Fault (i.e., the Upper Aterno fault system in Galadini and Galli, 2000), all of which experienced rupture on February 2, 1703. It is worth noting that, once again, the rupture did not occur along a single fault but rather involved a series of segments that likely ruptured simultaneously (Moro et al., 2013). As can be inferred from figure 4.4a, the area subjected to changes in Coulomb stress after the earthquake on January 14th is extensive. The two lobes of negative stress usually generated by slip on normal faults extend for tens of kilometers in the northeast-southwest direction, placing the Monte Vettore Fault (MVF) under a significant stress shadow zone.

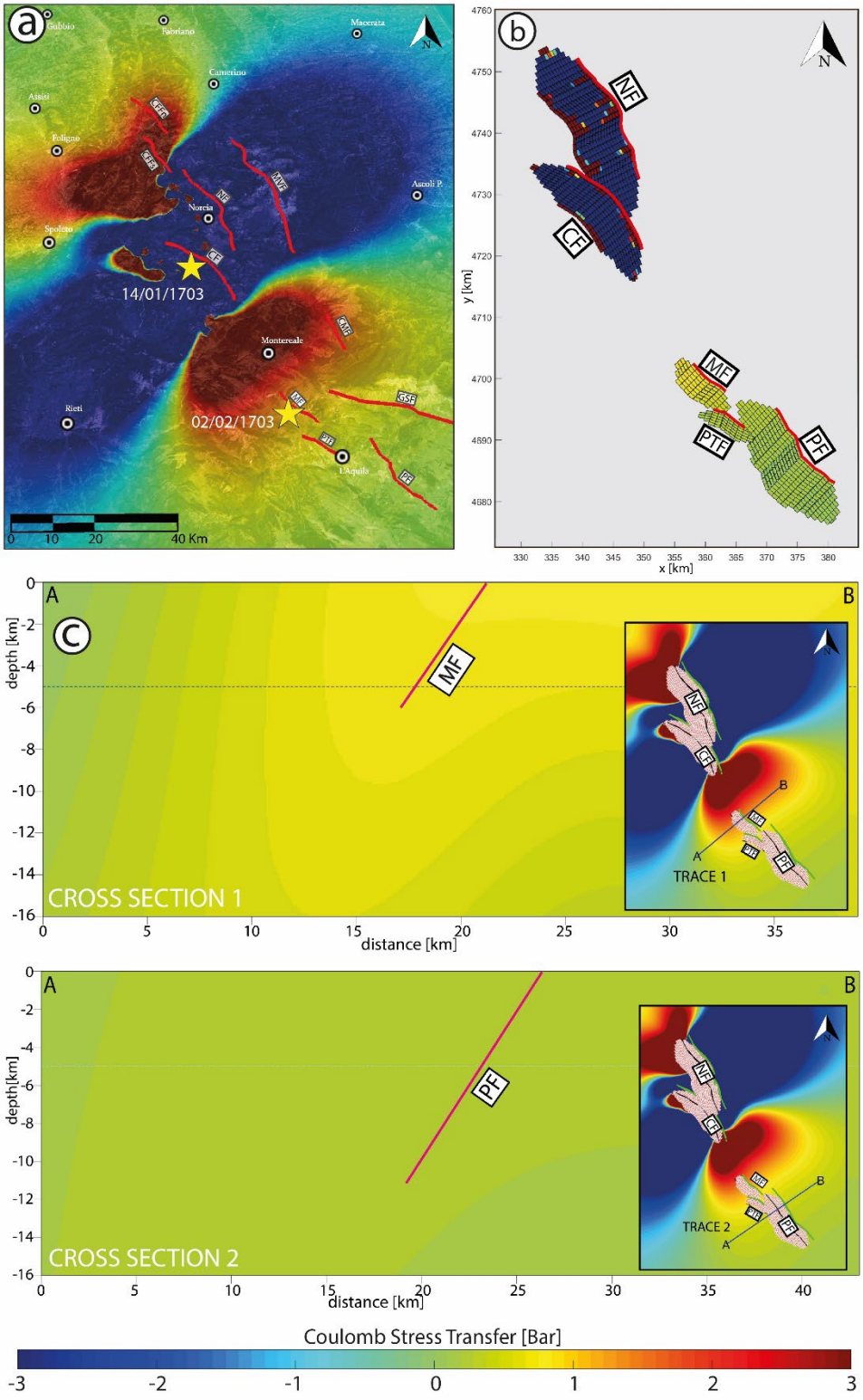

Figure 4.4 a) Plan view of the CST distribution on a plane located at a depth of 5 km. The causative faults belong to the Norcia Fault System and the receiver fault is the Paganica Fault. b) 3D view of the causative and receiver faults. Note that the CST is calculated on each of the rectangles that make up the entirety of the faults. c) Cross-sections perpendicular to the receiver faults (MF and PF), one at the northernmost part of the MF, near the causative faults

and the other Cross-section on the PF. Note the difference in the CST pattern when moving just a few kilometers away from the causative fault.

Within the shadow zone, a few kilometers west of the CF, a spot of positive stress appears, likely generated at the northern tip of the CF, creating heterogeneity in the CST pattern. However, there is no active fault present in the positively stressed zone. Two large lobes of stress increase (up to 5 bars) extend northwest and southeast from the middle zone between the two causative faults. The stress increase towards the northwest largely involves the Colfiorito fault system, branching towards Fabriano and Foligno, creating the classic "butterfly wing" pattern. This latter shape is absent in the positive lobe that extends from the causative faults towards the southeast. Here, the extent of the positively stressed crustal area appears larger and reaches to influence the Campotosto fault (CMF) and the northern tip of the Marine fault (MF). A modest increase in Coulomb stress is also recorded on the Pettino fault (PTF) and the northern tip of the Gran Sasso fault. In these last two cases, the stress increases by no more than 0.8 bars. It follows that the only fault involved in the earthquake on February 2nd, 1703, which received a significant CST "push" from the earthquake of January 14th of the same year, is the Marine fault. In the cross section and three-dimensional modeling (fig. 4.4b and fig. 4.4c), the northern tip of the Marine fault experiences an increase in stress of approximately 1 bar, gradually decreasing moving south along the fault. The Paganica fault, as shown in cross section 2, exhibits a slight stress increase of about 0.3 bar. Overall, the three receiver faults seem to have undergone a stress increase significantly lower than what would have been expected from an earthquake of such magnitude.

4.4.4 UPPER ATERNO EARTHQUAKE (MW 6.67, 02/02/1703) VS NORCIA FAULT

The last historical earthquake considered occurred days after the devastating earthquake that struck the Norcia area. On February 2, 1703, a probable cascading activation of three faults in the southern portion of the CAFS generated an earthquake with a magnitude of Mw 6.67. The causative faults were identified (Galli et al., 2011) as belonging to the Upper Aterno Fault System (Marine, Pettino, and Paganica-San

Demetrio faults). Given their sizes, these individual faults would not be capable of producing such magnitude on their own. Thus, a simultaneous activation of the entire fault system is implicated. The subsequent earthquake occurred in 1730, 27 years later, involving the southern half of the Norcia fault, which had also been previously activated in 1703. This Mw 6.04 earthquake was taken as a reference to decide the receiver fault for this simulation. The plan view modeling in Fig. 4.5a reveals a large stress shadow divided into two main lobes directed northeast and southwest. The first completely covers the Gran Sasso fault, depriving it of about 5 bars of stress. The Campotosto fault, especially its southern half, also underwent diminishing stress. The second lobe does not encompass any active and capable fault present in our study. The causative faults all lie within the stress shadow with localized spots of very high positive stress, which are not considered significant as the stress on the causative fault is assumed to reduce to zero after the stress drop due to its activation. Two lobes of positive stress radiate from the northern tip of the Marine fault northwestward and from the deep southern tip of the Paganica-San Demetrio fault southeastward. The first of these affects the southern half of the Cascia fault, transferring a maximum of 0.8 bars of positive stress. However, the next fault to activate was the Norcia fault, which received only 0.5 bars of positive stress exclusively at its southern tip. The minimal influence exerted by this earthquake on the Norcia fault is better seen in the three-dimensional modeling in Fig. 4.5b. The Vettore fault also underwent a very modest stress transfer of about 0.5 bars, again only in the southern portion. The stress lobe branching from the Paganica-San Demetrio fault southward, however, has a greater extent, reaching the cities of Avezzano and Sulmona. Given the meager stress transfer to the receiver fault, it was deemed unnecessary to proceed with the creation of cross sections along that fault.

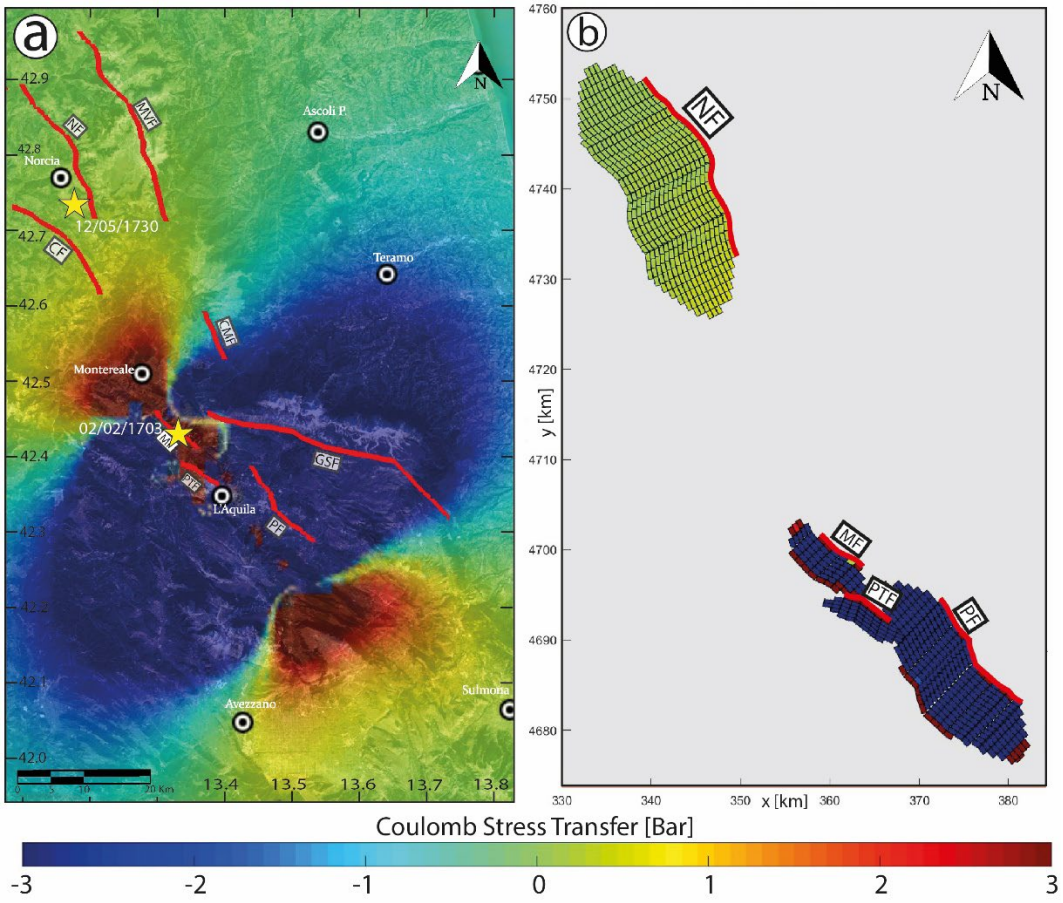

Figure 4.5 a) Plan view of the CST distribution on a plane located at a depth of 5 km. The causative faults are the Marine, Pettino and Paganica-San Demetrio faults (Upper Aterno Fault System) and the receiver fault is the Norcia Fault. b) 3D view of the causative and receiver faults. Note that the CST is calculated on each of the rectangles that make up the entirety of the faults.

4.4.5 COLFIORITO EARTHQUAKE (MW 5.97, 26/09/1997) VS VETTORE FAULT

The first earthquake considered from the instrumental catalogs is the 1997 earthquake that occurred in the Colfiorito Basin, in the northernmost part of the CAFS. This earthquake is considered analogous to the historical earthquake of 1279 (Galli and Galadini, 1999). Therefore, we modeled both earthquakes in the same manner, with the only difference being the generated seismic moment (and consequently, the slip), which is lower for the more recent earthquake. It should be noted that the inferred magnitude generated by the Colfiorito fault system in 1279 was Mw 6.2, while in 1997, the measured value for the 26 September mainshock was Mw 5.97. In addition to the

mainshock, a series of closely spaced events occurred, all between the months of September and October. A foreshock with a magnitude of Mw 5.66 alerted the population at 00:33, causing many people to leave their homes, thereby limiting injuries and fatalities. At 9:40, the mainshock of Mw 5.97 occurred, followed by a Mw 5.22 and a Mw 5.47 aftershocks. For this reason, it was appropriate to calculate the cumulative stress generated by all four major seismic events, resulting in a cumulative seismic moment of 1.92572E+25 dyne-cm, thereby approaching the seismic moment generated by the 1279 earthquake. The contribution of aftershocks and foreshocks in the overall CST framework resulted in only slight changes in the amount of stress (both positive and negative) transferred to the surrounding crust. Comparing the results of the 1279 and the 1997 earthquakes (see section 3.1), it can be observed that a modest increase in slip or magnitude has an important influence on the amount of Coulomb stress transfer (CST) around the causative faults. In this simulation, the receiver fault is the Monte Vettore fault, which activated in 2016, causing three devastating earthquakes in close succession. The aim is to understand if the 1997 earthquake played a role in the subsequent activation of the MVF in 2016.

Figure 6a shows the cumulative stress pattern generated at a depth of 5 km by the simultaneous activation of CFFn and CFFs in the 1997 sequence on faults with the same rake and strike as the MVF. The stress shadow stands out compared to the zones of positive CST, extending almost symmetrically in the northeast-southwest direction. The two positive lobes seem to be positioned like those generated by the 1279 earthquake, with no significant differences in intensity and extent reaching a positive stress value of 3 bars. However, as depicted in figure 6b and c, it is not enough to significantly influence the stress on the Monte Vettore fault, which remains almost unchanged, as if it had not been affected by the CST generated by the 1997 earthquake except in the northern tip, where the stress state depends on the fault depth. From 0 to 8 km depth, in the northern tip of the receiver fault, the effect of the stress shadow is clearly visible, with a stress reduction up to -1 bar. However, at greater depths in the same area, the Monte Vettore fault appears to have received modest positive stress (up to 0.4 bar). In figure 6a, it can be seen that only the northern tip of the Norcia fault undergoes a substantial increase in stress of about 1.5 bars, but just a few kilometers away towards the MVF, this amount gradually decreases until it is almost negligible.

The highest value of CST recorded on the MVF after the 1997 earthquake is only 0.4 bars. The same applies to the Cascia fault, of which only the northern tip is slightly influenced (0.2-0.4 bars) by the slip of the Colfiorito faults.

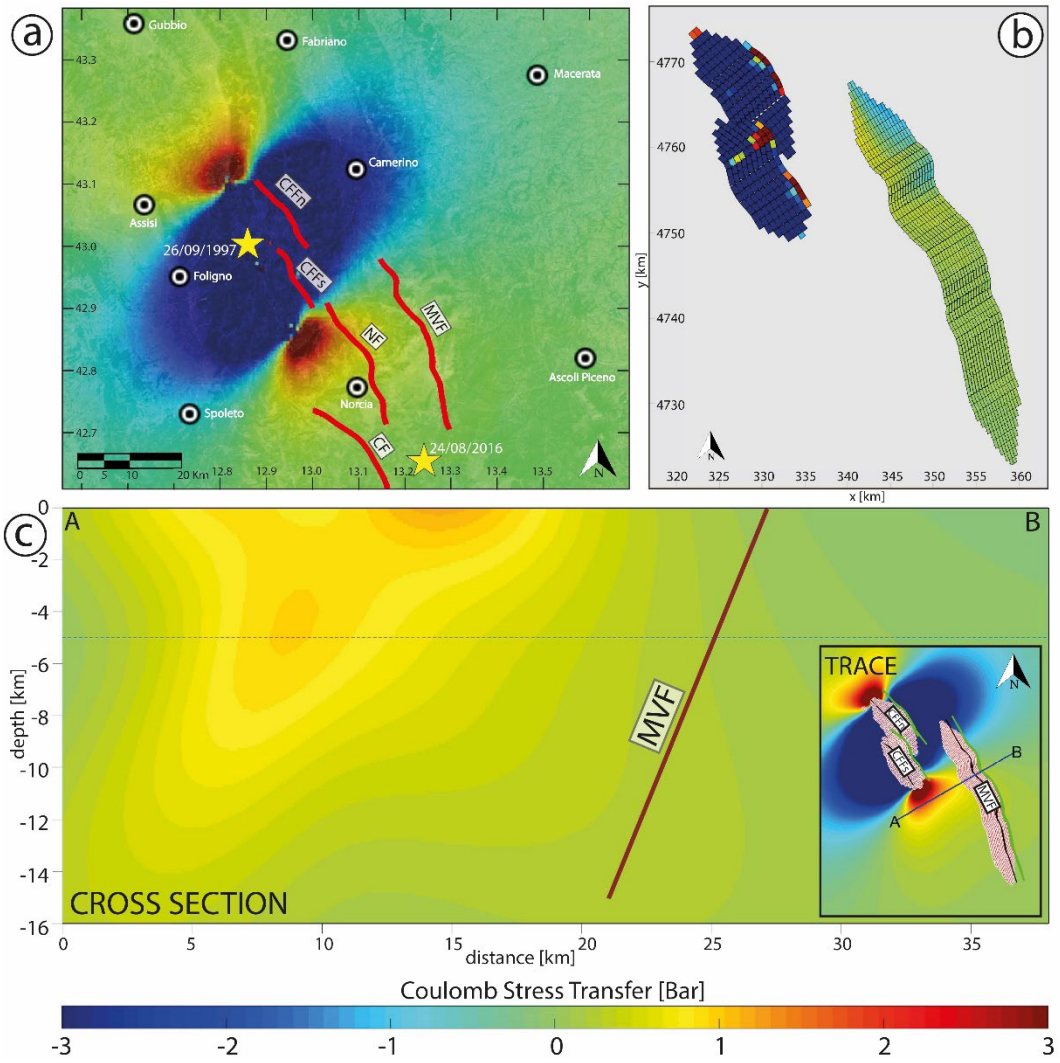

Figure 4.6 a) Plan view of the cumulative CST distribution on a plane located at a depth of 5 km. The causative faults are Colfiorito North and South, and the receiver fault is the Mt. Vettore Fault. b) 3D view of the causative and receiver faults. Note that the cumulative CST is calculated on each of the rectangles that make up the entirety of the faults. c) Cross-section perpendicular to the receiver fault (MVF).

4.4.6 PAGANICA EARTHQUAKE (MW6.29, 06/04/2009) VS VETTORE FAULT

On April 6, 2009, the Abruzzo city of L'Aquila was severely struck by a Mw 6.29 earthquake. The proximity of the epicenter to the city contributed to hundreds of casualties and significant buildings damages and collapses. The causative fault of this earthquake has been identified by several authors as the Paganica-San Demetrio fault (Anzidei et al., 2009; Gori et al., 2009; Walters et al., 2009; EMERGEO Working Group, 2010; Cinti et al., 2011; Galli et al., 2011; Chiaraluce, 2012; Pantosti and Boncio, 2012). This structure, spanning 16.6 km (at the surface), is an almost pure dip-slip fault and has generated at least two significant historical earthquakes (1461 and 1703). Just 7 years after the activation of the Paganica-San Demetrio fault, another earthquake struck an area located approximately 60 km to the north-northwest. The series of earthquakes that hit the central Apennines in 2016 were generated by the Monte Vettore fault, which had been silent for many centuries before (Galli et al., 2019). At the surface, the Monte Vettore fault is about 34 km long and was capable of generating multiple events within a short period. The seismic sequence produced an initial Mw 6.0 earthquake on August 24, 2016, followed by an Mw 5.9 on October 26. Finally, the most intense seismic event occurred on October 30, with a magnitude of Mw 6.5.

Given the short time interval between the earthquake of 2009 and those of 2016, we are interested in understanding the potential influence of the activation of the Paganica-San Demetrio fault on the Monte Vettore fault.

As expected, the distance between the two faults and the moderate magnitude of the L'Aquila earthquake are factors that leave the Monte Vettore fault almost untouched by the stress transfer resulting from the activation of the Paganica-San Demetrio fault. As evident from the plan view modeling in Fig. 4.7, the positive stress lobes extending from the fault tips towards the northwest and southeast have a limited extent of a few kilometers, partially embracing only the Marine and Pettino faults. Even the northwestern tip of the Gran Sasso fault receives moderately low positive stress (approximately 0.7 bar). Positive stress spots stand out as embedded within the stress shadow on the hanging wall of the causative normal fault, located about 4-5 km southwest of the surface trace. Towards the northeast, the stress shadow is more

extensive and covers the central third of the Gran Sasso fault. On the other hand, towards the southwest, no faults are inhibited by the zone of decreased Coulomb stress. The Monte Vettore fault, taken as the receiver fault in this calculation, experiences a stress transfer of no more than 0.2 bars, which is negligible. Three-dimensional analysis was not deemed necessary as the receiver fault did not show significant signs of stress transfer from the activation of the Paganica-San Demetrio fault, however, a cumulative three-dimensional modeling of all recent seismic events has been performed, as shown in Figure 4.11. Since the southern sector of the CAFS has recently only experienced the L'Aquila earthquake, this model can be referred to for a three-dimensional visualization of CST on the faults surrounding the Paganica-San Demetrio fault.

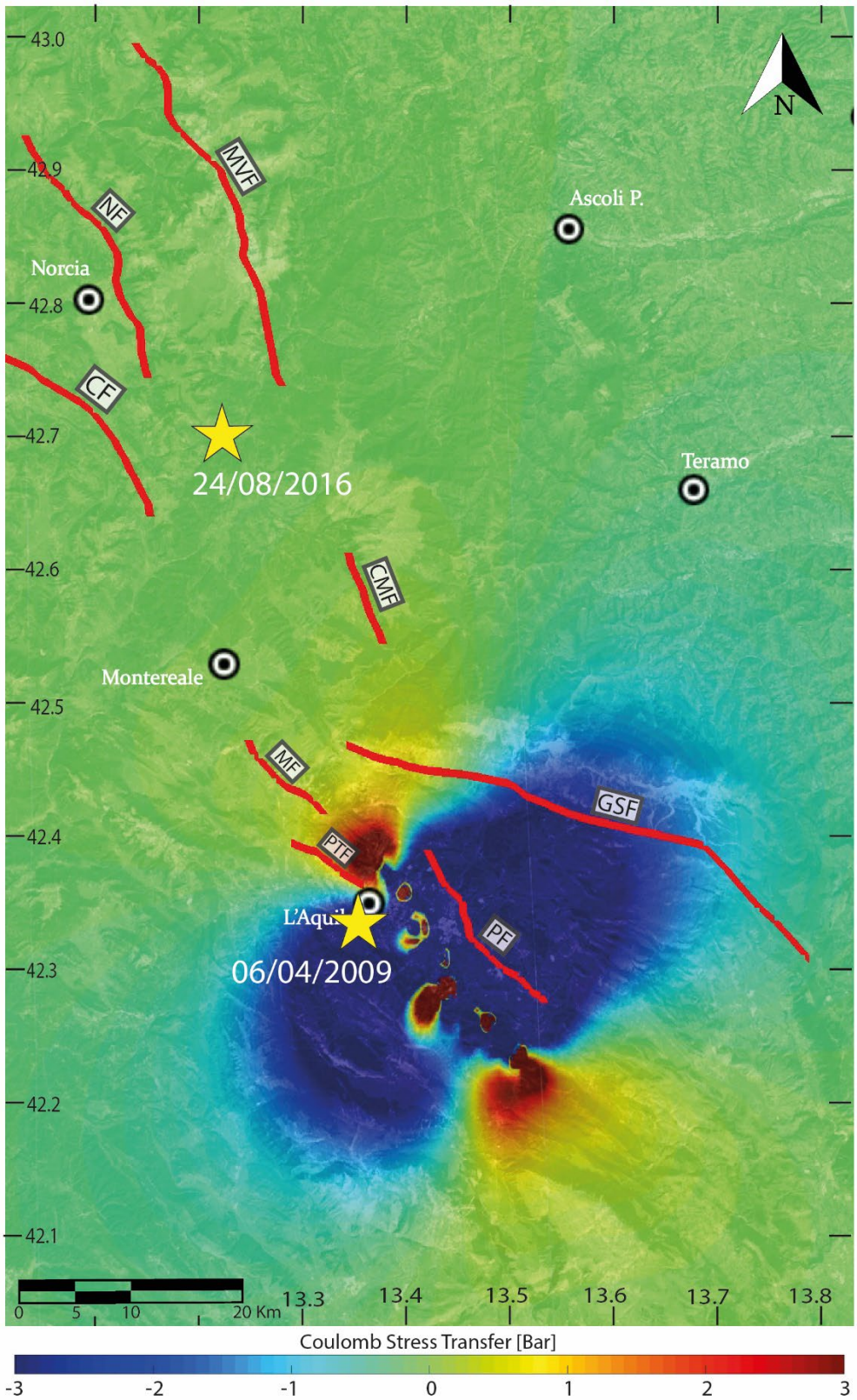

Figure 4.7 Plan view of the CST distribution on a plane located at a depth of 5 km. The causative fault is the Paganica-San Demetrio fault, and the receiver fault is the Mt. Vettore Fault.

4.4.7 THE 2016 MT. VETTORE FAULT SEISMIC SEQUENCE

The last seismic event in the catalogs struck the central Apennines in 2016. The Mt. Vettore fault system, comprising dozens of surface segments with an en-echelon arrangement, generated three earthquakes within a little over two months. The main seismogenic structure experienced partial activation, first at the southern fault tip on August 24th (Mw 6.0), involving also the Amatrice fault, which is located along the strike to the south (in our model, it is integrated with the southern tip of the Mt. Vettore fault), then at the northern fault tip on October 26th (Mw 5.9), and finally, the central segment was activated, involving the two previously activated tips, resulting in a catastrophic earthquake of magnitude Mw 6.5.

In this section, we analyze the results obtained from the modeling of both the partial activation and the entire rupture of the Monte Vettore fault. In this case study, the receiver fault is the same as the causative fault, infact we want to understand the influence that a partial rupture of one segment had on the remaining unactivated part of the fault. The objective is to determine if and how much the three subsequent events were driven by Coulomb stress transfer.

Regarding the complete rupture on October 30, we will analyze the CST on the Norcia fault, which is in a precarious position relative to the Monte Vettore fault. The Norcia fault raises concern due to its size, its proximity to several inhabited areas, and the time elapsed since its last total reactivation in 1703 (Galli et al., 2023). In order, we will analyze:

i) The effect of the southern tip partial rupture on the central-northern portion of the fault.

ii) The effect of the northern tip partial rupture on the central-southern portion of the fault.

iii) The effect of the entire fault surface rupture on the surrounding crust and, in particular, on the Norcia fault.

On August 24th, when the southern tip of the Monte Vettore fault ruptured together with the northern tip of the Amatrice fault, it generated a wide stress shadow that partially affected the southernmost section of the Norcia fault and part of the Cascia

fault, reducing stress by approximately 1 bar. The positive stress transfer involved two lobes radiating towards the northwest and southeast from the rupture surface (Fig. 4.8a). The southern lobe did not affect any of the faults in the CAFS except for the Campotosto fault, which, however, experienced a negligible CST (around 0.2 bar). Of interest is the northern lobe of positive stress that involves part of the central section of the same fault. The sections in Fig. 4.8c show that the locked zone of the fault closest to the ruptured portion, after the August 24th, is highly stressed over its entire width, and then the imparted stress decreases drastically as it moves away from the southern tip. From the three-dimensional modeling in figure 4.8b, this effect appears to be associated with a gentle bend at the boundary with the rupture. There is an accumulation of stress of up to 6 bars in the area confined between the end of the coseismic rupture and the hinge of the bend with the concavity facing southwest. However, the northern half of the fault seems untouched in terms of CST.

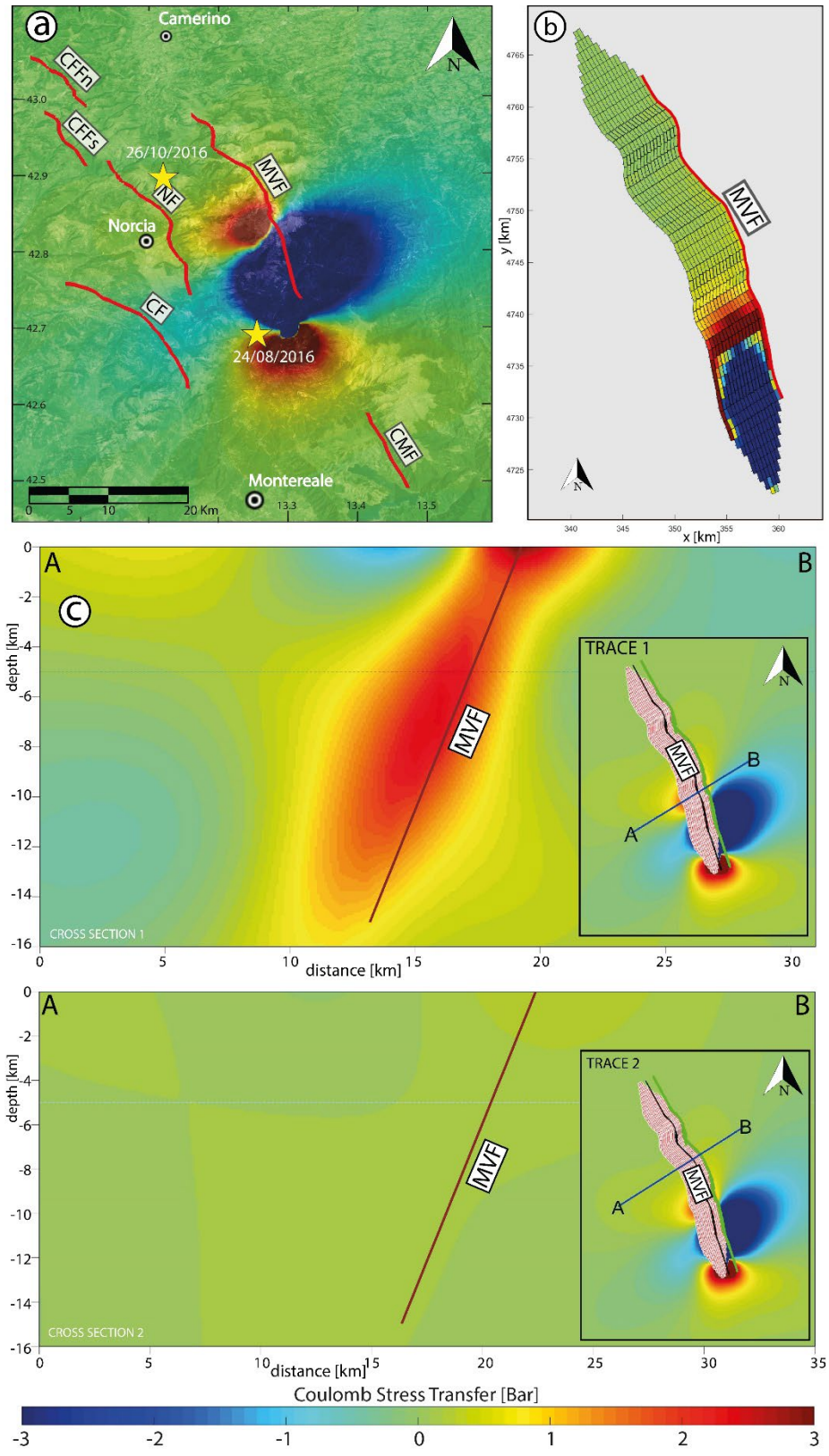

Figure 4.8 CST related to the 24/08/2016 earthquake. a) Oblique view of the CST distribution on a plane located at a depth of 5 km. The causative fault is the southernmost portion of the Mt. Vettore Fault and the receiver is its central and northern portion. b) 3D view of the CST

on the Mt. Vettore Fault. Note that the CST is calculated on each of the rectangles that make up the entirety of the fault. c) Cross-sections perpendicular to the MVF, one near the southern partial rupture and the other cross-section at the central portion of the MVF. Note the difference in the CST pattern when moving just a few kilometers away from the rupture.

A similar and specular situation was obtained by modeling the partial activation of the northern segment ruptured on October 26th. The seismic moment generated was lower than the earthquake on August 24th, approximately 8.81049E+24 dyne-cm compared to 1.24451E+25 dyne-cm of the previous earthquake, resulting in reduced intensity and extent of both the positive stress lobes and the stress shadow (Fig. 4.9a). The stress shadow weakly reaches the northwestern tip of the Norcia fault and the southeastern tip of the Colfiorito south fault, but with a stress reduction of about -0.4 bar. The positive lobes extend both towards the northwest and southeast, affecting the stress state of the southeastern tip of the Colfiorito fault, where the CST does not exceed 0.6 bars. The Monte Vettore fault experiences significant stress only in a narrow portion adjacent to the rupture zone. The two cross sections (Fig. 4.9c) about 12 km apart from each other demonstrate how the CST is concentrated only in the area adjacent to the rupture, dissipating drastically as it moves southeastward. The three-dimensional modeling in Fig. 4.9b reveals that the situation is very similar to that anticipated from the modeling on August 24th. Positive stress is concentrated around a bend, more pronounced in this case, with the same concavity as the one to the south of the fault. Starting from the bend towards the southeast, the CST gradually tends to zero within a few kilometers, leaving the stress state of the central part of the fault almost unchanged.

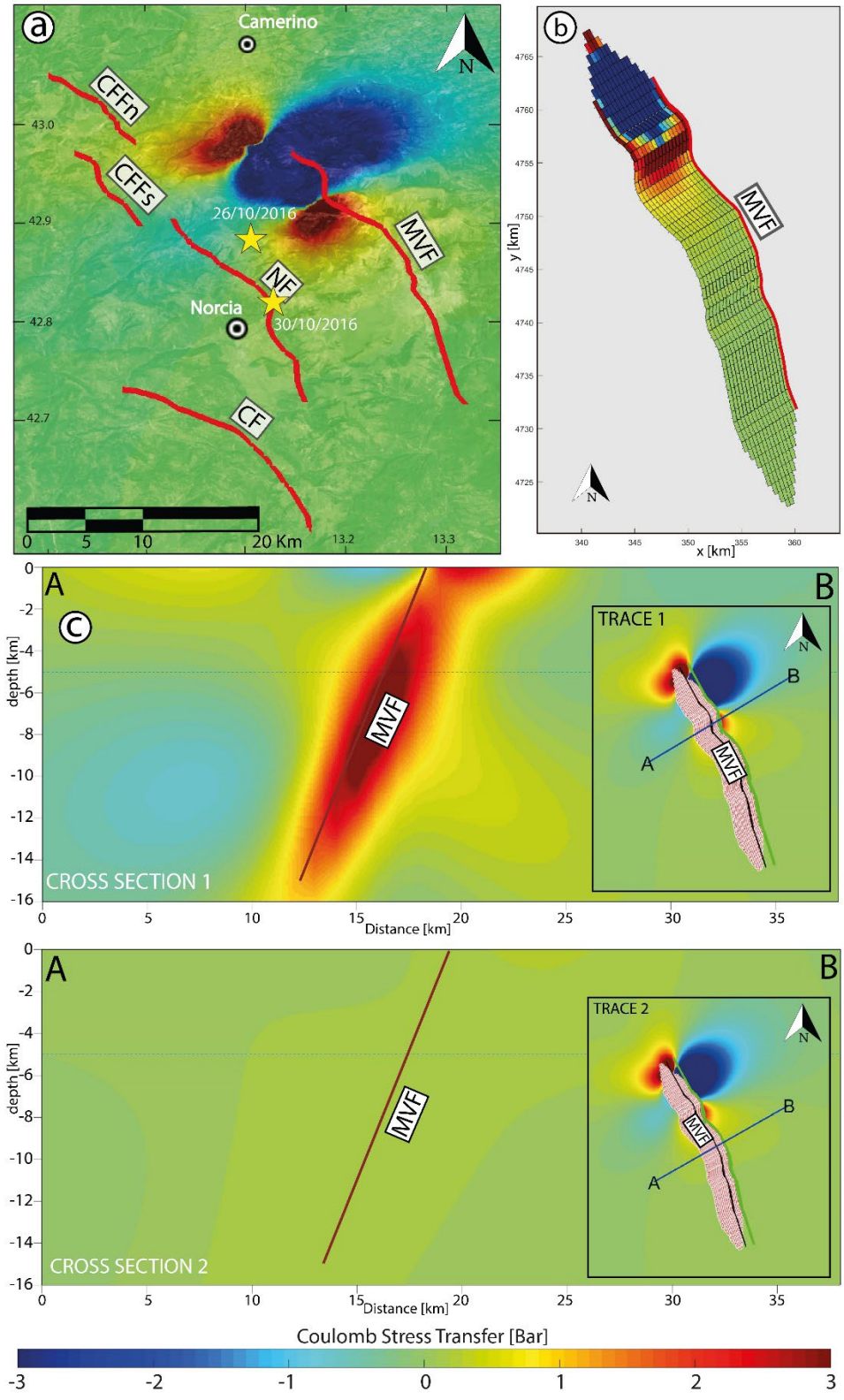

Figure 4.9 CST related to the 26/10/2016 earthquake. a) Oblique view of the CST distribution on a plane located at a depth of 5 km. The causative fault is the northernmost portion of the Mt. Vettore Fault and the receiver is its central and southern portion. b) 3D view of the CST on the Mt. Vettore Fault. Note that the CST is calculated on each of the rectangles that make

up the entirety of the fault. c) Cross-sections perpendicular to the MVF, one near the northern partial rupture and the other cross-section at the central portion of the MVF. Note the difference in the CST pattern when moving just a few kilometers away from the rupture.

On October 30th, a powerful seismic event originated from the activation of the central segment of the Monte Vettore fault system, concurrently reactivating its previously fractured northern and southern segments. The slip distribution for this comprehensive rupture exhibited an asymmetrical pattern, predominantly localized within the southern third of the fault. The ensuing Coulomb Stress Transfer (CST) pattern is markedly larger and more heterogeneous (Fig. 4.10a) when compared with prior two modeling attempts. Notably, the stress shadow enveloping the footwall is approximately five times broader than that observed over the hangingwall. The latter induces a significant stress diminution particularly impacting the faults of Norcia (primarily its southern half) and Cascia. This stress shadow extends over 60 km eastward on the footwall. The plan view modeling (Fig. 4.10a) at a depth of 5 km delineates four predominant lobes of increased stress, which are strategically positioned along the fault strike, confined to the hangingwall and the northern and southern fault tips. The most expansive stress augmentation zone emanates from the southern tip of the Monte Vettore fault, progressing southward and imparting a minor Coulomb stress transfer (approximately 0.5 bars) exclusively to the northern segment of the Campotosto fault. Positive CST is also evident in the northern sector, affecting the Colfiorito faults and the northern half of the Norcia fault. Nonetheless, upon scrutinizing the three cross sections depicted in Fig. 4.10c, it becomes evident that the Norcia fault (acting as the receiver fault in this simulation) undergoes a stress increase of up to 4 bars only within its shallower portion, spanning from approximately 4 km depth to the surface. This observation aligns with the conclusions of Galli et al. (2018), and Galderisi and Galli (2020), providing a rationale for the observed shallow coseismic ruptures on the Norcia fault due to the noted rise in surface stress. The fault's deeper segment is predominantly under the influence of the stress shadow, with negative values plummeting to around -4 bars. This distinct CST distribution along the Norcia fault is conspicuously discerned in the three-dimensional modeling (Fig. 4.10b). This representation further elucidates that both the stress shadow and the stress

rising zones display diminishing values as one transitions northward along the fault, consistent with the insights gleaned from the plan view.

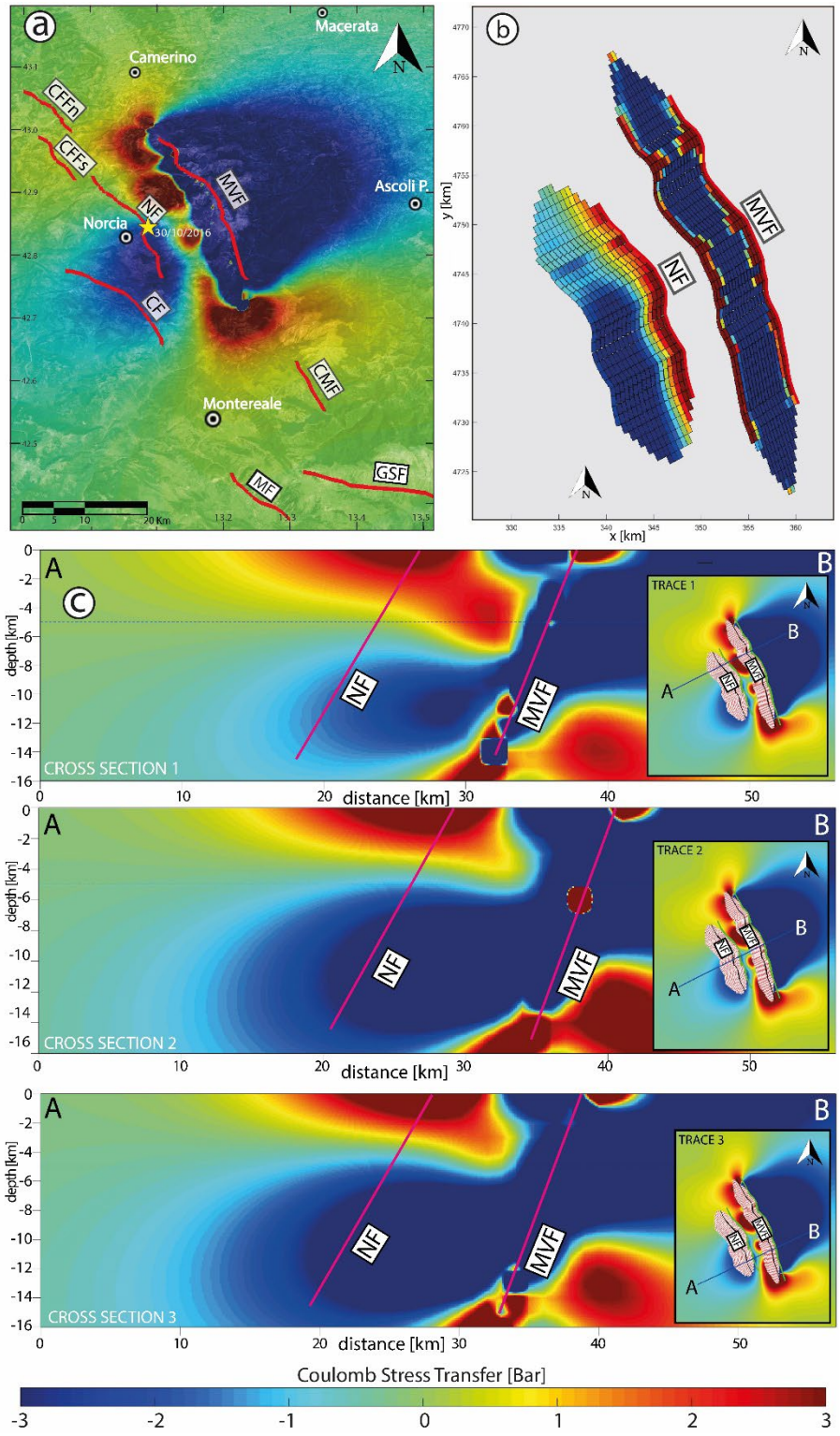

Figure 4.10 CST related to the 30/10/2016 earthquake. a) Oblique view of the CST distribution on a plane located at a depth of 5 km. The causative fault is the Mt. Vettore Fault and the

receiver is the Norcia fault. b) 3D view of the CST on the causative and receiver faults. Note that the CST is calculated on each of the rectangles that make up the entirety of the fault. c) three cross-sections perpendicular to the Norcia fault placed in different portions along the receiver fault.

4.4.8 CUMULATIVE COULOMB STRESS TRANSFER AFTER 1997, 2009 AND 2016 EARTHQUAKES

The final model we considered seeks to elucidate the cumulative CST effect arising from seismic events spanning from 1997 to 2016. The objective behind this attempt is to understand the current stress state of the faults within the CAFS. For the plan view of this model, we utilized parameters from a hypothetical receiver fault, adopting average values of strike, dip, and rake representative of all the faults in the CAFS. This approach facilitated a broader applicability, enabling a more realistic assessment of the effects across the entire CAFS fault system. Noteworthy is the fact that multiple tests using varied receiver fault parameters were executed, yielding strikingly similar outcomes. This consistency is primarily attributed to the closely aligned range of dip, rake, and strike values among the CAFS faults, which rendered the differences in individual test outcomes nearly indiscernible.

Initial analysis of the resulting plan view model (Fig. 4.11b) reveals complex interactions between the positive and negative stress lobes generated by different earthquakes. These lobes overlap, merge, and in some instances, cancel each other out or amplify each other. The resulting CST pattern is noticeably heterogeneous, characterized by dominant stress shadows interspersed with more localized regions of enhanced crustal stress. Delving deeper into the model at a depth of 5 km, we observed that the positive stress lobe, originating from the Mt Vettore fault activation and partially overlaying the Colfiorito fault, becomes obscured when juxtaposed with the pattern from the 1997 Colfiorito fault activation. Conversely, the positive stress lobe extending southeast from the Colfiorito fault is accentuated—intensifying the stress—upon the Monte Vettore fault activation. This implies a pronounced cumulative positive stress state on the Norcia fault, especially its northern segment, which sits at the intersection of these positive CST lobes. The southern segment of the Norcia fault,

however, remains predominantly in the stress shadow cast by the Monte Vettore fault, akin to the entirety of the Cascia fault.

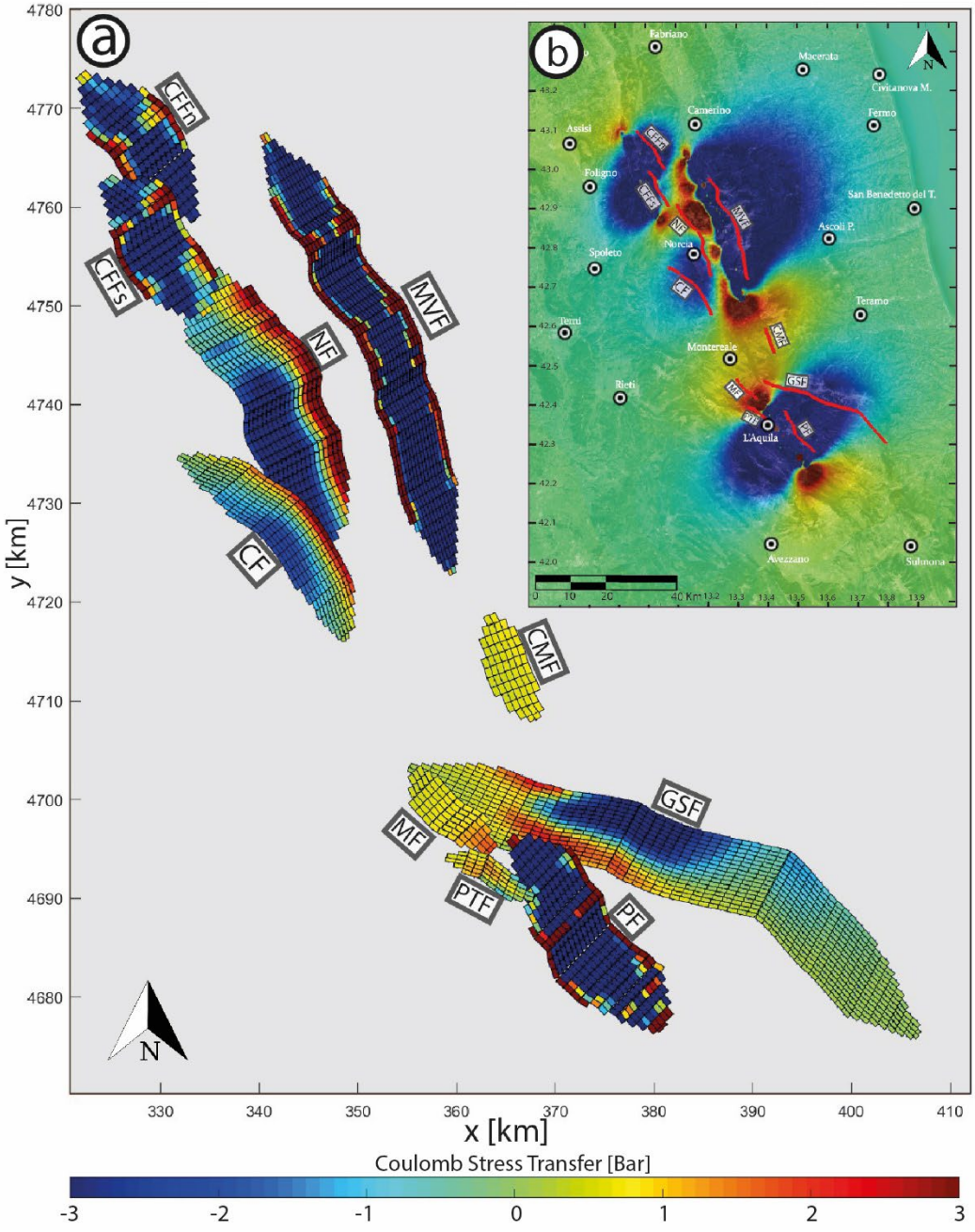

Figure 4.11 a) 3D view of the cumulative CST in the CAFS following the 1997, 2009 and 2016 seismic sequences. Note that the CST is calculated on each of the small rectangles that make up the entirety of the faults. b) Cumulative CST distribution at a depth of 5 km (plan view) following the 1997, 2009 and 2016 seismic sequences.

Shifting further south reveals a compelling interplay between the positive stress lobes emanating from the 2016 Monte Vettore fault (propagating south from its southern fault tip) and the 2009 Paganica-San Demetrio fault (extending north from its northern tip). Their convergence forges a broad region of elevated stress around the area spanning from Montereale city to the Campotosto fault, subjecting the latter to an increased stress of approximately 1.2 bars. Both the Pettino and Marine faults are also enveloped by this heightened stress zone—a manifestation of the compounded cumulative stress effects triggered by nearby fault activations within a relatively short time frame.

In the plan view modelling at a depth of 5 km, the Gran Sasso fault appears to be influenced by a vast stress shadow created on the footwall of the Paganica-San Demetrio fault, which activated in 2009. However, this stress shadow covers the central area of the Gran Sasso fault, leaving the northernmost fault tip positively stressed. Greater complexity is revealed by the analysis of the three-dimensional model described below.

While the plan view was shaped by the hypothetical receiver fault and provides a general perspective of potential CST patterns from recent seismic events, a more granular model was constructed to depict the CST effect on every individual rectangular segment of each fault. Instead of relying on the hypothetical receiver fault parameters, this detailed model was tailored according to the specific strike, dip, and rake values of each discretized fault segment, yielding a notably refined result for each fault (Fig. 4.11a). This representation unveils pronounced variations from the plan view. Key insights include the upper 5 km of the Norcia fault being predominantly affected by positive CST, with the northernmost section displaying stress penetration down to about 7 km. The superficial layer of the fault experiences considerable stress intensities of up to 5 bars. Below these depths, the fault lies predominantly in the stress shadow engendered by the 1997 and 2016 earthquakes. The Cascia fault mirrors this pattern, with its topmost 2-3 km undergoing about 3.5 bars of positive stress while the underlying surface is primarily in the stress shadow. The Campotosto fault, in contrast, exhibits a more uniform positive stress profile, averaging around 0.8 bars.

The Mt Marine fault exhibits more heterogeneity in stress reception. Its southernmost fault tip experiences the highest CST, approximately 1.5 bars, which gradually decreases northward to around 0.5 bars. In contrast, the Pettino fault is primarily stressed at its northern tip and central region (up to about 1.2 bars), with the southern half influenced by the stress shadow caused by the 2009 Paganica-San Demetrio fault activation.

The Gran Sasso fault also displays intriguing CST dynamics. Its central and northern segments, extending to a depth of about 8 km, fall under the stress shadow produced by the Paganica-San Demetrio fault. Below this stress shadow and at the northern fault tip, the fault appears to experience positive CST up to a maximum of 2 bars. However, this stress concentration is confined to specific limited areas, leaving the southern half largely uninfluenced except for a slight stress reduction from the prominent bend towards the south, and this only at the surface. The stress accumulation at the extreme northern tip of the Gran Sasso fault does not exceed 0.7 bars.

4.5 DISCUSSION

Our investigation into the dynamics of static stress transfer (CST) offers a comprehensive analysis of the CAFS, covering several centuries of Mw≥6 seismic events, from 1279 to 2016. This extensive temporal span allows a reliable understanding of the seismogenic sources behavior, capturing both the individual and cumulative CST effects of multiple seismic episodes and their implications for the current stress conditions within the CAFS.

The distribution of CST across the CAFS, characterized by concentrated areas of positive stress in some faults and shadow stress regions prevalent in others, underscores the complexity of seismic behavior within an interconnected fault system. The analyzed case studies have confirmed the role played by CST in adjacent faults, both in terms of earthquake triggering or inhibition. However, there are instances where this correlation is not so evident. The 1279 earthquake on the Colfiorito faults produced a zone of positive stress on the Norcia fault, that subsequently ruptured in 1328. Yet, the area of the Norcia fault affected by a considerable amount of stress is

minimal and confined almost exclusively to its northern tip (Campi fault in Galli et al., 2023). This founding let to speculate that the 1328 earthquake on the Norcia fault nucleated in the area of increased stress caused by the previous Colfiorito earthquake, to then engage the entire Norcia fault going southward. If so, the reactivation of the Norcia faults in 1328 might have been influenced by approximately 2 bars of positive stress at its northern extremity. As indicated by Galli et al., (2005; 2020), the 1328 earthquake did not involve the Cascia faults, as sometimes occurs in interconnected fault systems, but remained confined on the Norcia segments. In other words, the Cascia faults did not receive enough stress from the Colfiorito earthquake, supporting the hypothesis of stress transfer exclusively on the Norcia faults. A similar situation is observed in simulations performed on the subsequent devastating January 14, 1703 Norcia earthquake. In this case, the entire Norcia fault system, including the Cascia faults, activated, producing a much energetic earthquake than that of Colfiorito. In 1703, the positive stress lobes reached much greater distances and higher values (bar), significantly affecting the northern segment of the Upper Aterno fault system, i.e., the Mt Marine fault. Indeed, 19 days later, in the whole upper Aterno basin, a second devastating earthquake occurred, generated by the contemporary rupture of the Mt Marine, Mt Pettino and Paganica-San Demetrio fault, as also supported by the paleoseismological studies in Galli et al. (2010; 2011) and Moro et al. (2013). Despite the Paganica-San Demetrio fault was not affected by the CST generated by the January 1703 Norcia earthquake, the Mt Marine fault received enough stress to produce a cascade effect nucleating from this fault and then propagated southwards, involving, through dynamic and static stress transfer, also the other faults of the Upper Aterno fault system, in quick succession. Again, the influence of CST appears decisive.

However, it is worth noting that two and a half centuries earlier, the Gran Sasso fault system, running in the footwall of these faults, produced the most powerful earthquake in the CAFS. This Mw ~7.0 event put the UAFS, and in particular the upper part of the PSDFS into a situation of increasing stress. Even though much of the PSDFS was covered by the shadow zone of this large earthquake, it may have undergone dynamic stress transfer produced by the activation of the UAFS, which, on the contrary, were immersed in a substantial area of positive stress.

The 1703 Norcia earthquake also seems to have impacted the Campotosto fault, already in a critical situation in terms of CST from the 1349 Gran Sasso earthquake. Additionally, from the cumulative modeling of CST generated by recent instrumental earthquakes (Figs. 4.11 and 4.13f), a significant positive stress contribution from recent earthquakes emerges. According to our models and calculations, the Campotosto fault would have reached a stress accumulation over a millennium that makes its lack of reactivation highly unlikely (Figs. 4.12 and 4.13). Accordingly, the Campotosto fault has generated few seismic events with magnitudes just above Mw 5.0, both following the 2009 seismic sequence in L'Aquila and after the 2016 Mt. Vettore events (Cheloni et al., 2019). This observation supports the hypothesis of Tondi et al. (2020), who consider the Campotosto fault to be an actual zone of soft-linkage between the northern and southern faults of the CAFS, deeming it a direct participant in recent seismic events.

Another cryptic situation concerns the activation of the Norcia fault in 1730 (Mw 6.0) following its earlier activation in 1703 (Mw 6.9). As this fault surely ruptured in 1703, the 1730 occurence seems to challenge the theory that stress on the causative fault reduces to zero following its rupture. In order to generate another moderate magnitude earthquake only 27 years later, the fault would have needed to accumulate a significant amount of stress from neighboring faults, which really did not happen from 1703 to 1730. A possible explanation could be provided by Cowie et al. (2013), who demonstrated that in central Apennines nonlinear viscous deformation between 15 and 24 km depth dominates and promotes strain localization. Subsequently, Wedmore et al. (2017) calculated the interseismic loading of faults through continuous creep in shear zones at the base of each fault, below the locked brittle upper crust. Their study reveals that the Norcia fault, in the period between these two closely spaced earthquakes, managed to 'recharge' with interseismic stress due to deep viscous deformation, partly aided by coseismic stress from smaller magnitude earthquakes that occurred earlier. This peculiarity could thus explain the close temporal reactivation of this fault within such a short time span.

In 1979, the Norcia fault generated an earthquake with a magnitude of Mw 5.83. This event was not considered in the CST calculations of this study, as its magnitude falls below the chosen threshold. However, it is worth noting that, given the position of the

Colfiorito faults relative to the Norcia fault, this earthquake could have promoted stress to the Colfiorito fault system, facilitating its activation in 1997. It should also be mentioned that the faults responsible for the 1997 earthquake had already been subjected to considerable positive stress due to the devastating Norcia earthquake of 1703, further supporting the hypothesis that stress transfer played a crucial role.

While for historical earthquakes CST modeling may have been influenced by uncertainty regarding their real magnitude, CST calculations for recent earthquakes (1997 Colfiorito, 2009 L'Aquila, and 2016 Mt. Vettore earthquakes) are more reliable as slip data are available, and there is not error on the magnitude. This allowed us to model the slip on Mt. Vettore fault exactly as it occurred, divided into three main shocks that involved different portions of the fault.

In the case of Mt. Vettore, an unusual scenario is observed; the first partial activation predominantly impacted the southern tip, stressing the central region of the fault and sparing the northern tip. Nevertheless, the latter was the subsequent segment to activate. Historically, the northern segment has never been subjected to significant positive stress loading. However, Mildon et al. (2017) attributed this anomaly to the interseismic stress loading in the shear zone at 15–24 km depth, which would have positively stressed the deeper band of the fault. According to these authors, this would have predisposed the fault to a subsequent earthquake. After the August 24th (Mw 6.0) event, on October 26th (Mw 5.9) the northern tip ruptured, significantly increasing stress in the fault's central region. However, on October 30th, not only the central portion of the fault, but also the previously ruptured segments reactivated, indicating that the accumulated stress had not fully dissipated. The previous coseismic rupture of the Mt. Vettore fault occurred 1573 years earlier (Galli et al., 2019), and the recurrence interval for an earthquake of similar magnitude is approximately 1.8 ± 0.3 kyr, suggesting a slightly advanced recurrence time for the Mt. Vettore fault. Interestingly, the 1703 Norcia earthquake simulation reveals that the Mt. Vettore fault experienced significant negative inhibiting stress, with no other models displaying sufficient positive Coulomb Stress Transfer (CST) to compensate for the stress removed in 1703. Different mechanisms such as fluid migration, dynamic stress transfer or interseismic stress loading may be invoked in this situation (Oskin et al., 2008; Hetzel and Hampel, 2005; Brodsky and van der Elst, 2014, Wedmore et al., 2017).

The CST pattern generated in 2016 on the Norcia Fault aligns with the calculations made by Galderisi and Galli (2020), corroborating the theory that these two faults exchange CST in a mutually inhibitory manner. Moreover, our calculations indicate that the Norcia fault experiences significantly higher stress up to a depth of approximately 5 km, this data supports the findings of these authors, justifying the superficial coseismic ruptures on the Norcia fault with the aforementioned increase in surface stress.

The case study of the earthquake that struck the L'Aquila area in 2009 has revealed interesting implications for stress transfer to the Gran Sasso fault. Valoroso et al. (2013) conducted a thorough crustal study following this seismic event to analyze the distribution of aftershocks and deduce the geometry of the fault system. This detailed distribution of hypocenters suggests that some of them fall on the northern sector of the Gran Sasso fault. Galli et al. (2022) analyzed the distribution of these aftershocks in comparison with the two northern segments of the Gran Sasso fault, finding a precise correlation, with two aftershock clusters appearing to coincide perfectly with these fault segments. In particular, it seems that three significant aftershocks (Mw 4.0, Mw 4.7, Mw 5.1) are due to the reactivation of this major fault system. Our CST model in Figure 4.11 highlights the stress state of the Gran Sasso fault following recent seismic events. It can be stated that the stress pattern evident on the Gran Sasso fault is almost exclusively due to the 2009 L'Aquila earthquake, thus it is noticeable how the central deep and northern portions have been subjected to a significant increase in stress following the 2009 earthquake. The distribution of the L'Aquila earthquake aftershocks seems to coincide with the positively stressed areas of the GSF, corroborating the hypothesis of Galli et al. (2022). Indeed, we can observe how the two faults (PSDF and GSF), having different strikes, tend to converge towards their northwestern tips, making the stress transfer more effective in the northwest sector of the Gran Sasso fault compared to the southern half, which seems only partially influenced. The positive correlation between the stress pattern and the distribution of aftershocks provides further confirmation of the ability of CST to guide the evolution of seismic sequences.

Beyond the boundaries of the CAFS, two historically seismically-active regions to the north and south, Fabriano and Sulmona, respectively, have remained dormant in recent

centuries (Stucchi et al., 1991; Castelli and Monachesi, 2001; Gori et al., 2011; Galli et al., 2015; Bordoni et al., 2023; Gironelli et al., 2023). The following are estimates, as we do not know the exact position and kinematics of the Fabriano fault, making precise CST calculations impossible. Additionally, the Fabriano and Sulmona faults lie outside the CAFS; therefore, we did not include them in our calculations and did not incorporate the earthquakes they generated into our data. The stress pattern shown in Figure 11b refers to a receiver fault with kinematics and orientation corresponding to an average of those belonging to the CAFS. If the Fabriano fault significantly deviates from the orientation and kinematics of the CAFS faults, the result would be different. Despite this, interactions between the CAFS activity and the Fabriano and Sulmona faults can be hypothesized given their proximity and similar seismotectonic context. Below, we will make considerations about these two zones north and south of the CAFS, taking into account the uncertainty due to the lack of specific calculations but based on the extent of the stressed zones from historical and instrumental earthquakes of the CAFS. We are prepared to perform specific calculations should new scientific information emerge about the earthquake that struck the city of Fabriano in 1741. Our model suggests that these areas are minimally impacted by recent seismic sequences, recording only negligible stress changes (up to a maximum of 0.3 bars) (fig. 11b). Nevertheless, historical events amplify concerns. For example, the 1349 earthquake on the Gran Sasso fault transferred modest amounts of stress to the Mt Morrone fault, which borders the Sulmona basin. This calculation can be considered more precise compared to that of Fabriano because the Mt. Morrone fault, near Sulmona, has an orientation and kinematics similar to those of the CAFS. Moving north, the 1703 Norcia earthquake imparted positive stress to the crust surrounding Fabriano. Although the seismogenic source of the Fabriano earthquake is still debated in literature (Cello et al., 1997; Basili et al. 2008; Materazzi et al., 2022; Gironelli et al., 2023 and references therein), it triggered a significant Mw 6.1 earthquake in 1741, a few decades after the Norcia earthquake, suggesting probable stress transfer influence. In contrast, the Mt Morrone fault has not generated significant earthquakes for over 1800 years (Galli et al., 2015), heightening concern regarding this significant fault.

Examining the differences in seismic moment release across the three seismicity windows described by Valentini et al. (2023), further insights can be drawn. The authors characterize the seismic cycle of the CAFS over the past millennium as segmented into three periods of higher seismicity, each registering a distinct cumulative seismic moment. Assuming that a millennium is a sufficiently long period to characterize the seismic cycle of the CAFS, one can make considerations on its predictability and a possible recurrence model. Several authors have demonstrated that many fault systems exhibit a time-predictable nature (e.g., Shimazaki and Nakata, 1980; Rubinstein et al., 2012; Zechar and Nadeau, 2012; Scholz, 2019), while Tondi and Cello (2003) have suggested the time-and-slip-predictable nature of the CAFS. If we accept the latter assertion as correct and consider the significant difference in seismic moment (dependent on slip and thus directly proportional) between the first two seismicity windows (one between 1300 and 1400, one around 1700) and the most recent one (from 1979 to 2016), we can hypothesize the existence of a seismic moment gap in the current historical period. This hypothesis assumes the immutability of the displacement rate over such a short time frame, which over the last 700 ka is 1.6 cm/year (for the entire CAFS; Tondi and Cello, 2003). The lowest cumulative seismic moment is thus observed in the latest seismicity window, corresponding to the period from 1979 to 2016. Consequently, there appears to be a potential seismic gap in the current historical period, which, according to the authors calculations, could be filled with a seismic moment of approximately Mo=1.27E+26 dyne-cm, corresponding to a magnitude Mw=6.67 earthquake. Such magnitude might be generated by the Gran Sasso fault, which, as deduced from Fig. 11a, exhibits zones of particularly high stress. Moreover, this fault has shown no signs of reactivation since 1349 and, despite often falling within the stress shadows of adjacent faults, displays a considerably long temporal gap of inactivity. On the other hand, the Gran Sasso fault seems to be characterized by long recurrence times (2.8 ± 0.5 ky; Galli et al., 2022), and although CST may influence the characteristic return time (e.g. Wedmore et al., 2017), it still remains an extremely lengthy period.

The CAFS could be spatially divided into two sectors, the northern sector encompassing the fault systems of Colfiorito, Mt Vettore and Norcia, and the southern sector those of the Upper Aterno, Laga Mts, and Gran Sasso. During the latest

seismicity window, most of the seismic moment was generated by the northern sector, leaving the southern sector affected only by the southern segments of the UAFS, namely the Paganica-San Demetrio faults, which are insufficient to bridge the aforementioned seismic gap. This thesis supports the hypothesis that the causative fault for the seismic gap could belong to the southern sector.

Our study also highlights the cumulative nature of CST, with subsequent seismic events either amplifying or compensating for the stress effects of prior events. This iterative accumulation of stress alterations may result in stress conditions significantly different from those inferred from isolated events, emphasizing the importance of a comprehensive and long-term perspective on seismic sequences to understand their stress impacts. The importance of considering individual fault characteristics in CST modeling becomes evident from our analysis. While an aggregate model based on average fault parameters provides valuable insights into potential CST patterns, a detailed model designed for specific values of strike, dip, and rake for each fault segment offers a more refined understanding of the CST effects on each fault.

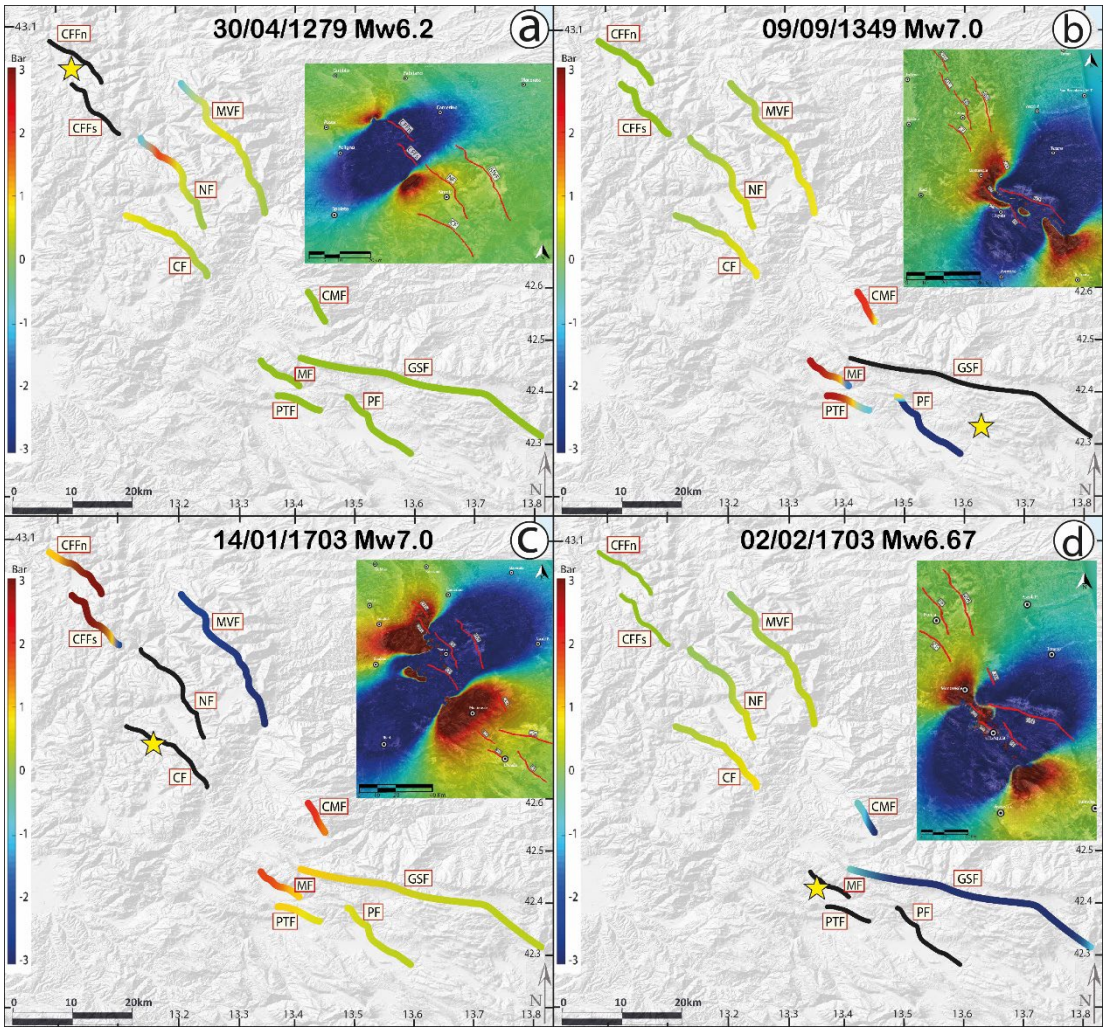

Figure 4.12 Summary visualization of the Calculated CST at a Depth of 5 km among the faults of the CAFS for each of the analyzed historical earthquakes. a) CST generated by the Colfiorito Fault System in April 1279. b) CST generated by the Gran Sasso Fault in September 1349. c) CST generated by the Norcia and Cascia Faults in January 1703. d) CST generated by the Paganica-San Demetrio fault, Marine, and Pettino Faults in February 1703. The fault traces drawn in black represent the causative faults. The insets of each figure illustrate the spatial distribution of the CST within the crust on a plane located at a depth of 5 km.

However, it is worth noting that the accuracy of our models depends on the precision of input parameters, which, although derived from the best available data, remain approximations. For example, so far, determining the slip patterns of historical earthquakes is impossible. Moreover, Vannucci et al. (2021) have pointed out that historical earthquakes might be overvalued in magnitude due to the challenges of estimating their size from macroseismic data. Such inaccuracies could result in

overrating the energy released during pre-instrumental seismic events. Furthermore, calculated CST changes do not necessarily forecast an earthquake but merely indicate the stress state of a fault. This aligns with observations by Hardebeck et al. (1998), who noted that although CST models offer valuable insights, their predictive ability remains inherently probabilistic.

Our study underscores the crucial role of spatial and temporal components of CST in understanding seismic dynamics. It emphasizes the value of considering the cumulative effects of multiple seismic events and the specific characteristics of individual faults in seismic behavior modeling. Future studies may seek to further refine these models by incorporating more detailed fault characteristics and broader geographic contexts to improve the precision of seismic risk predictions.

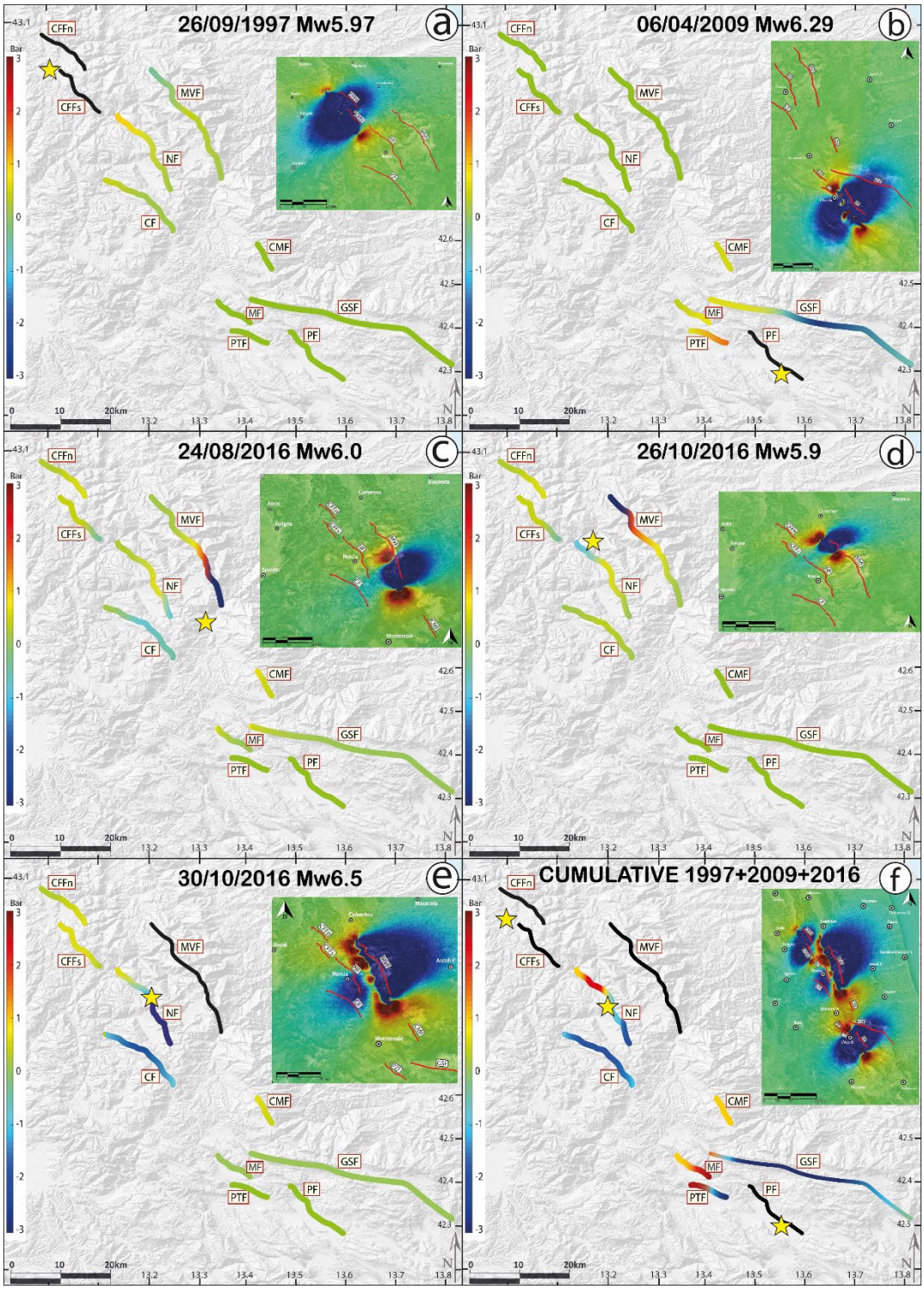

Figure 4.13 Summary visualization of the Calculated CST at a Depth of 5 km among the faults of the CAFS for each of the analyzed instrumental earthquakes. a) CST generated by the Colfiorito Fault System in September 1997. b) CST generated by the Paganica-San Demetrio Fault in April 2009. c) CST generated by the southern portion of the Mt. Vettore fault in August 2016. d) CST generated by the northern portion of the Mt. Vettore fault in October 26th 2016. e) CST generated by the complete rupture of the Mt. Vettore fault in October 30th 2016. f)

Cumulative CST from the last five instrumental earthquakes. The fault traces drawn in black represent the causative faults. The insets of each figure illustrate the spatial distribution of the CST within the crust on a plane located at a depth of 5 km.

4.6 CONCLUSIONS

The Central Apennines Fault System (CAFS) is an active tectonic region in central Italy which witnessed a series of devastating seismic events in the past Millenium. While the role of Coulomb Stress Transfer (CST) in triggering seismic events has been discussed in numerous studies, its specific influence within the CAFS over an extensive time span has remained analytically unexplored. This research addresses that gap by providing an in-depth analysis of the effects of CST on historical and instrumental seismic events associated with the CAFS.

Nine selected events from the CPTI15 catalog were tested for comprehensive CST analysis, based on their spatiotemporal proximity to subsequently activated faults. In addition, in order to isolate the static stress transfer for each seismic episode, we analyzed the cumulative CST of contemporary instrumental earthquakes, detailing the current stress landscape. Employing an innovative methodology, faults were conceptualized in a three-dimensional plane, with an ellipse-shaped area implying their 2D geometric representation. Given the sensitivity of CST to strike variations, a variable strike was integrated within a three-dimensional elliptical model, ensuring greater accuracy in estimates.

In many of the case studies, CST may have played an influential role within the CAFS, catalyzing the activation or inhibition of its faults. Several instances highlight fault reactivation following high stress transfer between closely outcropping active faults, in short periods. Some examples are described below:

- The 1279 Colfiorito earthquake positively stressed the northern tip of the Norcia fault, that actually ruptured few decades later, in 1328.
- The January 14, 1703 Norcia earthquake positively stressed the Mt. Marine fault, where few days later a huge earthquake nucleated, provoking a cascade effect engaging the whole Upper Aterno fault system, namely the Mt. Marine-Mt. Pettino-Paganica-San Demetrio faults.

- The August 24 and October 26, 2016 earthquakes seem to have stressed the bends and the central portion of the Mt. Vettore fault, probably facilitating the October 30 impressive fault rupture.
- The Colfiorito fault system stored conspicuous amount of positive stress from each of the earthquakes generated by the Norcia fault system, including the 1979 event (Mw 5.83), probably influencing its reactivation in 1997.
- The January 14, 1703 Norcia earthquake generated also a huge positive stress lobe towards the Fabriano area, where 38 years later a destructive earthquake struck.

Conversely, certain scenarios illuminate the calming effect of stress shadows. Some examples include:

- The Mt. Vettore fault generated only two earthquakes during the past two millennia. This could be linked to the existence of the parallel Norcia fault that ruptured at least 5 times in the same interval, transferring negative CST on the Vettore fault.
- The same hypothesis could be applied to the Gran Sasso fault, that ruptured only in 1349 in the past millennium, whereas the Upper Aterno and the Paganica-San Demetrio fault systems generated at least 3 strong earthquakes that transferred negative Coulomb stress on the Gran Sasso fault.

However, some events do not display a clear correlation, suggesting the influence of other factors, such as fluid dynamics, accumulated elastic strain energy, interseismic stress loading or dynamic stress transfer. Some examples of this lack of correlation are:

- The 1349 Gran Sasso earthquake enveloped the Paganica-San Demetrio fault in a huge stress shadow, but the latter ruptured 112 years later, in 1461.
- The February 1703 Upper Aterno earthquake exerted a negligible influence on the Norcia fault, but the latter ruptured 27 years later notwithstanding the huge stress drop on the fault during the previous January 1703 Norcia earthquake.

- The 1997 Colfiorito earthquake transferred a negligible amount of stress to the Mt. Vettore fault, and almost exclusively on its central portion, but the southernmost portion of the fault ruptured during the August 2016 earthquake.
- The CST caused by the 2009 Paganica-San Demetrio fault earthquake did not affect the Vettore fault that generated the 2016 earthquake.

The nuanced understanding of CST achieved through this research has both concrete and academic implications. By illuminating the interaction between faults in previous seismic episodes, it provides valuable insights into possible future earthquake sequences. Such awareness is essential: by anticipating seismic sequences, targeted risk mitigation tactics can be formulated, thereby protecting local communities from the catastrophic consequences of earthquakes.

Moreover, the complexity of the CAFS, observed in light of past seismic episodes like those in 1997, 2009, and 2016, underscores the intricate nature of stress patterns. These patterns emerge from interactions between seismic events, with stress lobes intertwining in ways that amplify, nullify, or diversify their impacts on nearby faults. It is noteworthy that while historically and currently seismic-active regions such as Fabriano and Sulmona have remained relatively quiescent, their potential for future activity and associated risks should not be overlooked. This research highlights the complex dynamics at play in a high-seismic-activity region like the CAFS. Through rigorous analyses and innovative modeling techniques, we offer insights that can guide future investigations and pragmatic strategies for seismic risk mitigation. This study stands as a testament to the profound ability of CST to influence the seismic narrative of a region and emphasizes the need for continued research in this field.

Acknowledgments

We would like to acknowledge Dr. Zoë Mildon and Dr. Manuel-Lukas Diercks for their kind assistance in using the "3D-Faults" MATLAB code. This work was supported by the FAR Unicam project “Novel Approach for Seismic Hazard Analysis—NoHard", responsible Emanuele Tondi.

Open Research

For the creation of this manuscript, data were sourced from the Italian Catalogue of Active and Capable Faults (ITHACA- ITaly HAzard from CApable faults; ITHACA Working Group, 2019; http://sgi2.isprambiente.it/ithacaweb/Mappatura.aspx) and the Database of Individual Seismogenic Sources (DISS; DISS Working Group, 2021; Basili et al., 2008; https://diss.ingv.it), comparing the data in these catalogs with those found in scientific literature for each fault. Earthquake data were cross-referenced with various seismic catalogs, including the Parametric Catalogue of Italian Earthquakes (CPTI15; Rovida et al., 2022; https://emidius.mi.ingv.it/CPTI15-DBMI15), the Italian Seismological Instrumental and Parametric Data-Base (ISIDe; ISIDe Working Group, 2007; https://terremoti.ingv.it/iside), the Catalogue of Strong Italian Earthquakes (CFTI; Guidoboni et al., 2018, 2019; https://storing.ingv.it/cfti/cfti5/), and the Italian Macroseismic Database (DBMI; Locati et al., 2022; https://emidius.mi.ingv.it/CPTI15-DBMI15). Some finite-fault rupture models were derived from the Earthquake Source Model Database (SRCMOD; Mai and Thingbaijam, 2014; http://equake-rc.info/srcmod) and were used as input for specific Matlab (MATLAB Version: 9.14.0.2137306 (R2023a) Prerelease – academic license; The MathWorks Inc. (2022) ;
https://www.mathworks.com) tools. The Matlab tools employed are “Coulomb3.4” (Lin and Stein, 2004; Toda et al., 2005; https://temblor.net/coulomb/) and “Faults 3D” (Mildon et al., 2016; https://github.com/ZoeMildon/3D-faults). Figures were created using Adobe Illustrator (version 28.3; Adobe Inc., 2019), Adobe Photoshop (version 25.5; Adobe Inc., 2019) and Google Earth Pro (http://www.google.com/earth/index.html).

References

Adobe Inc. (2019). Adobe Photoshop. Retrieved from https://www.adobe.com/products/photoshop.html

Adobe Inc. (2019). Adobe Illustrator. Retrieved from https://adobe.com/products/illustrator

Anderson, E.M., 1951. The Dynamics of Faulting. Oliver & Boyd, Edinburgh.

Aki K. and P. G. Richards; 1980: *Quantitative Seismology*, 2nd ed., edited by J. Ellis, Univ. Sci. Books, New York.

Alkan, H., Öztürk, S., & Akkaya, İ. (2023). Seismic Hazard Implications in and Around the Yedisu Seismic Gap (Eastern Türkiye) Based on Coulomb Stress Changes, b-Values, and S-wave Velocity. Pure and Applied Geophysics, 180(9), 3227-3248.

Amato A., Azzara R., Chiarabba C., Cimini G. B., Cocco M., Di Bona M., Margheriti L., Mele F., Selvaggi G., Basili A., Boschi E., Courbolex F., Deschamps A., Gaffet S., Bittarelli G., Chiaraluce L., Piccinini D. and Ripepe M.; 1998: *The 1997 Umbria-Marche, Italy, earthquake sequence: A first look at the main shocks and aftershocks*. Geophysical Research Letters, **25**(15), 2861-2864.

Anzidei, M., Boschi, E., Cannelli, V., Devoti, R., Esposito, A., Galvani, A., ... & Serpelloni, E. (2009). Coseismic deformation of the destructive April 6, 2009 L'Aquila earthquake (central Italy) from GPS data. Geophysical Research Letters, 36(17).

Asayesh, B. M., Zafarani, H., & Tatar, M. (2020). Coulomb stress changes and secondary stress triggering during the 2003 (Mw 6.6) Bam (Iran) earthquake. Tectonophysics, 775, 228304.

Barchi M., Galadini F., Lavecchia G., Messina P., Michetti A. M., Peruzza L., Pizzi A., Tondi E. and Vittori E.; 2000: *Sintesi delle conoscenze sulle faglie attive in Italia Centrale: parametrizzazione ai fini della caratterizzazione della pericolosità sismica*. GNDT-Monografie

Barnett J. A., Mortimer J., Rippon J. H., Walsh J. J. and Watterson J.; 1987: *Displacement geometry in the volume containing a single normal fault*. AAPG Bulletin, **71**(8), 925-937.

Basili R, Valensise G, Vannoli P, Burrato P, Fracassi U, Mariano S, Boschi E (2008) The database of individual seismogenic sources (DISS), version 3: summarizing 20 years of research on Italy's earthquake geology. Tectonophysics 453(1–4):20–43. https:// doi. org/ 10. 1016/j. tecto. 2007. 04. 014

Blumetti A.M. , 1995. Neotectonic investigation of evidence of paleoseismicity in the epicentral area of the January–February 1703, central Italy, earthquakes, Perspectives in Paleoseismology, Assoc. Eng. Geol. Bull., Special Publ.6, 83–100

Boncio, P., & Lavecchia, G. (2000). A structural model for active extension in Central Italy. Journal of Geodynamics, 29(3-5), 233-244.

Boncio, P., Lavecchia, G., & Pace, B. (2004). Defining a model of 3D seismogenic sources for Seismic Hazard Assessment applications: the case of central Apennines (Italy). Journal of Seismology, 8, 407-425.

Bordoni, P., Gori, S., Akinci, A., Visini, F., Sgobba, S., Pacor, F., ... & Doglioni, C. (2023). A site-specific earthquake ground response analysis using a fault-based approach and nonlinear modeling: The Case Pente site (Sulmona, Italy). Engineering Geology, 314, 106970.

Brodsky, E. E., & van der Elst, N. J. (2014). The uses of dynamic earthquake triggering. Annual Review of Earth and Planetary Sciences, 42, 317-339.

Byerlee, J. (1978). Friction of rocks. Pure Apply Geophys 116: 615–626.

Castelli, V., & Monachesi, G. (2001). Seismic history and historical earthquake scenario for the town of Fabriano (Central Italy). Italian Geotechnical Journal, 35(2), 36-46.

Cello, G., Mazzoli, S., Tondi, E., & Turco, E. (1995). Tettonica attiva in Appennino centrale ed implicazioni per l'analisi della pericolosità sismica del settore assiale della catena umbro-marchigiana-abruzzese. STUDI GEOLOGICI CAMERTI. NUOVA SERIE, 13(1), 115-138.

Cello G, Mazzoli S, Tondi E, Turco E (1997) Active tectonics in the central Apennines and possible
implications for seismic hazard analysis in peninsular Italy. Tectonophysics 272(1):43–68. https:// doi.org/ 10. 1016/ S0040- 1951(96) 00275-2

Cello G., Deiana G., Mangano P., Mazzoli S., Tondi E., Ferreli L., Maschio L., Michetti A.M., Serva L. and Vittori E.; 1998: *Evidence for surface faulting during the September 26, 1997, Colfiorito (Central Italy) earthquakes*. Journal of Earthquake Engineering, **2**(2), 303-324.

Cello G., Mazzoli S., Tondi E. and Turco E.; 1997: *Active tectonics in the central Apennines and possible implications for seismic hazard analysis in peninsular Italy*. Tectonophysics, **272**(1), 43-68.

Cheloni, D., D'Agostino, N., Scognamiglio, L., Tinti, E., Bignami, C., Avallone, A., ... & Mattone, M. (2019). Heterogeneous behavior of the Campotosto normal fault (Central Italy) imaged by InSAR GPS and strong-motion data: Insights from the 18 January 2017 events. Remote Sensing, 11(12), 1482.

Chiarabba C., Amato A., Anselmi M., Baccheschi P., Bianchi I., Cattaneo M., Cecere G., Chiaraluce L., Ciaccio M. G., De Gori P., De Luca G., Di Bona M., Di Stefano R.,

Faenza L., Govoni A., Improta L., Lucente F. P., Marchetti A., Margheriti L., Mele F., Michelini A., Monachesi G., Moretti M., Pastori M., Piana Agostinetti N., Piccinini D., Roselli P., Seccia D., Valoroso L.; 2009: *The 2009 L'Aquila (central Italy) MW6.3 earthquake: Main shock and aftershocks*. Geophysical Research Letters, **36**(18).

Chiarabba C. and De Gori P.; 2016: *The seismogenic thickness in Italy: constraints on potential magnitude and seismic hazard*. Terra Nova, **28**(6), 402-408.

Chiaraluce, L. (2012). Unravelling the complexity of Apenninic extensional fault systems: A review of the 2009 L'Aquila earthquake (Central Apennines, Italy). Journal of Structural Geology, 42, 2-18.

Chiaraluce L., Di Stefano R., Tinti E., Scognamiglio L., Michele M., Casarotti E., Cattaneo M., De Gori P., Chiarabba C., Monachesi G., Lombardi A., Valoroso L., Latorre D. and Marzorati S.; 2017: *The 2016 central Italy seismic sequence: A first look at the mainshocks, aftershocks, and source models*. Seismological Research Letters, ***88***(3), 757-771.

Chiaraluce L., Valoroso L., Piccinini D., Di Stefano R. and De Gori P.; 2011: *The anatomy of the 2009 L'Aquila normal fault system (central Italy) imaged by high resolution foreshock and aftershock locations*. Journal of Geophysical Research: Solid Earth, **116**(B12).

Cinti, F. R., Pantosti, D., De Martini, P. M., Pucci, S., Civico, R., Pierdominici, S., ... & Patera, A. (2011). Evidence for surface faulting events along the Paganica fault prior to the 6 April 2009 L'Aquila earthquake (central Italy). Journal of Geophysical Research: Solid Earth, 116(B7).

Collettini, C., & Sibson, R. H. (2001). Normal faults, normal friction?. Geology, 29(10), 927-930.

DISS Working Group (2021) Database of Individual Seismogenic Sources (DISS), version 3.3.0: a compilation of potential sources for earthquakes larger than M 5.5 in Italy and surrounding areas. Istituto Nazionale di Geofisica e Vulcanologia (INGV). https://doi.org/10.13127/diss3.3.0

Dong, P., Zhao, B., & Qiao, X. (2022). Interaction between historical earthquakes and the 2021 Mw7. 4 Maduo event and their impacts on the seismic gap areas along the East Kunlun fault. Earth, Planets and Space, 74(1), 42.

EMERGEO Working Group. (2010). Evidence for surface rupture associated with the Mw 6.3 L'Aquila earthquake sequence of April 2009 (central Italy). Terra Nova, 22(1), 43-51.

Faure Walker, J. P., G. P. Roberts, P. A. Cowie, I. D. Papanikolaou, P. R. Sammonds, A. M. Michetti, and R. J. Phillips (2009), Horizontal strain-rates and throw-rates across breached relay zones, central Italy: Implications for the preservation of throw deficits at points of normal fault linkage, J. Struct. Geol., 31(10), 1145–1160, doi:10.1016/j.jsg.2009.06.011.

Faure Walker, J. P., G. P. Roberts, P. R. Sammonds, and P. Cowie (2010), Comparison of earthquake strains over 102 and 104 year timescales: Insights into variability in the seismic cycle in the central Apennines, Italy, J. Geophys. Res., 115, B10418, doi:10.1029/2009JB006462

Fossen, H. (2016). Structural geology. Cambridge university press.

Galadini F. and Galli P.; 2000: *Active tectonics in the central Apennines (Italy)–input data for seismic hazard assessment.* Natural Hazards, **22**(3), 225-268.

Galadini F. , Galli P., 2003. Paleoseismology of silent faults in the Central Apennines (Italy): the Mt. Vettore and Laga Mts. faults, Ann. Geophys.465, 815–836.

Galadini F. and Messina P.; 2001: *Plio-Quaternary changes of the normal fault architecture in the central Apennines (Italy)*. Geodinamica Acta, **14**(6), 321-344.

Galderisi A. and Galli P.; 2020: *Coulomb stress transfer between parallel faults. The case of Norcia and Mt Vettore normal faults (Italy, 2016 Mw 6.6 earthquake)*. Results in Geophysical Sciences, 1, 100003.

Galli P. and Galadini F.; 1999: *Seismotectonic framework of the 1997-98 Umbria-Marche (Central Italy) earthquakes.* Seismological Res. Letters, **70** (4) 404-414

Galli P.; 2020: *Recurrence times of central-southern Apennine faults (Italy): hints from palaeoseismology*. *Terra Nova*, ***32***(6), 399-407.

Galli P., Galadini F. and Calzoni F.; 2005: *Surface faulting in Norcia (central Italy): a "paleoseismological perspective"*. Tectonophysics, **403**(1-4), 117-130.

Galli P., Galderisi A., Marinelli, R., Peronace E., Messina P. and Polpetta F.; 2019: *A reappraisal of the 1599 earthquake in Cascia (Italian Central Apennines): Hypothesis on the seismogenic source.* Tectonophysics, **774**, 10.1016/j.tecto.2019.228287.

Galli P., Galderisi, A., Ilardo, I., Piscitelli, S., Scionti, V., Bellanova, J. and Calzoni, F.; 2018: *Holocene paleoseismology of the Norcia fault system (Central Italy).* Tectonophysics, **745**, 154-169.

Galli, P., Giaccio, B., & Messina, P. (2010). The 2009 central Italy earthquake seen through 0.5 Myr-long tectonic history of the L'Aquila faults system. Quaternary Science Reviews, 29(27-28), 3768-3789.

Galli P. A., Giaccio B., Messina P., Peronace E. and Zuppi G. M.; 2011: Palaeoseismology of the L'Aquila faults (central Italy, 2009, M w 6.3 earthquake): Implications for active fault linkage. Geophysical Journal International, **187**(3), 1119-1134.

Galli, P., Giaccio, B., Peronace, E., & Messina, P. (2015). Holocene paleoearthquakes and early–late pleistocene slip rate on the Sulmona fault (central Apeninnes, Italy). Bulletin of the Seismological Society of America, 105(1), 1-13.

Galli P., Galadini F. and Pantosti D.; 2008: *Twenty years of paleoseismology in Italy*. Earth-Science Reviews, **88**(1-2), 89-117.

Galli P., Galderisi A., Messina P. and Peronace E.; 2022: *The Gran Sasso fault system: Paleoseismological constraints on the catastrophic 1349 earthquake in Central Italy*. Tectonophysics, **822**, 229156.

Galli P., Galderisi A., Peronace E., Giaccio B., Hajdas I., Messina P., Pileggi D. and Polpetta F.; 2019: *The awakening of the dormant Mount Vettore fault (2016 central Italy earthquake, Mw 6.6): Paleoseismic clues on its millennial silences*. Tectonics, **38**(2), 687-705.

Galli, P., Messina, P., Peronace, E., Galderisi, A., Ilardo, I., & Polpetta, F. (2023). Paleoseismic evidence of five magnitude 7 earthquakes on the Norcia fault system in the past 8,000 years (Central Italy). Frontiers in Earth Science, 11, 1188602.

Galli P., Peronace E., Bramerini F., Castenetto S., Naso G., Cassone F. and Pallone F.; 2016: *The MCS intensity distribution of the devastating 24 August 2016 earthquake in central Italy (MW 6.2)*. Annals of Geophysics, **59**.

Galli P., Peronace E. and Messina P.; 2022: *Archaeoseismic evidence of surface faulting in 1703 Norcia earthquake (Central Italian Apennines, Mw 6.9)*. Geosciences, **12**(1), 14.

Gasparini C., Iannaccone G. and Scarpa R.; 1985: *Fault-plane solutions and seismicity of the Italian peninsula*. Tectonophysics **117**, 59–78.

Gironelli, V., Volatili, T., Luzi, L., Brunelli, G., Zambrano, M., & Tondi, E. (2023). Ground motion simulations of historical earthquakes: the case study of the Fabriano (1741, Mw= 6.1) and Camerino (1799, Mw= 6.1) earthquakes in central Italy. Bulletin of Earthquake Engineering, 1-22.

Gori, S., Giaccio, B., Galadini, F., Falcucci, E., Messina, P., Sposato, A., & Dramis, F. (2011). Active normal faulting along the Mt. Morrone south-western slopes (central Apennines, Italy). International journal of earth sciences, 100, 157-171.

Guidoboni E., Ferrari G., Mariotti D., Comastri A., Tarabusi G., Sgattoni G., Valensise G. (2018) - CFTI5Med, Catalogo dei Forti Terremoti in Italia (461 a.C.-1997) e nell'area Mediterranea (760 a.C.-1500). Istituto Nazionale di Geofisica e Vulcanologia (INGV). doi: https://doi.org/10.6092/ingv.it-cfti5

Guidoboni E., Ferrari G., Tarabusi G., Sgattoni G., Comastri A., Mariotti D., Ciuccarelli C., Bianchi M.G., Valensise G. (2019), CFTI5Med, the new release of the catalogue of strong earthquakes in Italy and in the Mediterranean area, Scientific Data 6, Article number: 80 (2019). doi: https://doi.org/10.1038/s41597-019-0091-9

Gupta A. and Scholz C. H.; 2000: *A model of normal fault interaction based on observations and theory*. Journal of structural Geology, **22**(7), 865-879.

Hardebeck, J. L., Nazareth, J. J., & Hauksson, E. (1998). The static stress change triggering model: Constraints from two southern California aftershock sequences. Journal of Geophysical Research: Solid Earth, 103(B10), 24427-24437.

Harris, R. A., and R. W. Simpson (1992), Changes in static stress on southern California faults after the 1992 Landers earthquake, Nature, 360(6401), 251–254, doi:10.1038/360251a0.

Hetzel, R., & Hampel, A. (2005). Slip rate variations on normal faults during glacial–interglacial changes in surface loads. Nature, 435(7038), 81-84.

Iezzi, F., Francescone, M., Pizzi, A., Blumetti, A. M., Boncio, P., Di Manna, P., ... & Urbini, S. (2022, September). Paleoseismological surveys for the identification of capable faults in urban areas: the case of the Mt. Marine Fault (Central Apennines, Italy). In 11th International INQUA Meeting on Paleoseismology, Active Tectonics and Archeoseismology (PATA), France.

Iezzi, F., Roberts, G., Walker, J. F., & Papanikolaou, I. (2019). Occurrence of partial and total coseismic ruptures of segmented normal fault systems: Insights from the Central Apennines, Italy. Journal of Structural Geology, 126, 83-99.

Improta, L., Latorre, D., Margheriti, L., Nardi, A., Marchetti, A., Lombardi, A. M., ... & Moretti, M. (2019). Multi-segment rupture of the 2016 Amatrice-Visso-Norcia seismic sequence (central Italy) constrained by the first high-quality catalog of Early Aftershocks. Scientific Reports, 9(1), 6921.

ISIDe Working Group; 2007: *Italian Seismological Instrumental and Parametric Database (ISIDe)*. Istituto Nazionale di Geofisica e Vulcanologia (INGV). https://doi.org/10.13127/ISIDE

ITHACA Working Group (2019) ITHACA (ITaly HAzard from CApable faulting), a database of active capable faults of the Italian territory. Version December 2019. ISPRA Geological Survey of Italy. Web Portal http://sgi2.isprambiente.it/ithacaweb/Mappatura.aspx

King G. C., Stein R. S. and Lin, J.; 1994: *Static stress changes and the triggering of earthquakes*. Bulletin of the Seismological Society of America, **84**(3), 935-953.

Lin J. and Stein R. S.; 2004: *Stress triggering in thrust and subduction earthquakes and stress interaction between the southern San Andreas and nearby thrust and strike-slip faults*. Journal of Geophysical Research: Solid Earth, **109**(B2).

Locati M., Camassi R., Rovida A., Ercolani E., Bernardini F., Castelli V., Caracciolo C.H., Tertulliani A., Rossi A., Azzaro R., D'Amico S., Antonucci A. (2022). Database Macrosismico Italiano (DBMI15), versione 4.0 [Data set]. Istituto Nazionale di Geofisica e Vulcanologia (INGV). https://doi.org/10.13127/dbmi/dbmi15.4

Mai, P.M. and Thingbaijam, K.K.S. (2014). SRCMOD: An online database of finite-fault rupture models. Seismological Research Letters, 85(6), 1348-1357.

Maleki Asayesh, B., Hamzeloo, H., & Zafarani, H. (2019). Coulomb stress changes due to main earthquakes in Southeast Iran during 1981 to 2011. Journal of Seismology, 23(1), 135-150.

Marchandon, M., Vergnolle, M., & Cavalié, O. (2021). Fault interactions in a complex fault system: insight from the 1936–1997 NE Lut earthquake sequence. Geophysical Journal International, 224(2), 1157-1173.

Materazzi M, Bufalini M, Dramis F, Pambianchi G, Gentili B, Di Leo M (2022) Active tectonics and paleoseismicity of a transverse lineament in the Fabriano valley, Umbria–Marche Apennine (central Italy). Int J Earth Sci 111(5):1539–1549

Messina P., Galadini F., Galli P. and Sposato A.; 2002: *Quaternary basin evolution and present tectonic regime in the area of the 1997–1998 Umbria–Marche seismic sequence (central Italy)*. Geomorphology, **42**(1-2), 97-116.

Mildon Z.K. , Roberts G.P., Faure Walker J.P., Wedmore L., McCaffrey K.J.W., 2016a. Active normal faulting during the 1997 seismic sequence in Colfiorito, Umbria: did slip propagate to the surface?, J. Struct. Geol.91102–113.

Mildon, Z. K., Roberts, G. P., Faure Walker, J. P., & Iezzi, F. (2017). Coulomb stress transfer and fault interaction over millennia on non-planar active normal faults: The M w 6.5–5.0 seismic sequence of 2016–2017, central Italy. Geophysical Journal International, 210(2), 1206-1218.

Mildon, Z. K., Roberts, G. P., Faure Walker, J. P., & Toda, S. (2019). Coulomb pre-stress and fault bends are ignored yet vital factors for earthquake triggering and hazard. Nature communications, 10(1), 2744.

Mildon Z. K., Toda S., Faure Walker J. P. and Roberts G. P.; 2016: *Evaluating models of Coulomb stress transfer: Is variable fault geometry important?*. Geophysical Research Letters, **43**(24), 12-407.

Morewood N.C. , Roberts G.P., 2000. The geometry, kinematics and rates of deformation within an en echelon normal fault segment boundary, central Italy, J. Struct. Geol.22(8), 1027–1047.

Moro, M., Gori, S., Falcucci, E., Saroli, M., Galadini, F., & Salvi, S. (2013). Historical earthquakes and variable kinematic behaviour of the 2009 L'Aquila seismic event (central Italy) causative fault, revealed by paleoseismological investigations. Tectonophysics, 583, 131-144.

Nostro, C., Chiaraluce, L., Cocco, M., Baumont, D., & Scotti, O. (2005). Coulomb stress changes caused by repeated normal faulting earthquakes during the 1997 Umbria-Marche (central Italy) seismic sequence. Journal of Geophysical Research: Solid Earth, 110(B5).

Oskin, M., Perg, L., Shelef, E., Strane, M., Gurney, E., Singer, B., & Zhang, X. (2008). Elevated shear zone loading rate during an earthquake cluster in eastern California. Geology, 36(6), 507-510.

Pantosti D. and Boncio P.; 2012: *Understanding the April 6th, 2009 L'Aquila earthquake-the geological contribution: an introductory note to the special issue*. Italian Journal of Geosciences, **131**(3), 303-308.

Papanikolaou I.D. , Roberts G.P., Michetti A.M., 2005. Fault scarps and deformation rates in Lazio–Abruzzo, Central Italy: comparison between geological fault slip-rate and GPS data, Tectonophysics408(1–4), 147–176.

Papanikolaou I.D. , Roberts G.P., 2007. Geometry, kinematics and deformation rates along the active normal fault system in the southern Apennines: implications for fault growth, J. Struct. Geol.29(1), 166–188.

Pino, N. A., Convertito, V., & Madariaga, R. (2019). Clock advance and magnitude limitation through fault interaction: the case of the 2016 central Italy earthquake sequence. Scientific reports, 9(1), 5005.

Reasenberg, P. A., and R. W. Simpson (1992), Response of regional seismicity to the static stress change produced by the loma prieta earthquake, Science, 255(5052), 1687–1690, doi:10.1126/science.255.5052.1687.

Roberts G.P. , Michetti A.M., 2004. Spatial and temporal variations in growth rates along active normal fault systems: an example from The Lazio–Abruzzo Apennines, central Italy, J. Struct. Geol.26(2), 339–376.

Roberts G.P. , 2008. Visualisation of active normal fault scarps in the Apennines, Italy: a key to assessment of tectonic strain release and earthquake rupture, J. Virtual Explor.29(4), doi:10.3809/jvirtex.2008.00197.

Rovida A., Locati M., Camassi R., Lolli B., Gasperini P. and Antonucci A.; 2022: *Catalogo Parametrico dei Terremoti Italiani CPTI15, versione 4.0.*

Rubinstein, J. L., Ellsworth, W. L., Chen, K. H., & Uchida, N. (2012). Fixed recurrence and slip models better predict earthquake behavior than the time-and slip-predictable models: 1. Repeating earthquakes. Journal of Geophysical Research: Solid Earth, 117(B2).

Scholz, C. H. (2019). The mechanics of earthquakes and faulting. Cambridge university press.

Scognamiglio, L., Tinti, E., Quintiliani, M. (2006): Time Domain Moment Tensor (TDMT) [Data set], Istituto Nazionale di Geofisica e Vulcanologia (INGV), https://doi.org/10.13127/TDMT

Shan, B., Xiong, X., Wang, R., Zheng, Y., & Yang, S. (2013). Coulomb stress evolution along Xianshuihe–Xiaojiang Fault System since 1713 and its interaction with Wenchuan earthquake, May 12, 2008. Earth and Planetary Science Letters, 377, 199-210.

Shimazaki, K., & Nakata, T. (1980). Time-predictable recurrence model for large earthquakes. Geophysical Research Letters, 7(4), 279-282.

Stucchi, M., Monachesi, G., & Mandrelli, F. M. (1991). Investigation of 18th century seismicity in central Italy in the light of the 1741 Fabriano earthquake. Tectonophysics, 193(1-3), 65-82.

Stein, R. S. (1999). The role of stress transfer in earthquake occurrence. Nature, 402(6762), 605-609.

Stein, R. S., Barka, A. A., & Dieterich, J. H. (1997). Progressive failure on the North Anatolian fault since 1939 by earthquake stress triggering. Geophysical Journal International, 128(3), 594-604.

The MathWorks Inc. (2022). MATLAB version: 9.14.0.2137306 (R2023a) Prerelease, Natick, Massachusetts: The MathWorks Inc. https://www.mathworks.com

Toda S., Stein R. S., Richards-Dinger K. and Bozkurt S. B.; 2005: *Forecasting the evolution of seismicity in southern California: Animations built on earthquake stress transfer*. Journal of Geophysical Research: Solid Earth, **110**(B5).

Tondi E.; 2000: *Geological analysis and seismic hazard in the central Apennines (Italy)*. Journal of Geodynamics, **29**(3-5), 517-533.

Tondi E. and Cello G.; 2003: *Spatiotemporal evolution of the Central Apennines fault system (Italy)*. Journal of Geodynamics, **36**(1-2), 113-128.

Tondi E., Jablonská D., Volatili T., Michele M., Mazzoli S. and Pierantoni P. P.; 2020: *The Campotosto linkage fault zone between the 2009 and 2016 seismic sequences of central Italy: Implications for seismic hazard analysis*. GSA Bulletin, **133**(7-8), 1679-1694.

Valentini G., Volatili T., Galli P. and Tondi E.; 2023: New methodological approach in the evaluation of faults interaction: insights from the central apennine fault system. Bulletin of Geophysics and Oceanography.

Valoroso, L., Chiaraluce, L., Piccinini, D., Di Stefano, R., Schaff, D., & Waldhauser, F. (2013). Radiography of a normal fault system by 64,000 high-precision earthquake locations: The 2009 L'Aquila (central Italy) case study. Journal of Geophysical Research: Solid Earth, 118(3), 1156-1176.

Vannoli P., Burrato P., Fracassi U. and Valensise G.; 2012: *A fresh look at the seismotectonics of the Abruzzi (Central Apennines) following the 6 April 2009 L'Aquila earthquake (Mw 6.3)*. Italian Journal of Geosciences, **131**(3), 309-329.

Vannucci G., Lolli B. and Gasperini P.; 2021: *Inhomogeneity of macroseismic intensities in Italy and consequences for macroseismic magnitude estimation*. Seismological Research Letters, **92**(4), 2234-2244.

Vittori E., Deiana G., Esposito E., Ferreli L., Marchegiani L., Mastrolorenzo G., Michetti A.M., Porfido S., Serva L., Simonelli A.L. and Tondi E.; 2000: *Ground effects and surface faulting in the September–October 1997 Umbria–Marche (Central Italy) seismic sequence*. Journal of Geodynamics, **29**(3-5), 535-564.

Walker, J. F., Roberts, G. P., Cowie, P. A., Papanikolaou, I., Michetti, A. M., Sammonds, P., & Phillips, R. J. (2012). Relationship between topography, rates of extension and mantle dynamics in the actively-extending Italian Apennines. Earth and Planetary Science Letters, 325, 76-84.

Walsh J. J. and Watterson J.; 1987: *Distributions of cumulative displacement and seismic slip on a single normal fault surface*. Journal of Structural Geology, **9**(8), 1039-1046.

Walters, R. J., Elliott, J. R., D'agostino, N., England, P. C., Hunstad, I., Jackson, J. A., ... & Roberts, G. (2009). The 2009 L'Aquila earthquake (central Italy): A source mechanism and implications for seismic hazard. Geophysical Research Letters, 36(17).

Wang, L., Gao, H., Feng, G., & Xu, W. (2018). Source parameters and triggering links of the earthquake sequence in central Italy from 2009 to 2016 analyzed with GPS and InSAR data. Tectonophysics, 744, 285-295.

Wedmore L. N. J., Faure Walker J. P., Roberts G. P., Sammonds P. R., McCaffrey K. J. W. and Cowie P. A.; 2017: *A 667 year record of coseismic and interseismic Coulomb stress changes in central Italy reveals the role of fault interaction in controlling irregular earthquake recurrence intervals*. Journal of Geophysical Research: Solid Earth, **122**(7), 5691-5711.

Wilkinson, M., Roberts, G. P., McCaffrey, K., Cowie, P. A., Walker, J. P. F., Papanikolaou, I., & Watson, Z. K. (2015). Slip distributions on active normal faults measured from LiDAR and field mapping of geomorphic offsets: an example from L'Aquila, Italy, and implications for modelling seismic moment release. Geomorphology, 237, 130-141.

Xiong, W., Tan, K., Qiao, X., Liu, G., Nie, Z., & Yang, S. (2017). Coseismic, postseismic and interseismic coulomb stress evolution along the Himalayan main frontal thrust since 1803. Pure and Applied Geophysics, 174, 1889-1905.

Zechar, J. D., & Nadeau, R. M. (2012). Predictability of repeating earthquakes near Parkfield, California. Geophysical Journal International, 190(1), 457-462.

CHAPTER 5: Discussion and Conclusions

This doctoral thesis focuses on a detailed analysis of fault interactions in different tectonic settings, with a particular emphasis on Coulomb Stress Transfer (CST) (Harris and Simpson, 1992; Reasenberg and Simpson, 1992; King et al., 1994) and its role in the dynamics of fault interactions within the Central Apennines Fault System (CAFS, Cello et al., 1997). Through a meticulous investigation that spans seismic events with magnitudes of 5.8<Mw<7 from 1279 to 2016, this research provides an unprecedented insight into the behavior of seismogenic sources in this region. A fundamental aspect of the work involves the processing and interpretation of CST data, which has allowed for the identification of not only the individual effects but also the cumulative impacts of multiple seismic episodes on the current stress conditions within the CAFS. The precise and realistic modeling of seismogenic sources is a key point of this research; an accurate seismic hazard assessment also depends on the precision of input parameters; the closer they are to reality, the more truthful the output will be. True to this scientific and detailed approach, this thesis includes a study on surface faulting and the interaction between conjugate faults in a tectonic context different from that of the CAFS. This research project presents a detailed analysis of the immediate surface effects caused by the magnitude 6.4 Petrinja earthquake that struck central Croatia on December 29, 2020 (Chapter 2). Thanks to field surveys in the epicentral area, it was possible to document and catalog both primary coseismic effects, such as the geometry and dynamics of surface fracturing, and secondary effects, including phenomena of liquefaction, sinkhole formation, and landslides. The study of the impacts following the Petrinja earthquake highlights the essentiality of recognizing primary surface breaks to analyze the origin and surface evidence of earthquakes. The research has unveiled new data on strike-slip faults in the central Alpine-Mediterranean area, showing a complex pattern of aligned and en echelon fault segments, particularly around the Petrinja Fault Zone (PFZ). An in-depth investigation of the shear zone structure has revealed characteristic structural elements such as R and R' conjugate shears, T tension fractures, P shears, and X and Y shears (e.g. Ahlgren, 2001; Katz et al., 2004; Aktar et al., 2007), positioned at precise angles that define the Principal Displacement Zone (PDZ). These observations highlight the

influence of interactions between conjugate structures and their development during major seismic events in fault activation.

The application of InSAR imaging to map deformations has validated direct observations, although there are significant quantitative differences between direct displacement measurement data and satellite data (Livio et al., 2016). This discrepancy highlights the complexity of earthquake-induced deformations and the importance of combining various investigative approaches for an accurate estimation. Acknowledging the limitations in analyzing InSAR data and in precisely defining displacements, this analysis encourages a closer integration between field-collected data and geospatial methodologies to address these challenges. This work is part of a broader context of structural geology studies, offering crucial directions for future research focused on fault dynamics in areas of oblique plate convergence and the use of advanced techniques in seismic hazard assessment. This research contributes to the understanding of coseismic rupture mechanisms, showing the simultaneous activation of conjugate fault structures during earthquakes, an aspect previously underexplored. These findings underscore the urgency of precise and rapid monitoring of surface deformations to refine seismic hazard assessments related to capable faults, especially in areas characterized by complex fault interactions as demonstrated by the studied seismic events.

Geographically and geologically shifting to the CAFS, the research conducted in this doctoral thesis is set within a widely debated scientific context, that of Coulomb Stress Transfer and its influence on seismic dynamics and fault interactions, with a specific focus on the CAFS (Chapters 3 and 4). Comparing and relating the obtained results with those of previous studies, a picture of confirmations, extensions, and sometimes challenges to existing knowledge in the field of faults interaction emerges.

Before proceeding with the actual calculation of Coulomb Stress Transfer (CST), several preliminary analyses were conducted (Chapter 3). This phase was essential for carrying out a study that is as detailed as possible and minimizes simplifications.

The seismic cycle of the Central Apennines Fault System (CAFS) was reconstructed in light of the recent seismic sequences of 2009 and 2016 to observe how it has changed compared to the cycle produced by Tondi and Cello (2003). Over the last millennium, the analysis of the distribution of cumulative seismic moment has revealed the existence of three main time-windows of seismicity, interspersed by approximately 300-350 years, in line with the hypothesis proposed by Tondi and Cello (2003). These authors had previously defined the seismic cycle based on the calculation of cumulative coseismic slip, derived from the decomposition of the seismic moment. Our methodology, on the other hand, directly considered the cumulative seismic moment.

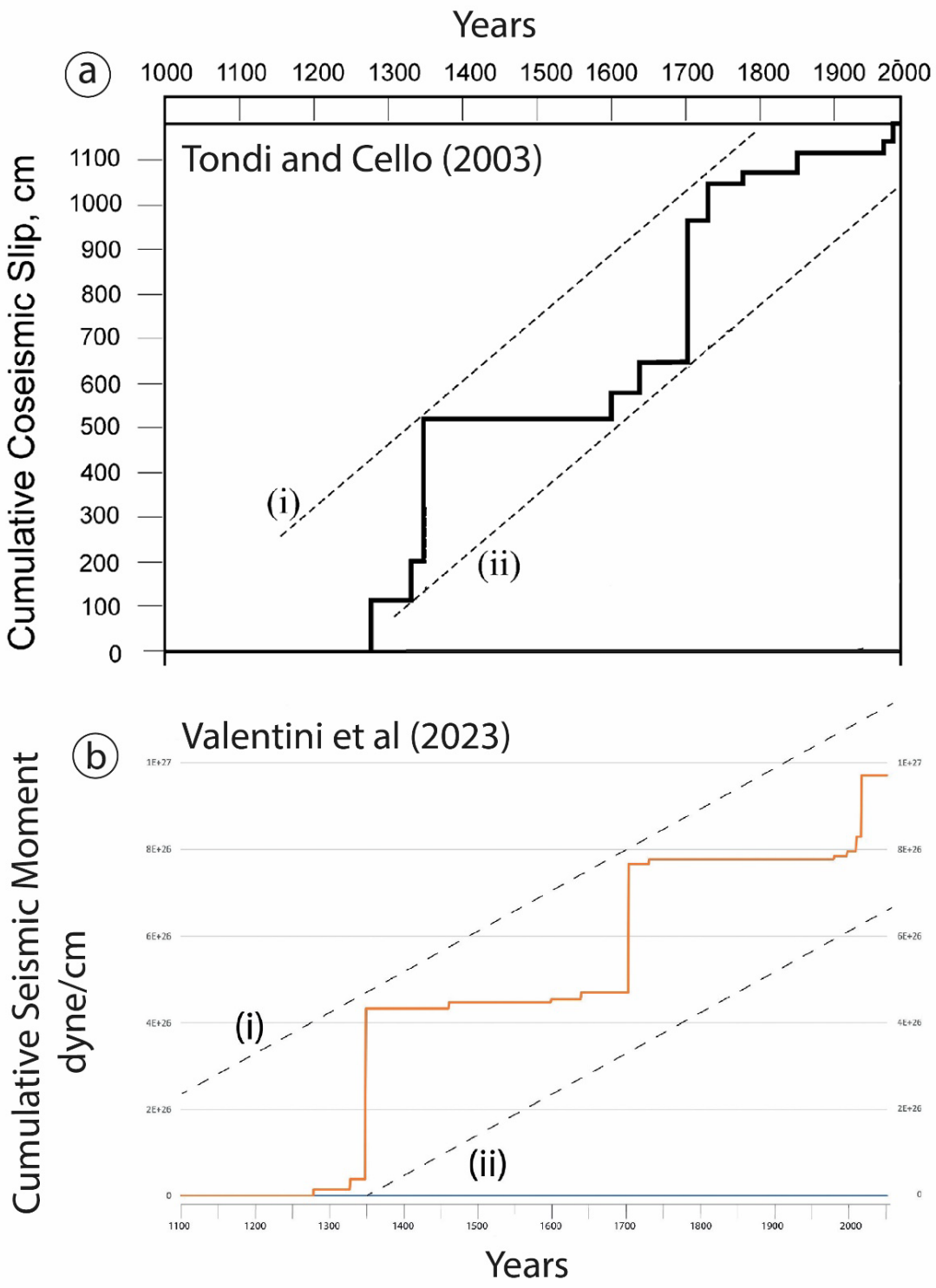

Figure 5.1 Comparison between a) the seismic cycle of the CAFS before the revision of historical events and the addition of the latest seismic events of 2009 and 2016 (modified after Tondi and Cello, 2003) and b) the updated seismic cycle by Valentini et al. (2023).

The resulting seismic cycle indicates that most of the seismic energy released in the last millennium can be attributed to three distinct "steps" in time: one between 1300 and 1400 AD, one around 1700 AD, and the last covering the most recent events, from 1979 to 2016. However, the amount of energy released is not constant among the three time windows of seismicity examined (Fig. 5.1 and Fig. 5.2). The seismic moment released during the first time window of seismicity was found to be the highest and decreases approaching the present. This could be due to a multitude of factors, primarily it can be hypothesized that a millennium may not represent a sufficiently long time span to define the seismic cycle. It is also desirable to consider the overestimation of the seismic moment generated by historical earthquakes, although some of them have been proven by detailed paleoseismological studies. In this case, the seismic moment generated by the first time window of seismicity might be overestimated or that of the second time window underestimated. In both these hypotheses, the last instance remains valid: a potential seismic gap in the current time window. This gap could be filled with a seismic moment of approximately Mo=1.27E+26 dyne-cm, corresponding to a magnitude Mw=6.67 earthquake. If this is true, it is urgent to understand which faults could be most plausible for potential future activation, for this reason, a model that represents as faithfully as possible the current stress state of the CAFS faults was necessary.

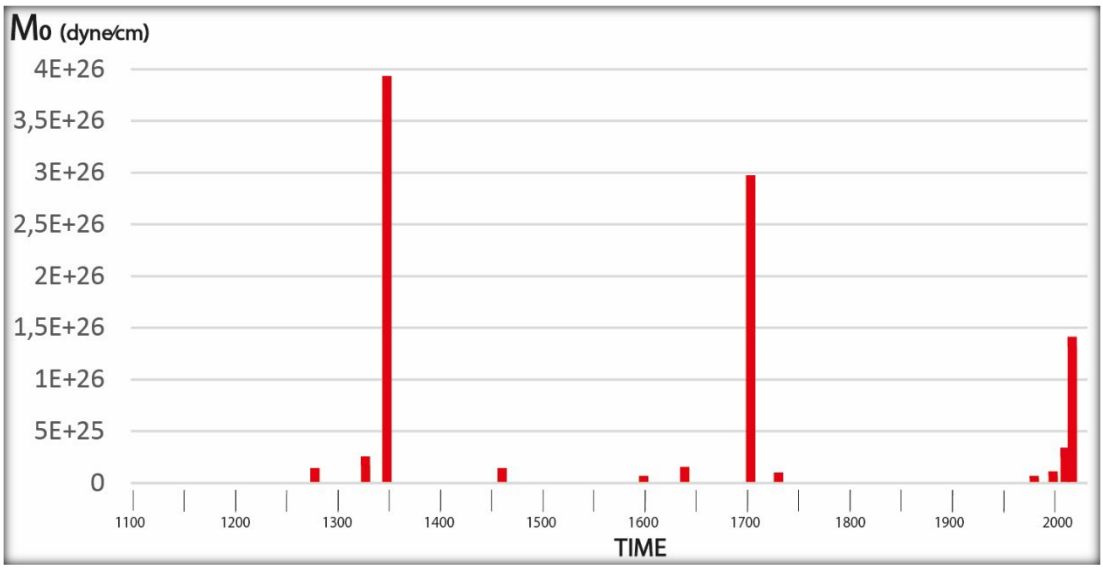

Figure 5.2 Distribution of seismic moment from the year 1100 to the present.

This discrepancy in the seismic moment generated across different seismicity windows suggests a significant variation in the energy release capacity of the CAFS over the considered time span. The gradual decrease in cumulative seismic moment through the three seismicity windows highlights the intrinsic complexity of the region's seismic cycle and raises questions about the underlying mechanisms governing such variations. A deep understanding of these dynamics is crucial to further refine seismicity forecasting models and develop more effective seismic risk mitigation strategies.

Following the analysis of the updated seismic cycle, an intensive study was conducted on the existing literature concerning the association between historical earthquakes and their causative faults. Numerous paleoseismological studies in the central Apennine area have allowed for a fair association (Falcucci et al., 2015; Blumetti, 1995; Galadini and Galli, 2003; Galli et al., 2005; 2008; 2011; 2018; 2020; 2022; 2023; Iezzi et al., 2023), although some sources remain debated. The study is prepared to be updated should new paleoseismological evidence on fault ruptures in historical times be published. For current knowledge, the most up-to-date data available in the literature, both regarding causative faults (or fault segments in case of partial rupture) and estimated magnitude, were adhered to. The latter is still a subject of discussion; although seismic catalogs are exhaustive and drafted with the best techniques available at the time, they are nonetheless subject to an error related to the scarcity and imprecision of written testimonies from centuries ago (Vannucci et al., 2021). The seismicity of the Central Apennines is not confined to the faults presented in this work but also extends to other active faults present in literature (e.g., the Fucino, Valle del Salto, Rieti, Leonessa, and Liri Valley Faults; Mildon et al., 2022; and Roberts et al., 2024). However, our study focuses exclusively on the two main fault sets within the CAFS that have generated historical earthquakes with magnitudes greater than Mw6, specifically within the NW-SE oriented belt stretching from Colfiorito to just south of L'Aquila. We chose not to expand our study area laterally (westward), both due to the scarcity of seismic events listed in the CPTI15 catalog, which are predominantly concentrated within the axial zone of the central Apennine, and to maintain consistency in our results with respect to the CAFS. Nonetheless, it would be of significant interest in future studies to analyze the influence of earthquakes outside

the axial zone of the CAFS (e.g., the 1298 earthquake near Spoleto and Rieti) on the seismic cycle of the CAFS.

It is also worth notice that the Laga Fault, also known as Monte Gorzano Fault in literature (Blumetti and Guerrieri, 2007; Civico et al., 2018; Wedmore et al., 2017; Mildon et al 2022) in this work is not reported following the outcome of Tondi et al. (2020). These authors suggest that the Laga Fault may have an older origin and is likely not directly connected to the recent seismic events of the 2009 and 2016 seismic sequences for several reasons. They highlight that the fault exhibits geomorphological and structural features indicative of an earlier geological evolution, possibly coeval with the compressive tectonic phase taking place during the Miocene. Finally, since the presented analysis focuses on faults that have generated historical and instrumental earthquakes with magnitudes greater than Mw6, minor faults (e.g. the Montereale Fault) that generated historical earthquakes with lower magnitudes and affected by lacks of geological constraints have been excluded in order to do not charactheri have been omitted compromise the precision and rigor of this study.

Another preliminary analysis was conducted to hypothesize the actual deep geometry of the faults within the Central Apennines Fault System (CAFS). The now-established assumption that the shape of a fault at depth is irregular but closer to an ellipse than to a rectangle (Barnett et al., 1987; Walsh and Watterson, 1987; Gupta and Scholz, 2000) was relied upon (the rectangular geometry has been used so far in all CST calculations in the literature). Bibliographic sources and analyses of aftershocks and foreshocks hypocenters from instrumental earthquakes were utilized to define the average geometric ratios between the major and minor axes of a hypothetical ellipse representing the fault plane.

Although this methodology requires future enhancements, I strongly believe it is far more realistic than the traditional rectangular shape, as demonstrated in the articles included in this thesis. The most influential aspect of this new geometry concerns the greater depth extension of the faults compared to their surface trace. This makes adjacent faults more prone to receive or transfer stress, whether negative or positive,

consequently increasing the interaction between faults, especially those positioned along strike from one another. The influence of this new modeling on parallel faults, however, has not brought about substantial changes in the stress pattern generated on the receiving fault.

The resulting more realistic geometry turns out to be elliptical and with a variable strike (Mildon et al., 2016), the latter factor being crucial. In most models for calculating the CST so far, a fixed-strike model has been used, taking the average strike of the surface trace. However, CST is strongly dependent on the orientation of faults and fault segments, so the generated stress pattern is affected by bends and sudden changes in strike along the faults. Including the variable strike (i.e., the real geometry of the fault plane) means bringing to light stress configurations that would not be evident with planar faults. It is not rare for a fault rupture to nucleate in a small stressed portion of the fault (e.g., a bend) and then propagate. Conversely, it's equally possible that bends along the fault act as barriers to coseismic rupture, limiting it to a portion of the fault and generating partial rupture, as likely happened in the case of the 2016 seismic sequence. Variable strike has therefore been included so that these variations are revealed. However, it is important to consider that these are projections of the fault trace at depth, but a simplification exists: the surface trace does not perfectly reflect the irregularities (e.g., jogs, steps, bends) present on the fault plane at depth. Nevertheless, at the moment, this remains the least approximate solution that can be adopted.

This new fault geometry affects both the extent and shape of the stress shadow produced by the causative fault, which can induce negative stress on normal faults positioned along strike or partially overlapping the causative fault, as well as on the lobes of positive stress. The effect of strike variability becomes apparent when bends are pronounced, creating a pattern with vertical stress bands (along the fault plane) of varying intensity compared to the surrounding areas. Alterations in fault orientation have been shown to significantly influence Coulomb stress transfer, with a mere 10-20 degree change in orientation sufficient to switch stress from positive to negative. Faults with the most marked stress discrepancies are those exhibiting pronounced bends. If positive stress bands appear on the surface of the causative fault and it

ruptures completely without partial activations, then the stress accumulation bands become negligible in terms of triggering new mainshocks, as the rest of the fault's surface has already released the previously accumulated stress, rendering such narrow positive stress bands inadequate to cause a new mainshock. Exploring the potential correlation between these positive stress zones and the occurrence of aftershocks to confirm a possible relationship would be intriguing. However, the simplification persists that these bends extend in depth maintaining the same surface geometry. Another simplification concerns the slip pattern, which was often assumed as a bullseye pattern due to the absence of slip data for historical earthquakes. Indeed, a significant variation in the stress transmitted to the receiving faults has been noticed depending on the slip pattern of the causative faults.

The impact of this new semi-realistic model has been tested on both imaginary faults positioned in different spatial relationships and on real faults, using three historical earthquakes as examples (Colfiorito 1279, Norcia 1328, Cascia 1599). This new methodology has been applied to these case studies to test its feasibility, effectiveness, and improvements over the methodology used so far.

This methodological paper (Chapter 3) has demonstrated how more precise inputs in Coulomb Stress Transfer (CST) modeling led to results significantly different from those obtained with the classical methodology used until now. However, there are non-negligible computational limitations. In addition to the limitations mentioned so far, it is worth noting that modeling a single elliptical fault with variable strike and its corresponding coseismic slip requires considerable computational power, sometimes necessitating whole weeks for a single CST computation. Therefore, the development of a MATLAB code that automates the processes and calculations previously performed by the user, possibly through a GUI simplifying the input parameter entry operations, becomes necessary.

Upon devising, implementing, and testing the new technique, a specific study was conducted on the relationship between the evolution of seismic sequences and Coulomb stress transfer within the CAFS (Chapter 4). Our study on CST in the CAFS examined seismic events with magnitudes Mw>5.8, spanning from 1279 to 2016. This broad temporal range allowed us to closely observe fault activity, detecting both

individual and collective impacts of CST on various earthquakes and how these influenced the current stress conditions in the system. A complex CST pattern has been identified, with some faults subjected to intense positive stress and others in stress shadow zones, revealing the complex dynamics among interconnected faults. The studied cases demonstrate CST as both a factor in seismic activation and inhibition, although the relationship is not direct in some examples.

The 1279 Colfiorito earthquake increased stress in a limited area of the northern part of the Norcia fault, which then exhibited seismic activity in 1328. This phenomenon suggests that the 1328 rupture may have been triggered in this area of increased stress, subsequently extending along the entire length of the Norcia fault. A similar dynamic occurred with the Norcia earthquake on January 14, 1703, where the effects of positive stress extended further, affecting the Monte Marine fault in the Upper Aterno system. This led to another severe earthquake 19 days later, resulting from the joint rupture of multiple faults (Monte Marine, Monte Pettino, and Paganica-San Demetrio), highlighting a cascade effect.

More than two centuries earlier, the Gran Sasso seismic event, with a magnitude of about 7.0, created a condition of accentuated stress only on the superficial part of the Paganica-San Demetrio fault system. Despite the stress shadow over much of this system, a dynamic stress transfer is presumed due to the activation of the Alto Aterno faults in 1703, these last situated in a zone of considerable positive stress.

The 1703 Norcia earthquake also affected the Campotosto fault, already compromised by the 1349 Gran Sasso earthquake. CST modeling, based on more recent seismic events, reveals a notable increase in stress. The models indicate that, over a millennium, the Campotosto fault has accumulated enough stress to make its inactivity unlikely. Indeed, following the 2009 L'Aquila seismic sequence and the 2016 Monte Vettore events, it produced earthquakes with magnitudes slightly above 5.0. These observations reinforce the idea that the Campotosto fault serves as a dynamic link between the northern and southern faults of the CAFS, playing an active role in recent seismic activity (Tondi et al., 2020).

The case of the Norcia fault's reactivation in 1730, only 27 years after a prior event in 1703, raises questions about the theory that stress within a fault completely zeroes out after its full rupture. It appears that, despite no significant stress accumulation from other faults during that period, this fault may have recharged with interseismic stress due to deep viscous deformation (Cowie et al., 2013; Wedmore et al., 2017), partly facilitated by coseismic stress from earlier lower magnitude earthquakes. This phenomenon might explain its unusual reactivation in such a short time span.

Considering more recent earthquakes, like those of Colfiorito in 1997, L'Aquila in 2009, and Monte Vettore in 2016, the reliability of CST calculations increases thanks to the availability of more precise fault slip data, free from magnitude uncertainties. This allowed us to accurately reconstruct the activation of the Monte Vettore fault, which exhibited an atypical sequence of events: initial activation impacted the southern part, leaving the northern tip unstressed which then activated later. This unconventional behavior has been linked to intersismic stress loading in the shear zone at 15-24 km depth, which would have positively stressed the fault's deeper portion (Cowie et al., 2013; Wedmore et al., 2017). On October 30, not only the central portion of the fault but also the previously ruptured segments reactivated, indicating that the accumulated stress had not fully dissipated. Interestingly, the simulation of the 1703 Norcia earthquake reveals that the Monte Vettore fault experienced significant negative inhibitory stress, with no other models showing sufficient positive Coulomb Stress Transfer (CST) to compensate for the stress removed in 1703. Various mechanisms such as fluid migration, dynamic stress transfer, or intersismic stress loading may be invoked in this situation.

It's also notable that despite a long inactivity, the 2016 CST model indicates a complex interaction between the Norcia and Monte Vettore faults, with a mutual inhibitory effect at depth and positive stress at the surface highlighting the importance of both surface and deep stress loading in seismic dynamics.

The analysis of the 2009 L'Aquila earthquake revealed significant outcomes regarding the stress effect on the Gran Sasso fault. Careful observation of the aftershock sequence indicates that some occurred in the northern part of the Gran Sasso fault. Our CST study highlights how the areas hit by L'Aquila aftershocks correspond to those

where the Gran Sasso fault was more stressed. This link between stress zones and the aftershock sequence emphasizes the influence of CST in shaping seismic sequences.

The analysis of past seismic events in the areas of Fabriano and Sulmona (outside the CAFS) raises questions: the 1349 earthquake slightly influenced the Mt Morrone fault, near Sulmona. Moving towards the northern sector, the 1703 Norcia earthquake increased stress around Fabriano. This city experienced a notable earthquake, magnitude 6.1, shortly after Norcia's, indicating a possible connection with stress transfer (which in this case, from the models, turns out positive). Conversely, the Mt Morrone fault has not shown signs of significant activity for nearly two millennia, raising concerns about its seismic stability. This last fault indeed results positively stressed by the CAFS activity over the last millennium.

As previously mentioned, seismic activity in the Central Apennines Fault System (CAFS) over the last thousand years has been divided into three main phases of intense seismic activity, each marked by a different total seismic moment. The most recent phase, between 1979 and 2016, recorded the least accumulation of seismic moment, suggesting the presence of a seismic gap that could be filled by an earthquake of magnitude Mw=6.6. This magnitude could result from the activation of the Gran Sasso fault, identified as a high-risk area due to its elevated stress level. However, the Gran Sasso fault has not shown activity since 1349 and, despite often falling under the influence of positive stress from adjacent faults, has exhibited a prolonged period of quiescence. It is known that this fault has rather extended return times, estimated at about 2.8 ky, and although Coulomb Stress Transfer (CST) may alter these intervals, the time between seismic events remains significantly wide.

The iterative accumulation of stress changes can result in stress conditions significantly different from those inferred from isolated events, underscoring the importance of a comprehensive and long-term perspective on seismic sequences to understand their stress impacts. However, it is important to note that the accuracy of our models depends on the precision of input parameters, which, although derived from the best available data, remain approximations. Moreover, calculated CST changes do not necessarily predict an earthquake but merely indicate the stress state of

a fault, although CST models offer valuable insights, their predictive capacity remains inherently probabilistic.

Our study emphasizes the critical role of spatial and temporal components of CST in understanding seismic dynamics. It highlights the value of considering the cumulative effects of multiple seismic events and the specific characteristics of individual faults in seismic behavior modeling. Future studies might seek to further refine these models by incorporating more detailed fault characteristics and broader geographic contexts to enhance the precision of seismic risk predictions. Additionally, while three-dimensional models offer significant advantages over previously adopted approaches, their computational complexity and the need for detailed data for parameterization pose a challenge for large-scale application.

Furthermore, despite the introduction of advanced three-dimensional models, these still rely on approximations of the physical properties of faults and the surrounding environment. Variability in fault geometry, mechanical properties of materials, and the role of fluids in the subsurface are factors that can significantly influence stress transfer but are often simplified in current models. Future research might explore more sophisticated modeling approaches that account for these complex variables, potentially through the simulation of seismic scenarios based on more detailed physical principles.

A promising future perspective involves precisely relating the stress state of a fault to the variation it causes in terms of the characteristic return time. In other words, there is a need to answer the following question: how does such an amount of positive or negative stress received by a fault alter its characteristic return time? Future research could answer this question, making studies on CST quantifiable and practically applicable to seismic hazard maps.

Furthermore, there is a necessity to integrate research findings into seismic warning systems and urban and territorial planning strategies. The transformation of scientific knowledge into practical applications requires close collaboration among seismologists, engineers, urban planners, and policymakers, as well as the

development of tools and methodologies that can effectively translate research outcomes into risk mitigation measures.

In conclusion, the research presented through these studies meticulously explores the influence of Coulomb Stress Transfer (CST) on fault interaction dynamics, with a special focus on the Central Apennines Fault System (CAFS) and on the primary and secondary coseismic effects following the seismic event in Petrinja (Croatia) on December 29, 2020. Through detailed analysis and innovative methodologies, these works illuminate complex seismic mechanisms, offering significant insights for understanding seismic sequences and for developing more effective risk mitigation strategies.

The field observation and mapping of coseismic effects generated by the Petrinja earthquake revealed intense activity along the pre-existing PFZ (Petrinja Fault Zone), characterized by strike-slip kinematics and conjugate fault structures, highlighting the importance of analyzing regional geodynamics through the direct observation of coseismic effects. This phenomenon, along with detailed fault rupture mapping and fault mechanism analysis, underscores the need for accurate and timely monitoring of coseismic deformations to improve seismic hazard assessments and future event prediction in the Alpine-Dinarides-Albanides orogen.

Moderate magnitude seismic events, although with focal mechanisms different from those in Croatia, have struck central Italy in the last two decades. Updating the seismic cycle of the CAFS following the 2009 and 2016 events and analyzing the spatiotemporal evolution of seismicity reveals that CAFS seismicity over the last 1000 years appears divided into three time-windows of seismicity separated by about 300-350 years of time gap. The cumulative seismic moment shows discordance among the different seismicity windows, gradually decreasing towards the present. A thorough analysis of the CST was necessary to assess whether this progressive decrease in seismic moment could be due to a potential seismic gap, and if so, to outline the most probable future seismic scenario based on the amount of stress received by each fault. Introducing an elliptical geometry in the studied faults has produced significant changes in the transmission of static stress. This approach not only enhances our understanding of the contribution of CST in fault interactions but also paves the way

for future advanced applications in estimating the rupture susceptibility of active faults, integrating multidisciplinary data for a more comprehensive and integrated seismic risk assessment.

Lastly, the detailed analysis of CST in the CAFS, examining nine seismic events selected from the CPTI15 catalog, demonstrates how CST may have played a key role within the system, catalyzing the activation or inhibition of its faults in various historical contexts. Many seismic events were catalyzed by a concentration of positive static stress on the causative fault following preceding earthquakes with spatiotemporal proximity. In other cases, it seems reasonable to speculate on the dilation of the characteristic return time of an earthquake due to the effect of the stress shadow on the receiving fault. However, there are several examples where CST appears to have been completely uninfluential on the rupture of some faults, suggesting interaction with other triggering factors such as dynamic stress transfer or underground fluid circulation, or, ultimately, shortcomings in the CST model due to lack of data or erroneous estimates of historical magnitudes.

Understanding CST not only has concrete and academic implications, illuminating fault interactions in previous seismic episodes but also provides valuable insights for possible future earthquake sequences, essential for formulating targeted risk mitigation tactics to protect local communities from the catastrophic consequences of earthquakes. Through the processing of the current CST scenario, is evident that faults with higher stress concentration are the Mt. Marine Fault, Pettino Fault, Campotosto fault (the latter seems to have released part of the stress accumulated during the 2009 seismic sequence), the northern sector of the Gran Sasso fault, and a fault outside the boundaries of the CAFS: the Mt. Morrone fault, dangerously close to the city of Sulmona.

The outcomes of these studies highlight the complex dynamics at play in high seismic activity regions like the CAFS and the Dinarides, showing how a detailed understanding of CST and fault interactions can provide crucial insights for seismic risk management. The adoption of innovative modeling techniques and the integration of historical and instrumental data in these works not only significantly advance

earthquake knowledge but also lay the groundwork for future seismic risk mitigation strategies, emphasizing the need for ongoing research in this vital field.

References

Ahlgren, S. G. The nucleation and evolution of Riedel shear-zones as deformation bands in porous sandstone. J. Struct. Geol. 23(8), 1203–1214. https:// doi. org/ 10. 1016/ S0191-8141(00) 00183-8 (2001).

Aktar, M., Karabulut, H., Ozalaybey, S. & Childs, D. A conjugate strike-slip faults within the extensional tectonics of Western Turkey. Geophys. J. Int. 171(3), 1363–1375. https:// doi. org/ 10. 1111/j. 1365- 246X. 2007. 03598.x (2007).

Barnett J.A., Mortimer J., Rippon J.H., Walsh J.J. and Watterson J.; 1987: Displacement geometry in the volume containing a single normal fault. AAPG Bull., 71, 925-937.

Blumetti A.M. , 1995. Neotectonic investigation of evidence of paleoseismicity in the epicentral area of the January–February 1703, central Italy, earthquakes, Perspectives in Paleoseismology, Assoc. Eng. Geol. Bull., Special Publ.6, 83–100

Blumetti, A. M., & Guerrieri, L. (2007). Fault-generated mountain fronts and the identification of fault segments: implications for seismic hazard assessment. *BOLLETTINO-SOCIETA GEOLOGICA ITALIANA*, *126*(2), 307.

Civico, R.& the Open EMERGEO Working Group. Surface ruptures following the 30 October 2016 Mw 6.5 Norcia earthquake, central Italy. Journal of Maps, 14, 151-160, DOI: 10.1080/17445647.2018.1441756 (2018).

Cello G, Mazzoli S, Tondi E, Turco E (1997) Active tectonics in the central Apennines and possible implications for seismic hazard analysis in peninsular Italy. Tectonophysics 272(1):43–68. https:// doi.org/ 10. 1016/ S0040- 1951(96) 00275-2

Cinti, F. R., Civico, R., Blumetti, A. M., Chiarini, E., La Posta, E., Pantosti, D., ... & Brunori, C. A. (2018). Evidence for surface faulting earthquakes on the Montereale fault system (Abruzzi Apennines, central Italy). Tectonics, 37(9), 2758-2776.

Cowie, P. A., Scholz, C. H., Roberts, G. P., Faure Walker, J. P., & Steer, P. (2013). Viscous roots of active seismogenic faults revealed by geologic slip rate variations. Nature Geoscience, 6(12), 1036-1040.

Falcucci, E., Gori, S., Moro, M., Fubelli, G., Saroli, M., Chiarabba, C., & Galadini, F. (2015). Deep reaching versus vertically restricted Quaternary normal faults: Implications on seismic potential assessment in tectonically active regions: Lessons from the middle Aterno valley fault system, central Italy. Tectonophysics, 651, 186-198.

Galadini F. , Galli P., 2003. Paleoseismology of silent faults in the Central Apennines (Italy): the Mt. Vettore and Laga Mts. faults, Ann. Geophys.465, 815–836.

Galli P. A., Giaccio B., Messina P., Peronace E. and Zuppi G. M.; 2011: Palaeoseismology of the L'Aquila faults (central Italy, 2009, M w 6.3 earthquake): Implications for active fault linkage. Geophysical Journal International, 187(3), 1119-1134.

Galli P., Galadini F. and Calzoni F.; 2005: Surface faulting in Norcia (central Italy): a “paleoseismological perspective”. Tectonophysics, 403(1-4), 117-130.

Galli P., Galadini F. and Pantosti D.; 2008: Twenty years of paleoseismology in Italy. Earth-Science Reviews, 88(1-2), 89-117.

Galli P., Galderisi A., Messina P. and Peronace E.; 2022: The Gran Sasso fault system: Paleoseismological constraints on the catastrophic 1349 earthquake in Central Italy. Tectonophysics, 822, 229156.

Galli P., Galderisi, A., Ilardo, I., Piscitelli, S., Scionti, V., Bellanova, J. and Calzoni, F.; 2018: Holocene paleoseismology of the Norcia fault system (Central Italy). Tectonophysics, 745, 154-169.

Galli P.; 2020: Recurrence times of central-southern Apennine faults (Italy): hints from palaeoseismology. Terra Nova, 32(6), 399-407.

Galli, P., Messina, P., Peronace, E., Galderisi, A., Ilardo, I., & Polpetta, F. (2023). Paleoseismic evidence of five magnitude 7 earthquakes on the Norcia fault system in the past 8,000 years (Central Italy). Frontiers in Earth Science, 11, 1188602.

Geol. Soc. Am. Bull., 133, 1679-1694, doi: 10.1130/B35788.1.

Gupta A. and Scholz C.H.; 2000: A model of normal fault interaction based on observations and theory. J. Struct. Geol., 22, 865-879.

Harris, R. A., and R. W. Simpson (1992), Changes in static stress on southern California faults after the 1992 Landers earthquake, Nature, 360(6401), 251–254, doi:10.1038/360251a0.

Katz, Y., Weinberger, R. & Aydin, A. Geometry and kinematic evolution of Riedel shear structures, Capitol Reef National Park Utah. J. Struct. Geol. 26(3), 491–501. https:// doi. org/ 10. 1016/j. jsg. 2003. 08. 003 (2004).

King G. C., Stein R. S. and Lin, J.; 1994: Static stress changes and the triggering of earthquakes. Bulletin of the Seismological Society of America, 84(3), 935-953.

Livio, F., Serva, L. & Gürpinar, A. Locating distributed faulting: contributions from InSAR imaging to probabilistic fault displacement hazard analysis (PFDHA). Quatern. Int. https:// doi. org/ 10. 1016/j. quaint. 2016. 09. 034 (2016).

Mildon Z.K., Toda S., Faure Walker J.P. and Roberts G.P.; 2016: Evaluating models of Coulomb stress transfer: is variable fault geometry important?. Geophys. Res. Lett., 43, 12407-12414, doi: 10.1002/2016GL071128.

Mildon, Z. K., Roberts, G. P., Faure Walker, J. P., Beck, J., Papanikolaou, I., Michetti, A. M., ... & Vittori, E. (2022). Surface faulting earthquake clustering controlled by fault and shear-zone interactions. *Nature Communications*, *13*(1), 7126.

Reasenberg, P. A., and R. W. Simpson (1992), Response of regional seismicity to the static stress change produced by the loma prieta earthquake, Science, 255(5052), 1687–1690, doi:10.1126/science.255.5052.1687.

Roberts, G. P., Sgambato, C., Mildon, Z. K., Iezzi, F., Beck, J., Robertson, J., ... & Mitchell, S. (2024). Spatial migration of temporal earthquake clusters driven by the transfer of differential stress between neighbouring fault/shear-zone structures. *Journal of Structural Geology*, *181*, 105096.

Tondi E. and Cello G.; 2003: Spatiotemporal evolution of the Central Apennines fault system (Italy). Journal of Geodynamics, 36(1-2), 113-128.

Tondi E., Jablonská D., Volatili T., Michele M., Mazzoli S. and Pierantoni P.P.; 2020: The Campotosto linkage fault zone between the 2009 and 2016 seismic sequences of central Italy: implications for seismic hazard analysis.

Valentini G., Volatili T., Galli P. and Tondi E.; 2023: New methodological approach in the evaluation of faults interaction: insights from the central apennine fault system. Bulletin of Geophysics and Oceanography.

Vannucci G., Lolli B. and Gasperini P.; 2021: Inhomogeneity of macroseismic intensities in Italy and consequences for macroseismic magnitude estimation. Seismological Research Letters, 92(4), 2234-2244.

Walsh J.J. and Watterson J.; 1987: Distributions of cumulative displacement and seismic slip on a single normal fault surface. J. Struct. Geol., 9, 1039-1046.

Wedmore L. N. J., Faure Walker J. P., Roberts G. P., Sammonds P. R., McCaffrey K. J. W. and Cowie P. A.; 2017: A 667 year record of coseismic and interseismic Coulomb stress changes in central Italy reveals the role of fault interaction in controlling irregular earthquake recurrence intervals. Journal of Geophysical Research: Solid Earth, 122(7), 5691-5711.

RINGRAZIAMENTI

La mia più profonda gratitudine va al mio supervisor, nonché Prorettore vicario dell'Ateneo, il Prof. Emanuele Tondi, per il suo incrollabile incoraggiamento e la sua lungimiranza. La sua guida è stata un pilastro non solo per questa tesi, ma anche per il mio percorso accademico e personale. La sua visione e il suo supporto sono stati indispensabili.
Desidero ringraziare di cuore Tiziano Volatili, per la sua preziosa supervisione e guida. La sua competenza ha avuto un'influenza significativa nel plasmare il mio percorso accademico, e sono profondamente grato per il suo sostegno.
Un grande riconoscimento va ai miei colleghi e amici della sezione di Geologia di Unicam. Il loro spirito di collaborazione e il costante supporto hanno giocato un ruolo importante nel raggiungimento dei miei obiettivi. Il loro aiuto e il piacevole ambiente di ricerca che hanno contribuito a creare, hanno avuto un'influenza decisamente positiva nella mia carriera.
Il percorso di dottorato mette a dura prova il sistema nervoso, soprattutto se condividi lo studio con Giorgio. Per questo ringrazio Veronica e la sua infinita pazienza, infondo quante altre persone sarebbero state disposte a sopportarmi 8 ore al giorno per 4 anni?

E dopo le 8 ore di lavoro qualcun altro ha sempre sacrificato la sua pazienza per me, grazie Marika, sei stata un punto di riferimento insostituibile, ti sarò sempre riconoscente.
Grazie Naze, Kledy, Alessandro, Cristina, Elisa, Fils, Ines, Moja e Mommy; la nostalgia dei tempi d'oro del nostro gruppo sconvolgerà il mio umore ancora a lungo, ma mi permetterà di ricordare quanto sono stato fortunato a conoscervi e a ricevere il vostro supporto durante tutti questi anni.
È normale, alcuni se ne vanno, ognuno prende la sua strada e piano piano, i gruppi si smembrano, ma alcuni no, alcuni rimangono legati indissolubilmente nonostante qualsiasi intemperia. Guglielmo, Valerio, Davide, Daniele, Matteo; questi sono solo alcuni dei membri della seconda famiglia a cui devo un enorme grazie! Sapere che, nonostante la divergenza delle nostre vite, nulla è mai cambiato mi rende immensamente fiero di avervi con me.

Κάποιες φορές, όταν είσαι έτοιμος να χάσεις τις ελπίδες σου, μπαίνει στη ζωή σου αυτός ο άνθρωπος που ανάβει τη φωτιά που είχε σβήσει εδώ και χρόνια. Στη ζωή μου, αυτός ο άνθρωπος ονομάζεται Σοφία. Θα έπρεπε να σε ευχαριστήσω για χίλια πράγματα, αλλά υπάρχει ένα συγκεκριμένο, πολύ σημαντικο: έκανες ένα μαγικό, μου θυμισες τι σημαίνει να ΑΓΑΠΑΣ.
Μιας και τα ευχαριστήρια είναι αρκετά γλυκανάλατα, τώρα είναι η στιγμή να σπάσουμε τη μαγεία ευχαριστώντας την Πολυξένη Ζάχου, την πιο μαλακισμένη απ'όλες! Εμείς είμαστε η απόδειξη ότι η φιλία μεταξύ άνδρα και γυναίκας όχι μόνο μπορεί να υπάρξει αλλά μπορεί να είναι και κάτι ξεχωριστό.

Gli "scienziati" non dovrebbero credere a queste cose, ma troppo spesso percepisco la tua presenza, il tuo calore e la tua influenza in molti avvenimenti della mia vita. Sono convinto che tu abbia badato a me per tutti questi anni. Grazie Noemi.

Mi sento fortunato, se dovessi ringraziare tutte le persone che sono state al mio fianco in questo percorso avrei bisogno di troppe pagine, troppi alberi tagliati. Sono sempre stato circondato da persone incredibili che, tassello dopo tassello, hanno contribuito a plasmare il Giorgio che sono ora, una di queste persone sei tu, tu che stai leggendo questo testo! Grazie.

DEDICO QUESTA TESI ALLA MIA FAMIGLIA, mia Madre, mio Padre e mia Sorella. Non avrei potuto desiderare niente di meglio! Grazie per il vostro Amore, supporto e per la grande pazienza che avete dimostrato di avere.